Technische Universität Wien

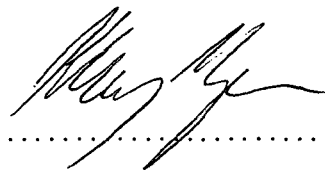DISSERTATION

Space-Time Processing
for UMTS/TDD

ausgeführt zum Zwecke der Erlangung des akademischen Grades
eines Doktors der technischen Wissenschaften

eingereicht an der
Technischen Universität Wien
Fakultät für Elektrotechnik und Informationstechnik

von

Dipl.–Ing. Klaus KOPSA
Matr.Nr. 9227528
Edmund-Weiß Gasse 1/16, A–1180 Wien

Wien, im September 2003

Betreuer:

O.Univ.Prof. Dipl.–Ing. Dr.techn. Ernst BONEK

Institut für Nachrichtentechnik und Hochfrequenztechnik
Technische Universität Wien

Zweitbegutachter:

Ao.Univ.Prof. Dipl.–Ing. Dr.techn. Franz HLAWATSCH

Institut für Nachrichtentechnik und Hochfrequenztechnik
Technische Universität Wien

Zusammenfassung

Ziel des EU-Projektes ANTIUM war die Entwicklung eines Analysegerätes für UMTS-
und DVB-T-Netze, welches die Ermittlung der vorliegenden Störsignalkonstellation er-
laubt. Diese Information kann dann vom Netzbetreiber für Optimierungen verwendet
werden. In der in dieser Dissertation vorgestellten Arbeit, die sich auf UMTS/TDD-
Systeme beschränkt, werden Algorithmen entwickelt, die die sogenannten Broadcast-
Kanäle (BCHs) von möglichst vielen umliegenden Basisstationen auslesen. Da im Rahmen
von ANTIUM mehrere Empfangsantennen zur Verfügung stehen, bietet sich dafür eine
räumlich-zeitliche Signalverarbeitung an. Die Aufgabe des Auslesens der BCHs zerfällt
in die funktionellen Einheiten *Synchronisation, Kanalschätzung* und *Datendetektion.*

Ziel der Synchronisationsstufe ist es zunächst, das Empfangssignal nach dem Vorhan-
densein von Synchronisationssequenzen zu durchsuchen, um die Anzahl der Basisstations-
signale festzustellen. Danach können die zeitlichen Lagen der BCHs sowie Informatio-
nen über die verwendeten Trainingssequenzen (basic midambles) und Spreizcodes gewon-
nen werden. Die drei hier vorgestellten Synchronisationsalgorithmen basieren auf einem
binären Hypothesentest, der mittels eines verallgemeinerten Likelihood-Verhältnisses eine
Entscheidungsstatistik für das Vorhandensein der Synchronisationssequenzen liefert. Eine
Mittelung über mehrere Rahmen verbessert diese Entscheidungsstatistik erheblich.

Da die Zusammensetzung der von UMTS/TDD zur Kanalschätzung angebotenen
Trainingssequenzen von der unbekannten Anzahl der Datenkanäle abhängt, muß sie vor
der eigentlichen Kanalschätzung ermittelt werden. Für diese Aufgabe werden zwei ver-
schiedene Methoden vorgestellt. Mit den geschätzten Trainingssequenzen kann dann eine
Mehrbenutzerkanalschätzung basierend auf dem MMSE-Prinzip erfolgen, wobei auch eine
modifizierte Kanalschätzmethode mit Störungsunterdrückung vorgestellt wird.

Mit Hilfe der Kanalimpulsantworten ist es der Datendetektionsstufe möglich, die
Kanäle zu entzerren und die Daten zu gewinnen. Die Schätzung der von einem räumlich-
zeitlichen MMSE-Entzerrer benötigten Korrelationsmatrix ist allerdings nicht mit aus-
reichender Genauigkeit möglich. Als Ausweg bietet sich an, die Korrelationsmatrix nicht
zu schätzen, sondern zu berechnen, wofür die Anzahl der vorhandenen Datenkanäle und
deren Sendeamplituden ermittelt werden müssen. Da dies am besten für die stärkste
Basisstation funktioniert, wird eine Störungsunterdrückungsstruktur verwendet.

Abschließend wird der Einfluß von Ungenauigkeiten der Synchronisations- und Kanal-
schätzstufen auf die Ergebnisse der Detektionsstufe untersucht. Simulationen des Gesamt-
systems ergeben zwar überwiegend zufriedenstellende Resultate, zeigen aber auch, daß die
Kanalschätzgenauigkeit großen Einfluß auf die Detektionsergebnisse hat.

Abstract

The goal of the EU-funded project ANTIUM was to develop a monitoring device for UMTS and DVB-T networks which allows to assess the interference situation present. The information provided by this device should enable operators to optimise their network. More specifically, for UMTS/TDD, to which this thesis is restricted, algorithms had to be developed which read the so-called broadcast channels (BCHs) of as many surrounding base stations as possible. Since the ANTIUM device is equipped with multiple antennas at the receiver, space-time signal processing can beneficially be used. The task of reading the BCHs splits up into *synchronisation, channel estimation,* and *data detection.*

The first step of the synchronisation stage is scanning the received data for the presence of synchronisation codes to determine the number of impinging base station signals. Subsequently, the temporal locations of the BCHs and information on the used training sequences (basic midambles) and scrambling codes are extracted. The three synchronisation algorithms presented in this thesis are based on a binary hypothesis test which uses a generalised likelihood ratio to obtain a decision statistic for the presence of synchronisation codes. Averaging over several frames turns out to improve this decision statistic considerably.

Since the composition of the midambles offered by UMTS/TDD for the purpose of channel estimation depends on the unknown number of data channels present, this composition has to be estimated prior to channel estimation. For this estimation task, two different methods are presented. Using the estimated midambles, multiuser channel estimation based on the MMSE principle can then be performed. We also develop a modified channel estimation technique with interference cancellation.

Knowledge of the channel impulse responses enables the data detection stage to equalise the channel and to recover the data. It turns out that for the conventional space-time MMSE filter, the required correlation matrix cannot be estimated with sufficient accuracy. The solution we propose is to explicitly calculate the correlation matrix instead of estimating it. For this task, we have to detect the data channels present and estimate their respective transmit amplitudes. Since this can be done with greatest accuracy for the strongest base station, we use an interference cancellation approach.

We finally investigate the influence of synchronisation and channel estimation errors on the performance of the detection stage. Simulations of the overall receiver system yield mostly satisfactory results, but they also show that the accuracy of channel estimation has a strong impact on data detection performance.

Acknowledgment

I would like to thank all the persons who contributed to this thesis in various ways:

"Begin at the beginning," the King said, very
gravely, "and go on till you come to the end:
then stop" — *Lewis Carrol*

Contents

Chapter 1

Introduction

Mobile communications has been the technology with the greatest impact on everyday life in the last few years. After the analogue first-generation systems which never became very popular, the tremendously successful *Global System for Mobile Communications* (GSM) offered voice communications with seamless roaming in almost the entire world. GSM is based on digital data transmission (referred to as second generation) and was originally developed for speech applications only. Although some evolutions of GSM towards the delivery of data contents—most notably the *General Packet Radio Service* (GPRS) system—were made, the inherent limitations of second-generation systems prohibit high-rate data services.

These high data rates which are required to enable wireless access to the Internet will in the near future be provided by so-called third-generation systems like UMTS. Using CDMA with various spreading factors, packet-switching techniques, and high bandwidths, the UMTS system has been developed from the outset for flexible data traffic. Within UMTS there exist two different modes, namely *frequency division duplex* (FDD) and *time division duplex* (TDD). Whereas the first FDD networks started operation in spring 2003, TDD services, which were developed mainly for microcell and indoor environments, have not been rolled out so far.

1.1 A Network Monitoring Device for UMTS

In cellular CDMA system such as UMTS, co-channel interference is inherently present and cannot be avoided. In order to serve as many users as possible with satisfactory quality, operators have to carefully balance the interference level. Besides thorough network planning, constant monitoring of the interference situation is hence necessary to effectively optimise the network. For the task of interference analysis, operators will need accurate measurement devices. In UMTS, a widely used measurement device is the classical trace mobile which is a common mobile terminal equipped with additional measurement software and interfaces. Its capability of online measurements makes this tool very useful for large-scale measurements, but because of its limited signal processing power it may not be able to resolve interference accurately enough in some critical situations.

Within the EU-funded ANTIUM project, one goal was to develop a network monitoring device for UMTS which outperforms the trace mobile by using multiple antennas and sophisticated signal processing. To classify interference, this network monitoring device determines which base stations contribute to the overall received signal and what their respective power levels are. This information is gained by reading the broadcast channels (BCHs) of as many surrounding base stations as possible. A prerequisite for recovering the BCH data in the data detection stage is successful synchronisation and channel estimation. Due to the multiple antennas available and the off-line processing implemented by the ANTIUM device, advanced and sophisticated signal processing techniques can be used to perform these tasks.

In this work, we will identify suitable algorithms for synchronisation, channel estimation, and data detection and adapt them to match the demands of UMTS/TDD interference analysis. We note that descriptions of our results have been published in [KMAH02, KAMH03, AKH03].

1.2 Selecting Suitable Receiver Techniques

Selecting an appropriate signal processing algorithm is a delicate task, because a vast number of methods are available, all with their specific advantages and drawbacks. According to the used receiver architecture, signal processing schemes can be coarsely classified into temporal, spatial and space-time algorithms.

Temporal processing is often necessary due to multipath propagation present in a mobile radio environment [Rap96]. The transmitted signals propagate along paths with different lengths and reach the receiver with different delays. This causes effects like fading and inter-symbol interference (ISI). The main goal of *temporal equalisers* is now to remedy the ISI and to restore the original signal. The optimum temporal equaliser in the sense of minimum sequence error probability is the *maximum-likelihood sequence estimator* (MLSE) [For72]. It can be shown that the MLSE criterion is equivalent to the problem of estimating the state of a discrete-time finite-state machine [Pro95]. An efficient way of performing the trellis search needed to solve these kinds of problems is the Viterbi algorithm [For73]. Nevertheless, the greatest drawback of the MLSE is that its computational complexity grows exponentially with the channel length. For many channels of practical interest, the MLSE is thus prohibitively expensive and therefore suboptimal but computationally affordable algorithms have to be used.

A popular class of suboptimal temporal equalisers are *linear transversal filters*, where different algorithms can be distinguished by the way the filter weights are chosen. A widely used criterion to select the weights is the *mean square error* (MSE) that leads to *minimum mean square error* (MMSE) equalisation [Geo65]. In the context of CDMA, a popular special case of the linear transversal equaliser is the so-called *RAKE receiver* [PG58] that correlates the received signal with delayed versions of the used spreading code. The fact that the correlator outputs collect the different multipath contributions somehow analogously to an ordinary garden rake led to the name "RAKE receiver."

Since the mobile environment changes with time, equalisation accuracy would decrease continuously if fixed filter weights were used. Often, a frequent re-calculation of the filter weights is computationally not feasible and inaccuracies have to be expected. This problem is avoided by *adaptive* equalisers that continuously track the channel variations and update the weights accordingly. The most popular adaptive equaliser is the so-called *least mean square* (LMS) algorithm [Wid66].

Another possibility of constructing suboptimal equalisers is to exploit previously detected symbols to suppress their influence on the present symbol. This class of equalisers is referred to as *decision-feedback* (DFB) equalisers [Aus67]. Besides the conventional transversal filter (*feedforward* filter), DFB equalisers use a second filter (*feedback* filter), whose output is subtracted from the feedforward filter output prior to decision. This leads to a superiority of the DFB equaliser over linear equalisers as long as decision error propagation is not too severe [Mon71].[1] In the case of error propagation, the performance of DFB equalisers is not easily assessed but nevertheless some bounds can be found [AB93]. A more detailed review on temporal equalisation algorithms can be found in [Pro95, Qur85].

The limiting factor for the capacity of any *cellular* mobile communication system is the inherent presence of co-channel interference. Since the interfering signals often impinge from different directions than the desired signal, a straightforward approach for mitigating the influence of co-channel interference is the use of an antenna array and spatial processing. Although this approach has been used in RADAR applications for decades, in mobile communications spatial processing is only starting to become popular. The principle of array processing is that the signals collected by different antenna elements are multiplied by a set of so-called *antenna weights* and combined in the receiver. Similarly to the temporal equalisers, different algorithms can be distinguished by the way the weights are chosen. A very simple possibility is to select the signal of the currently strongest antenna element (weight 1) while switching off the others (weight 0). This approach, which is also known as *selection diversity*, requires only one switch and a power sensor per antenna element and is hence very easy to implement. A way to better exploit the potential gains of spatial processing is to choose the weights such that the output signal-to-noise ratio (SNR) is maximised. This technique is known as *maximum ratio combining* (MRC) [Bre59] and works best if the interference is spatially white. In the case of spatially coloured interference, however, we can use *optimum combining* [Win84], where the weights are chosen to maximise the signal-to-interference-and-noise ratio (SINR). As for the temporal filters, also adaptive methods for weight computation (e.g. *constrained LMS* [Fro72]) have been proposed. One common feature of the so-called *diversity techniques* presented in this paragraph is that their performance is best when the different antenna elements are uncorrelated.

Methods that explicitly assume correlated antenna elements are the class of *beamforming* algorithms. They compute the antenna weights based on the *directions-of-arrival* (DOAs) of incoming signals. Algorithms for estimating these DOAs can be divided into

---

[1] In the theoretical analysis of the performance of the DFB, error propagation is usually neglected.

two classes, *spectrum-based* and *parametric* algorithms. The former ones use the highest peaks of a spectrum-like function (e.g. the azimuth power spectrum (APS)) as DOA estimates. Popular methods include the Fourier-based *Bartlett beamformer* [Bar48], the *minimum variance method* (MVM) [CGK67] and *MUSIC* [BK79]. Parametric methods, on the other hand, estimate the DOAs directly from the received data and usually offer higher resolution than spectrum-based methods. Two of the most popular algorithms are the maximum-likelihood (ML) based *SAGE* algorithm [FH94] and *ESPRIT* [RPK86], which uses invariance properties of the antenna array. A widely used derivative of ESPRIT is the computationally cheap *Unitary*-ESPRIT [HN95]. See [Fuh97, App76, VB88, KV96] for a more detailed review of DOA estimation methods and beamforming.

Since common mobile telecommunications systems encounter both multipath propagation and co-channel interference, a combination of purely temporal and purely spatial processing is advantageous. This leads directly to the class of so called *space-time* (ST) processing algorithms. For CDMA systems, such an extension of the temporal RAKE receiver to the spatial domain is the *2D-RAKE* [NP94, TGM96]: A beamforming front-end followed by a temporal RAKE receiver is yielding enhanced performance. But more generally, if we replace the scalar input of an arbitrary temporal equaliser by a vector input containing the signals of the different antenna elements, we can formulate the same optimality criteria as in temporal equalisation also in the space-time domain. From a sequence-error point of view, the optimal space-time equaliser will thus be the *ST-MLSE* [MS95]. Unfortunately, the inclusion of the spatial domain further increases the complexity of the temporal MLSE, and thus the demand for suboptimal methods is even stronger in space-time processing. A good compromise in this field are the *ST-MMSE* receiver [PP97] and also space-time DFB algorithms [KKB96]. For a more detailed review on space-time methods, refer to [PP97, vRLvW00].

Due to the structure of the ANTIUM network monitoring device, the following two constraints existed for possible signal processing algorithms:

1. multiple, uncalibrated receive antennas;

2. off-line processing.

With these constraints, we selected our signal processing algorithms for UMTS/TDD based on the following considerations. Because of the obvious performance advantages, space-time processing had to be preferred against purely spatial algorithms. The relatively low spreading factor of UMTS/TDD limits the performance of the RAKE receiver and its space-time version, and we thus did not use a RAKE-type receiver. But also structures with a beamforming front-end followed by more sophisticated temporal equalisers were not considered, since they rely on an array of calibrated antenna elements. Although the measurement equipment performs signal processing off-line, which allows more complex algorithms to be used, the computational complexity of the ST-MLSE was prohibitive. This is especially due to the fact that we are dealing with a multiuser environment, where we want to detect the signals of several base stations jointly [Ver98]. The use of adaptive algorithms was not necessary, since the off-line characteristic of the measurement device

4

enables block-processing. After removing all the other candidates, the ST-MMSE filter and the ST-DFB equaliser finally remained and were thus chosen for channel estimation and data detection, respectively.

1.3 Outline

In the following chapters, we will adapt these signal processing algorithms to the requirements of the ANTIUM device and develop methods which perform the tasks of synchronisation, channel estimation, and BCH data detection. We first provide an outline of the contents of the individual chapters.

Chapter 2. We start by reviewing the most important goals and constraints of ANTIUM. Subsequently, the simulation parameters and scenarios used in later chapters are described.

Chapter 3. Within the ANTIUM project, we focused on signal processing algorithms for the UMTS/TDD mode. In this chapter, we give a short overview of those structures and parameters of the UMTS/TDD standard which will be relevant for developing our algorithms.

Chapter 4. This chapter addresses synchronisation. The goal is to determine how many base station signals are present and where the corresponding BCHs are located temporally. Synchronisation is based on the synchronisation channels (SCHs) offered by UMTS/TDD and consists of primary and secondary synchronisation. We present three different detection algorithms—all based on the generalised likelihood ratio test— which are able to detect the presence of the primary synchronisation code in the received signal. We then discuss the use of these algorithms for secondary synchronisation, i.e., for determining the actual location of the BCHs and the scrambling code groups used by different base stations.

Chapter 5. The channel estimation stage is discussed next. This stage uses training information transmitted in the midamble of each timeslot. Since only the so-called basic midamble is known from synchronisation and the composition of the actual midamble is unknown, we first present two different methods for midamble estimation. We then consider methods for MMSE channel estimation; in particular, we introduce the novel *successive cancellation MMSE* (SC-MMSE) channel estimation algorithm.

Chapter 6. The last step in reading the BCHs of the different base stations is data detection. We develop a space-time MMSE equaliser which detects the BCH data of all base stations jointly. Since the required correlation matrix cannot be estimated with sufficient accuracy, we propose to calculate the correlation matrix rather than estimating it. This approach leads to two different decision feedback (DFB) equaliser structures.

Chapter 7. After our discussions of the synchronisation, channel estimation, and data detection stages in the last three chapters, we now consider the overall system. We present simulations which show the influence of imperfect synchronisation and channel estimation

results on the performance of the data detection stage.

Chapter 8. Finally, we summarise the most important contributions of this thesis and provide a short discussion of open problems and possible future improvements of our receiver.

Chapter 2

The ANTIUM Project

The work presented in this thesis has been carried out within the ANTIUM project, funded by the European Union in the course of the IST programme of the 5th framework programme. In the following, we will shortly introduce ANTIUM and present its motivation and goals.[1] The second part of the chapter explains the basic assumptions and parameter settings used later on in our simulations.

2.1 Objectives of ANTIUM

One of the approaches under discussion for satisfying the increased demand for interactive and asymmetric services concerns the cooperation of broadcasting and mobile communications systems. Cooperation or even convergence of these systems would allow the use of digital terrestrial broadcast standards such as DAB and DVB-T as a downlink for flexible transmission of multimedia content at higher data rates than those achieved by UMTS alone. In this case, broadcasting networks have to be built in a cellular fashion where frequency reuse enables high data rates on small areas for individual content delivery. This cellular concept for DAB and DVB-T will lead to problems similar to those encountered in mobile telecommunications systems, namely significant co-channel interference. For such scenarios, a measurement equipment is needed that can analyse the interference situation in both UMTS and DVB-T networks.

Especially in situations where radio planning becomes difficult (e.g. high-density urban, or indoor environments) operators will rely on accurate analysis of the current interference situation. In UMTS, a widely used measurement device is the classical trace mobile that is a common mobile terminal equipped with additional measurement software and interfaces. Its capability of online measurements makes this tool very useful for large-scale measurements, but because of its limited signal processing power it may not be able to resolve interference accurately enough in some crucial situations.

The ANTIUM project aims at providing operators with an innovative system for deployment and maintenance of future mobile radio networks. The objective is to build a demonstrator system suited for UMTS and DVB-T networks that is able to accurately detect and identify interferers. This knowledge will help operators to efficiently exploit

---

[1]For more detailed information about ANTIUM, see www.pcrd-antium.com.

their spectrum. The ANTIUM equipment is using multiple antennas and advanced signal processing techniques to resolve interference with high accuracy. However, because of the off-line processing and the relatively long processing time, the ANTIUM equipment will rather be used for spot measurements in problematic areas than for large-scale drive tests.

The way the ANTIUM equipment will be used is depicted in Figure 2.1, where a vehicle carries the device into places where problems have occurred. In the UMTS case, interference is analysed by reading the broadcast channels (BCHs) of as many surrounding base stations as possible.[1] The information carried on the BCHs together with the received power levels allows to classify the interference of surrounding base stations. With this knowledge, the operator is able to remedy the problems by optimising the network.
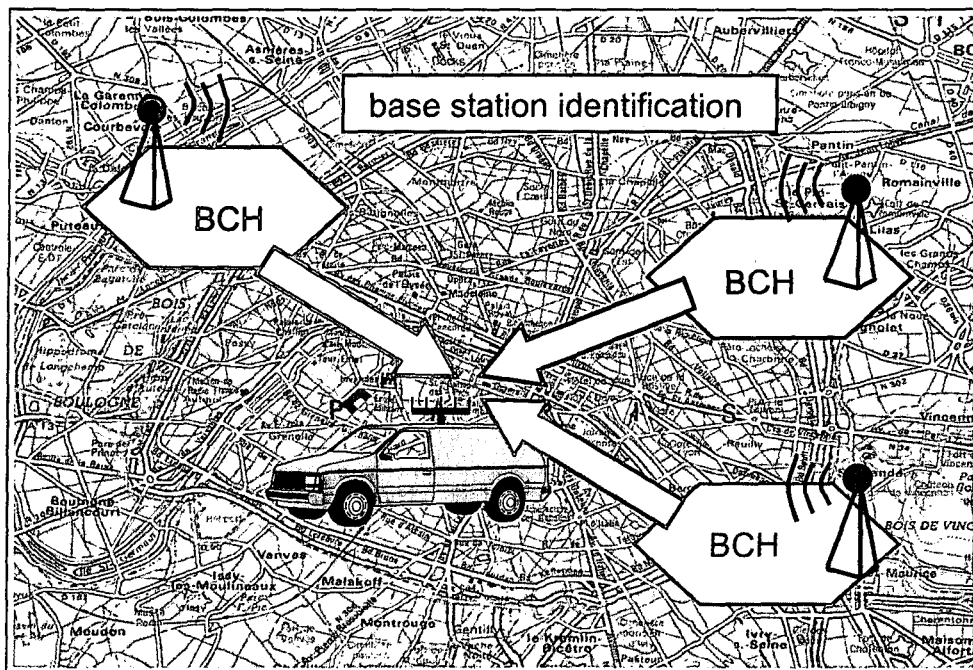
Figure 2.1: *Operational use of the ANTIUM measurement equipment.*

The goal of the ANTIUM project is to study, develop, validate, and test a demonstrator of a measurement device that will be able to perform the tasks of radio network monitoring and identification of co-channel interference for UMTS/FDD, UMTS/TDD, and DVB-T. This goal is achieved trough three main objectives:

1. Define the requirements of an advanced radio monitoring equipment.

2. Develop or adapt signal processing techniques that fulfill these requirements.

3. Develop a demonstrator implementing the selected techniques.

This demonstrator has the structure shown in Figure 2.2. Five antenna elements collect the signals and feed them into a multi-channel receiver. After transferring the signal to

---

[1]In DVB-T, the so-called *transmission parameter signalling* (TPS) is read.

the intermediate frequency of 5 MHz, the data is sampled (2 times oversampling) and stored on the hard disk of a PC. The actual signal processing algorithms that decode the BCH information run off-line on the recorded data sets. The demonstrator is additionally equipped with a GPS unit to record the coordinates of the measurement points.
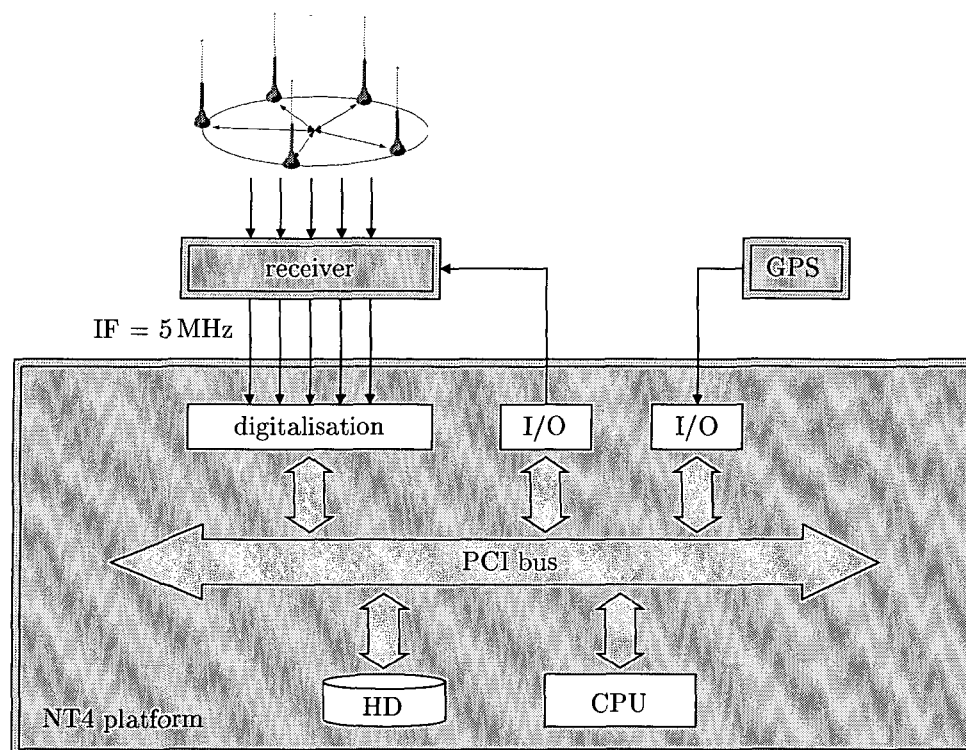
Figure 2.2: *Structure of the ANTIUM demonstrator.*

After the development phase, the demonstrator is to be validated through field tests carried out in UMTS and DVB-T networks. Since before the end of the ANTIUM project there is no UMTS/TDD network available where tests could be conducted, the demonstrator development was only made for UMTS/FDD and DVB-T. However, since the TDD mode is an integral part of UMTS, an algorithmic study has been made in order to prepare signal processing algorithms for a future integration of the UMTS/TDD mode in the demonstrator. This algorithmic study for UMTS/TDD has been carried out at Vienna University of Technology and its results are presented in this thesis. A list of the other participants of the ANTIUM project can be found in Table 2.1.

2.2 Simulation Environment and Parameters

For the algorithmic study of the UMTS/TDD mode we used the simulation environment depicted in Figure 2.3. The signals of K base stations (BS) are transmitted over the channel, where they encounter multi-path propagation and fading. The five antenna elements ($M = 5$) of the ANTIUM equipment collect the signals and feed them, together

9

Table 2.1: *List of participants of the ANTIUM project.*

Participant Name	Country
Thales Communications France	France
Vienna University of Technology	Austria
Télédiffusion de France	France
Bouygues Telecom	France
Telefonica I+D	Spain
University of Marne la Vallée	France
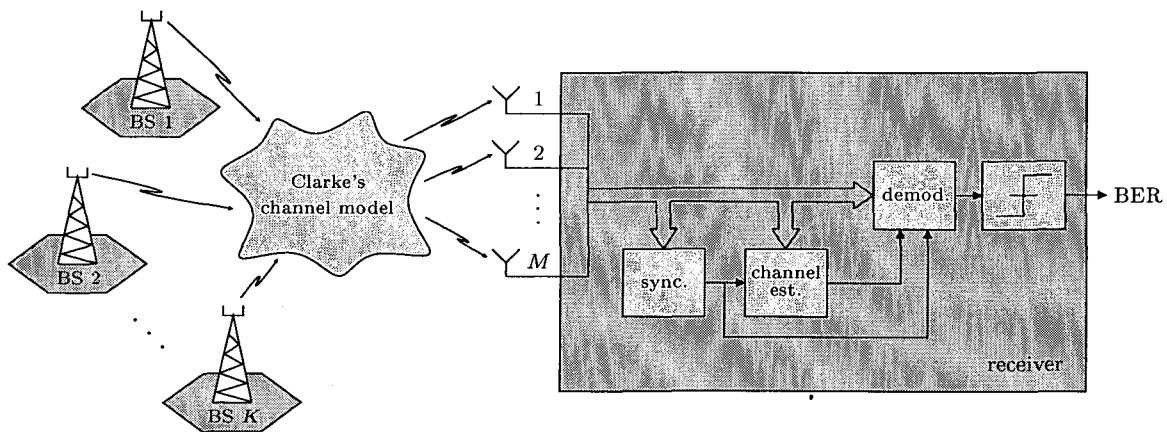
Figure 2.3: *Simulation environment.*

with additive white Gaussian noise, into the receiver. This receiver, consisting of a synchronisation (sync.), channel estimation (channel est.), and data detection/demodulation (demod.) part, is the actual object of the algorithmic study.

The synchronisation block detects the presence of surrounding base stations and calculates the slot timing. By knowing the temporal position of the slot borders, the training data[1] can be localised within the received data sequence. The training data aided channel estimation stage provides the demodulator with estimates of the channel impulse responses. After the influence of the channel has been mitigated by a multichannel equaliser, the BCH signals of different base stations are extracted. Feeding the decoded and deinterleaved data signals into a decision device, the bit error rate (BER) is finally calculated by comparing the received bits with the transmitted bits.

2.2.1   Interference Scenarios

The purpose of the ANTIUM equipment is to analyse interference present in a network. To test the performance of the developed signal processing algorithms, we use various simulation parameter settings to model different interference situations encountered in practice. Since UMTS/TDD is mainly designed for urban areas, we focus on two test

---

[1]In UMTS/TDD, training data is contained in a *midamble* (see Chapter 3).

environments termed "Outdoor to Indoor and Pedestrian" and "Indoor Office" [ETS98], which will be described in the following.

2.2.1.1 Outdoor to Indoor and Pedestrian Test Environment

The outdoor to indoor and pedestrian (short: *pedestrian*) test environment covers microcells in an urban environment. Microcells are characterised by moderate cell radius ($R = 270$ m) and low mobile velocity (walking speed, $v = 5$ km/h). Considering non-line-of-sight (NLOS) situations, the pathloss in dB can be modelled as [ETS98]

$$P_L = 40 \log d + 30 \log f + 49, \tag{2.1}$$

where d is the base station – mobile station distance in kilometres and f is the carrier frequency in MHz.

All base stations use the power levels given in Table 2.2 to transmit the different channels (cf. Chapter 3), and the noise power was set to -99 dBm.

Table 2.2: *Base station transmit powers for the pedestrian environment.*

Channel	Power
SCH	21 dBm
P-CCPCH	21 dBm
DCH	20 dBm
Maximum BS power	33 dBm

To test our algorithms in different interference situations that can occur in a network, we used the following three scenarios (Figure 2.4):

Scenario 1. The mobile is inside the middle cell whose signal is the strongest one.

Scenario 2. The mobile is at the boundary of two cells. The signals of the base stations of these two cells are received with the same average power.

Scenario 3. The mobile is at the boundary of three cells. The signals of the base stations of these three cells are received with the same average power.
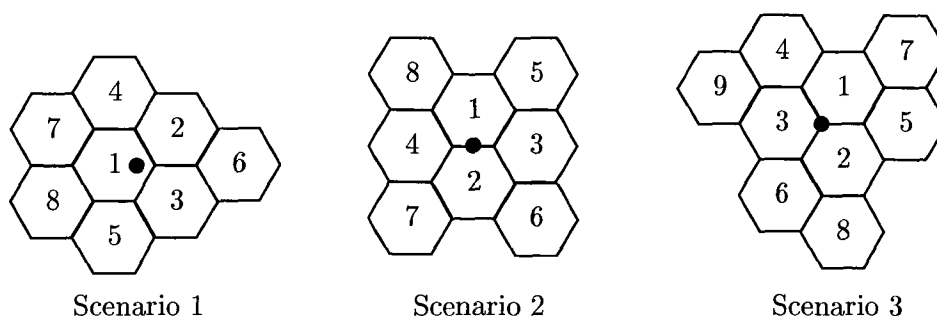

Scenario 1   Scenario 2   Scenario 3

Figure 2.4: *Simulation scenarios for the pedestrian environment. The bullet • indicates the receiver position.*

While there is only one dominant signal present in scenario 1, the mobile receives two and even three equally strong[1] signals in scenario 2 and scenario 3, respectively. For the interference cancellation algorithms used in the ANTIUM receiver, scenario 3 will hence be the most challenging one.

With the cell configurations of the three scenarios (Figure 2.4), and using the pathloss of (2.1) and the transmit powers of Table 2.2, we obtain the power levels and the relative powers received at the mobile station as listed in Table 2.3.

Table 2.3: *Received power levels (for maximum transmit powers) and relative powers received from different base stations in the pedestrian environment.*

Scenario 1					Scenario 2			
BS	Distance	Received Power	Relative Power		BS	Distance	Received Power	Relative Power
1	$2R/3$	$-85\,\mathrm{dBm}$	$-1\,\mathrm{dB}$		1	$\sqrt{3}R/2$	$-89\,\mathrm{dBm}$	$-3.6\,\mathrm{dB}$
2	$\sqrt{13}R/3$	$-95\,\mathrm{dBm}$	$-11\,\mathrm{dB}$		2	$\sqrt{3}R/2$	$-89\,\mathrm{dBm}$	$-3.6\,\mathrm{dB}$
3	$\sqrt{13}R/3$	$-95\,\mathrm{dBm}$	$-11\,\mathrm{dB}$		3	$3R/2$	$-99\,\mathrm{dBm}$	$-13.6\,\mathrm{dB}$
4	$\sqrt{31}R/3$	$-102\,\mathrm{dBm}$	$-18\,\mathrm{dB}$		4	$3R/2$	$-99\,\mathrm{dBm}$	$-13.6\,\mathrm{dB}$
5	$\sqrt{31}R/3$	$-102\,\mathrm{dBm}$	$-18\,\mathrm{dB}$		5	$\sqrt{21}R/2$	$-106\,\mathrm{dBm}$	$-20.6\,\mathrm{dB}$
6	$7R/3$	$-106\,\mathrm{dBm}$	$-22\,\mathrm{dB}$		6	$\sqrt{21}R/2$	$-106\,\mathrm{dBm}$	$-20.6\,\mathrm{dB}$
7	$7R/3$	$-106\,\mathrm{dBm}$	$-22\,\mathrm{dB}$		7	$\sqrt{21}R/2$	$-106\,\mathrm{dBm}$	$-20.6\,\mathrm{dB}$
8	$7R/3$	$-106\,\mathrm{dBm}$	$-22\,\mathrm{dB}$		8	$\sqrt{21}R/2$	$-106\,\mathrm{dBm}$	$-20.6\,\mathrm{dB}$

Scenario 3			
BS	Distance	Received Power	Relative Power
1	R	$-92\,\mathrm{dBm}$	$-5.1\,\mathrm{dB}$
2	R	$-92\,\mathrm{dBm}$	$-5.1\,\mathrm{dB}$
3	R	$-92\,\mathrm{dBm}$	$-5.1\,\mathrm{dB}$
4	$2R$	$-104\,\mathrm{dBm}$	$-17.1\,\mathrm{dB}$
5	$2R$	$-104\,\mathrm{dBm}$	$-17.1\,\mathrm{dB}$
6	$2R$	$-104\,\mathrm{dBm}$	$-17.1\,\mathrm{dB}$
7	$\sqrt{7}R$	$-109\,\mathrm{dBm}$	$-22.1\,\mathrm{dB}$
8	$\sqrt{7}R$	$-109\,\mathrm{dBm}$	$-22.1\,\mathrm{dB}$
9	$\sqrt{7}R$	$-109\,\mathrm{dBm}$	$-22.1\,\mathrm{dB}$

2.2.1.2 Indoor Office Test Environment

The indoor office (short: *indoor*) test environment is used to model picocells inside buildings. The cells have a very small radius ($R = 30\,\mathrm{m}$) and the mobile moves with walking speed ($v = 5\,\mathrm{km/h}$). The three-dimensional nature of indoor propagation is taken into account by including base stations on different floors. The distance between two adjacent

---

[1]On average.

floors is assumed to be $h = 3\,\mathrm{m}$. Considering NLOS situations, the pathloss in dB is modeled as [ETS98]

$$P_L = 37 + 30 \log d + 18.3\, n^{\frac{n+2}{n+1}-0.46}, \tag{2.2}$$

where d is the base station – mobile station distance in metres and n is the number of floors in the path.

The power levels given in Table 2.4 are used by the base stations to transmit the different channels (cf. Chapter 3), the noise power was again set to $-99\,\mathrm{dBm}$.

Table 2.4: *Base station transmit powers for the indoor environment.*

Channel	Power
SCH	14 dBm
P-CCPCH	14 dBm
DCH	13 dBm
Maximum BS power	26 dBm

As in the pedestrian environment, we used three different, increasingly challenging scenarios (Figure 2.5):

Scenario 1. This scenario is analogous to scenario 1 of the pedestrian test environment. The mobile is located inside the middle cell, from where the most powerful signal is received. There are no base stations on other floors.

Scenario 2. The mobile is at the boundary of two cells on the same floor. Two additional base stations, which are located exactly one floor below and above the mobile, are the strongest ones, while the base stations on the same floor are weaker.

Scenario 3. The mobile is inside the middle cell. Two additional base stations are considered which are located exactly one floor above and below the border point of three cells. The position of the mobile in the cell is chosen in such a way that the base stations 1–3 have the same average receive power.
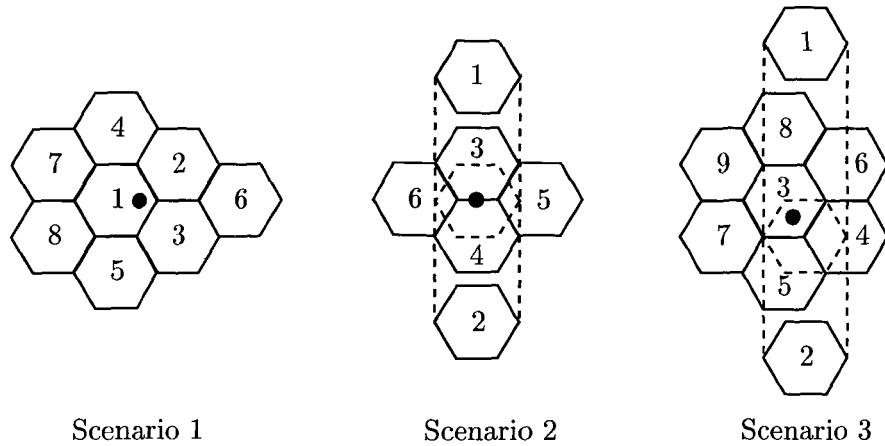

Scenario 1   Scenario 2   Scenario 3

Figure 2.5: *Simulation scenarios for the indoor environment. The bullet • indicates the receiver position.*

With the cell configurations of the three scenarios (Figure 2.5), and using the pathloss of (2.2) and the transmit powers of Table 2.4, we obtain the power levels and the relative powers received at the mobile station as listed in Table 2.5.

Table 2.5: *Received power levels (for maximum transmit powers) and relative powers received from different base stations in the indoor environment.*

Scenario 1					Scenario 2			
BS	Distance	Received Power	Relative Power		BS	Distance	Received Power	Relative Power
1	$2R/3$	$-50\,$dBm	$-1.7\,$dB		1	h	$-44\,$dBm	$-3.6\,$dB
2	$\sqrt{13}R/3$	$-58\,$dBm	$-9.7\,$dB		2	h	$-44\,$dBm	$-3.6\,$dB
3	$\sqrt{13}R/3$	$-58\,$dBm	$-9.7\,$dB		3	$\sqrt{3}R/2$	$-53\,$dBm	$-12.6\,$dB
4	$\sqrt{31}R/3$	$-63\,$dBm	$-14.7\,$dB		4	$\sqrt{3}R/2$	$-53\,$dBm	$-12.6\,$dB
5	$\sqrt{31}R/3$	$-63\,$dBm	$-14.7\,$dB		5	$3R/2$	$-61\,$dBm	$-20.6\,$dB
6	$7R/3$	$-66\,$dBm	$-17.7\,$dB		6	$3R/2$	$-61\,$dBm	$-20.6\,$dB
7	$7R/3$	$-66\,$dBm	$-17.7\,$dB					
8	$7R/3$	$-66\,$dBm	$-17.7\,$dB					

Scenario 3			
BS	Distance	Received Power	Relative Power
1	6.07 m	$-53\,$dBm	$-6.1\,$dB
2	6.07 m	$-53\,$dBm	$-6.1\,$dB
3	24.72 m	$-53\,$dBm	$-6.1\,$dB
4	32.96 m	$-57\,$dBm	$-10.1\,$dB
5	32.96 m	$-57\,$dBm	$-10.1\,$dB
6	57.54 m	$-64\,$dBm	$-17.1\,$dB
7	57.54 m	$-64\,$dBm	$-17.1\,$dB
8	74.41 m	$-67\,$dBm	$-20.1\,$dB
9	74.41 m	$-67\,$dBm	$-20.1\,$dB

2.2.2 Clarke's Channel Model

For our simulations, we used Clarke's channel model [Cla68] according to which the $M \times 1$ channel weight vector associated to the kth base station and the pth propagation path $(p = 0, \ldots, L-1)$ is given as

$$\mathbf{h}_{k,p}(n) = \alpha_{k,p} \sum_{q=1}^{N_{k,p}} c_{k,p}^{(q)} \exp\left\{ j\left[-2\pi n \frac{v}{\lambda}\cos(\theta_{k,p}^{(q)} - \gamma) + \varphi_{k,p}^{(q)} \right] \right\} \mathbf{s}_{k,p}^{(q)}. \qquad (2.3)$$

Here, M is the number of antenna elements, $\alpha_{k,p}$ is the amplitude of the pth path, $N_{k,p}$ is the number of subpaths associated to the pth propagation path, and $c_{k,p}^{(q)}$, $\theta_{k,p}^{(q)}$, $\varphi_{k,p}^{(q)}$, and $\mathbf{s}_{k,p}^{(q)}$ are respectively the attenuation, azimuth, phase, and steering vector of the qth

14

subpath of the pth path. The speed of the mobile is denoted as v, while γ is the azimuth angle of the mobile's motion, and λ is the wavelength.

This model is very flexible, and various environments can be modelled with proper parameter selection. For the actual simulations we slightly simplified the model (2.3) according to

$$\mathbf{h}_{k,p}(n_s) = \alpha_{k,p} \sum_{q=1}^{N_{k,p}} b_{k,p}^{(q)}(n_s)\, \mathbf{s}_{k,p}^{(q)}, \tag{2.4}$$

where the $b_{k,p}^{(q)}(n_s)$ are independently Rayleigh distributed for every p, q, and k. Regarding the time dependence, we assumed the channel taps $\mathbf{h}_{k,p}(n_s)$ to be constant during the duration $T_s = 666.67\,\mu s$ of one timeslot[1] and highlighted that by replacing the chip index n by the slot index n_s. However, to incorporate some channel variation, the Rayleigh coefficients $b_{k,p}^{(q)}(n_s)$ of *different* slots have a Jakes Doppler spectrum [Jak74].

For the tap powers $\alpha_{k,p}$, we used two different channel parameter settings called A and B for each environment [ETS98]. For the pedestrian environment, channel A has 3 paths with a maximum delay of only 2 chips, and channel B has 8 paths with a maximum delay of 15 chips. For the indoor environment, channel A has 3 taps with a maximum delay of 2 chips, whereas channel B has 4 taps with a maximum delay of 3 chips. The actual delay values and corresponding powers are given in Tables 2.6–2.7. Note that all paths $p = 0, \ldots, L - 1$ that are not listed in the table are equal to zero.

Table 2.6: *Tapped-delay line parameters for the pedestrian environment.*

Path	Channel A		Channel B	
	Rel. Delay (chips)	Avg. Power (dB)	Rel. Delay (chips)	Avg. Power (dB)
1	0	0	0	0
2	1	−12.5	1	−2.5
3	2	−25.0	3	−7.2
4	–	–	4	−10.8
5	–	–	5	−9.0
6	–	–	9	−10.2
7	–	–	10	−12.5
8	–	–	15	−24.5

Table 2.7: *Tapped-delay line parameters for the indoor environment.*

Path	Channel A		Channel B	
	Rel. Delay (chips)	Avg. Power (dB)	Rel. Delay (chips)	Avg. Power (dB)
1	0	0	0	0
2	1	−10	1	−5.0
3	2	−33	2	−15.1
4	–	–	3	−26.0

---

[1]With a velocity of $v = 5\,\text{km/h}$, the mobile moves only $0.006\,\lambda$ during one timeslot.

Chapter 3

Overview of the UMTS/TDD-Standard

To be able to develop signal processing algorithms for detecting and decoding the broadcast channels (BCHs) of surrounding base stations, we have to be familiar with the structure of the received signals. In this chapter, we will thus review some physical layer parameters of UMTS/TDD that are important in the context of ANTIUM.

Since the ANTIUM equipment is a network monitoring device without an active connection to the monitored network, the only available data are the *downlink signals* of the different base stations. The main focus of the following description will hence lie on the *parameters needed to locate the BCH* in the received signal, and on the structure of the BCH itself. However, more details about UMTS/TDD can be found in the specifications [3GP01a, 3GP01b, 3GP01c], and on www.3gpp.org.

3.1   Physical Channels

The 3.84 Mchip/s option of the UMTS/TDD mode uses the frame structure depicted in Figure 3.1. One *radio frame* has the duration of 10 ms and consists of 15 *timeslots*, where each timeslot contains 2560 *chips* of length 0.26 μs each.
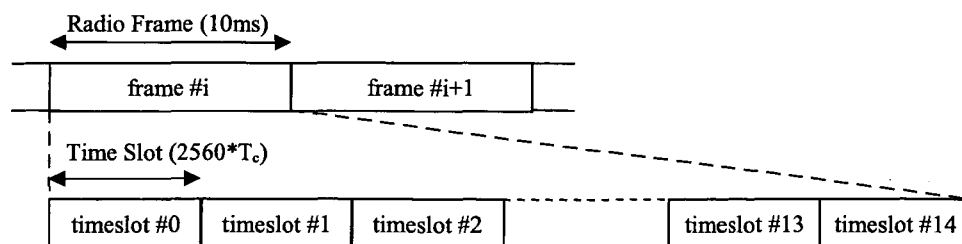

Figure 3.1: *Physical channel signal format* [3GP01a].

Each timeslot can be individually allocated for uplink or downlink in a flexible manner to be able to cope with asymmetric uplink/downlink traffic (Figure 3.2). The content of a timeslot is called a *burst*. Two different burst types are defined for downlink transmission.

17
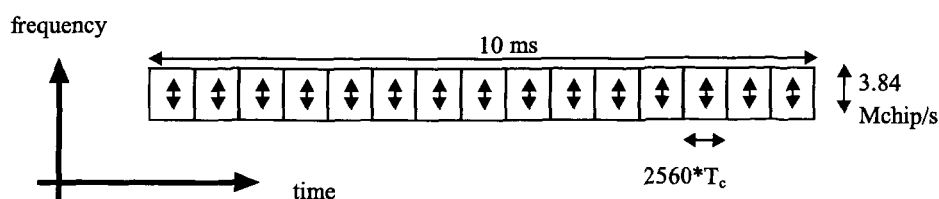
Figure 3.2: *Each timeslot can be individually allocated for uplink (↑) or downlink (↓) in a flexible manner* [3GP01a].

Data symbols 976 chips	Midamble 512 chips	Data symbols 976 chips	GP 96 CP

$$2560 * T_c$$
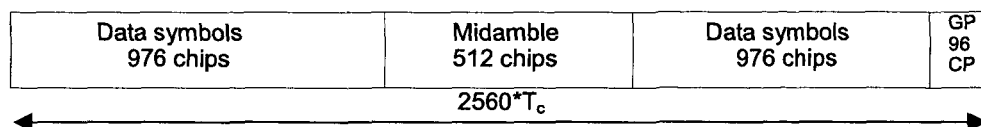
Figure 3.3: *Burst structure of burst type 1. GP denotes the guard period and CP the chip period* [3GP01a].

Burst type 1 contains two *data fields* of length 976 chips, a *midamble* of length 512 chips in the middle, and a *guard period* of 96 chips at the end of the timeslot (Figure 3.3). Burst type 2 has a shorter midamble (256 chips) and longer data fields (1104 chips each).

In UMTS, services offered to higher layers by the physical layer are called *transport channels*. Most important for ANTIUM is the BCH, a downlink transport channel that is used to broadcast system- and cell-specific information. Transport channels are carried by so-called *physical channels* which are defined by frequency, timeslot, spreading code, and burst type. Downlink physical channels in UMTS/TDD either use spreading factor $Q = 16$, or the whole burst is occupied by a single, unspread physical channel ($Q = 1$).

Concerning the BCH, one higher layer transport block that consists of 246 bits is mapped onto the *primary common control physical channel* (P-CCPCH) as shown in Figure 3.4. The P-CCPCH uses burst type 1 and is transmitted in only a single timeslot per frame, whose position is indicated by the *synchronisation channel* (SCH). Since the transmission time interval (TTI), which is equal to the interleaving period, is 20 ms, every BCH transport block is mapped onto two succeeding radio frames. Note also that no transmit power control (TPC) information and no transport format combination indicator (TFCI) is used for the BCH. Table 3.1 summarises the most important parameters.

Table 3.1: *Parameters of the BCH* [3GP01d].

Transport block size	246 bit
CRC	16 bit
Coding	convolutional coding, $R = 1/2$
TTI	20 ms
Midamble	512 chips
Codes and timeslots	$Q = 16 \times 1 \times 1$ timeslot
Modulation format	QPSK
TFCI	0 bit
TPC	0 bit

Figure 3.4: *Channel coding for the BCH* [3GP01d].

Like all downlink physical channels, the P-CCPCH is QPSK-modulated and spread with a so-called *orthogonal variable spreading factor* (OVSF) code of length 16 ($Q = 16$). Figure 3.5 shows the arrangement of these codes in a code tree.

Figure 3.5: *Code tree for generation of OVSF codes* [3GP01c].

19

Each stage in the code tree corresponds to a spreading factor, indicated by the value of Q in the figure. Starting from the root code wor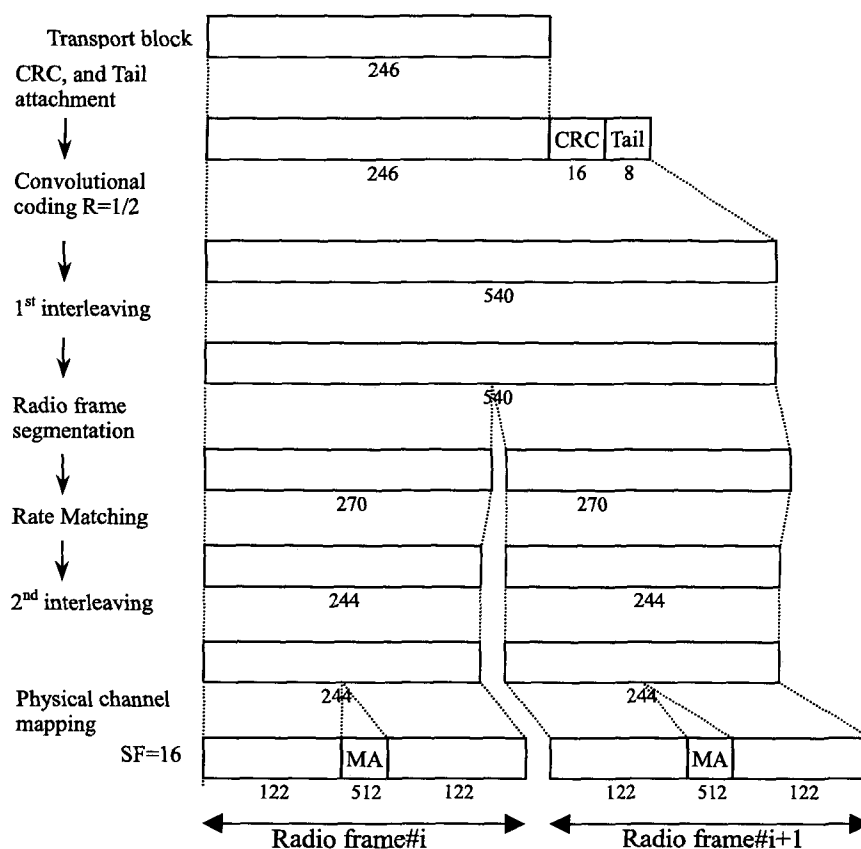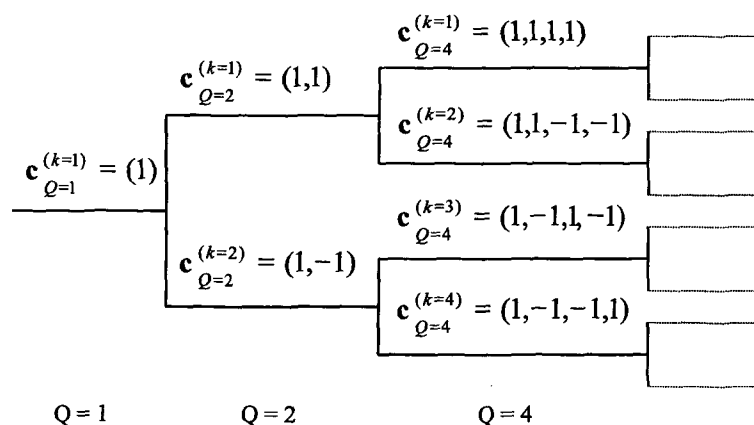d $c_{Q=1}^{(k=1)} = (1)$ in the first stage, the code tree is constructed by appending inverted and non-inverted replicas of the current code word and placing them in the lower and upper branch of the succeeding stage, respectively. For the second stage we obtain

$$c_{Q=2}^{(k=1)} = (c_{Q=1}^{(k=1)}, c_{Q=1}^{(k=1)}) \quad , \quad c_{Q=2}^{(k=2)} = (c_{Q=1}^{(k=1)}, -c_{Q=1}^{(k=1)}),$$

and the next stages are constructed in the same way. The most important property of the OVSF code tree is that a specific code word is orthogonal to every other code word that is neither lying on the path connecting the specific code word with the root of the tree nor in the sub-tree below the specific code word.[1] In particular, all code words of the same stage are orthogonal and since all downlink channels use $Q = 16$, there is a maximum of 16 parallel downlink channels with orthogonal codes. The P-CCPCH always uses $c_{Q=16}^{(k=1)}$; the number of other, parallel data channels in a P-CCPCH timeslot is restricted to 12 [3GP01a], with the remaining three codes left unused.

To be able to separate the data channels of different base stations,[2] the data is multiplied by a base-station-specific scrambling code of length 16 chips [3GP01c] after spreading. In total there are 128 different scrambling codes, partitioned into 32 so-called *code groups* of four codes each. Adjacent base stations should be assigned different code groups in order to limit interference. The scrambling operation does not change the bandwidth of the signal, because it is performed on the chip level. Moreover, since the spreading factor of the P-CCPCH equals the scrambling code length, we can treat the product of spreading code and scrambling code as a single effective spreading code in the detection process of the BCH.

Besides the scrambling code, the code group of a cell also determines which one of the 128 basic midamble codes of length 456 chips (for burst type 1) is used.[3] Repeating this basic midamble code twice to get a sequence of 912 chips, we can extract the eight final midambles $m^{(l)}$, $l = 1, \ldots, 8$ from this sequence as portions of 512 chips defined by eight different starting-points. This midamble construction scheme has the advantage that in the uplink, a single cyclic correlation with the basic midamble code is sufficient for channel estimation for all data channels present. For downlink transmission, this advantage is lost but the same midambles are nevertheless used in order to keep a similarity with the uplink. The final midambles are assigned to the different physical channels of one slot in a fixed way: The P-CCPCH always uses $m^{(1)}$, while $m^{(2)}$ is only used in case of block space-time transmit diversity (block STTD). Midambles $m^{(3)}$–$m^{(8)}$ are used by data channels.

To assure a constant power level over the whole slot, the transmit amplitudes of the midambles are adjusted to the amplitudes of the corresponding data channels $a^{(l)}$. Figure 3.6 shows the composition of a BCH timeslot. The P-CCPCH and its midamble $m^{(1)}$ are

---

[1] E.g., $c_{Q=2}^{(k=1)}$ is orthogonal to $c_{Q=4}^{(k=3)}$, but not to $c_{Q=1}^{(k=1)}$ and $c_{Q=4}^{(k=2)}$.

[2] The same set of 16 spreading codes is used by each base station. The codes are assigned to the different data channels irrespective of the code allocation in adjacent cells.

[3] As for the scrambling code, the code group determines only which set of four midambles is used.

1 Frame = 10ms

P-CCPCH	$m^{(1)}$	P-CCPCH		a_{ref}
+				
data channel	$m^{(3)}$	data channel		$a^{(3)}$
+				
data channel	$m^{(4)}$	data channel		$a^{(4)}$
+				
data channel	$m^{(5)}$	data channel		$a^{(5)}$
+				

1 Timeslot = 2560 chips
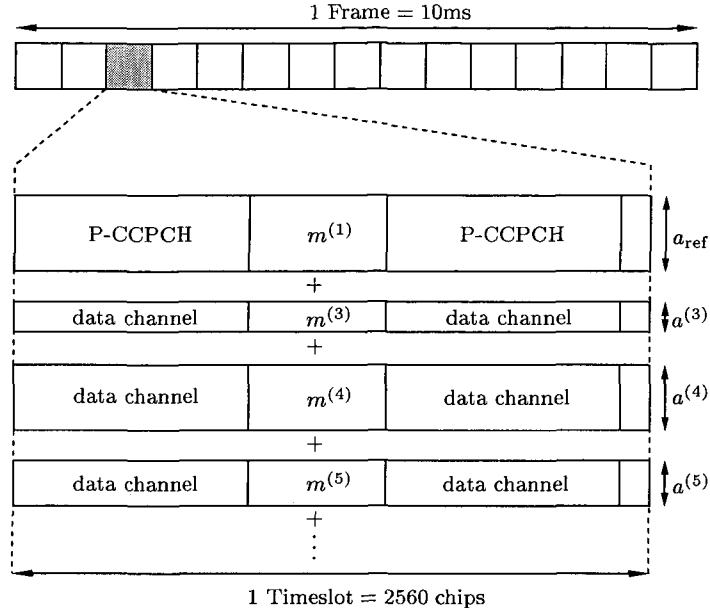
Figure 3.6: *Structure of a BCH timeslot.*

transmitted with reference amplitude a_{ref}, while the data channels and their respective midambles are using different amplitudes because of power control.

The total timeslot consisting of the data fields, midambles,[1] and guard periods of different physical channels is finally filtered by a root-raised-cosine pulse-shaping filter with frequency roll-off factor $\alpha = 0.22$ prior to transmission.

3.2 The Synchronisation Channel

As mentioned earlier, the synchronisation channel (SCH) indicates the timeslot where the P-CCPCH is transmitted. But also some other important parameters are carried by the SCH as we will explain in the following.

The SCH is a downlink channel. In order not to limit the uplink/downlink asymmetry, it is mapped on only one or two downlink slots per frame. There are two different cases of SCH and P-CCPCH allocation:

- Case 1: SCH and P-CCPCH allocated to timeslot k, $k = 0, \ldots, 14$

- Case 2: SCH allocated to two timeslots: k and $k + 8$, $k = 0, \ldots, 6$; P-CCPCH allocated to timeslot k.

The number of the P-CCPCH timeslot within the frame (value of k) is not known a priori and cannot be derived from the SCH alone. But the SCH allows to locate the P-CCPCH in the received data sequence, and the BCH can be detected and decoded without knowing

---

[1]Note that the midambles are not scrambled.

k. Since the value of k is transmitted on the BCH, the frame borders can be identified after BCH detection.

As shown in Figure 3.7, the SCH has a length of 256 chips and consists of a primary synchronisation code c_p and three secondary synchronisation codes $c_{s,j}$, $j = 1, 2, 3$ multiplied by QPSK symbols b_j. The primary synchronisation code c_p is the same in all UMTS/TDD networks and enables the mobile to detect the presence of surrounding base stations. For this purpose, c_p is constructed as a so-called hierarchical Golay sequence with good aperiodic autocorrelation properties [3GP01c].
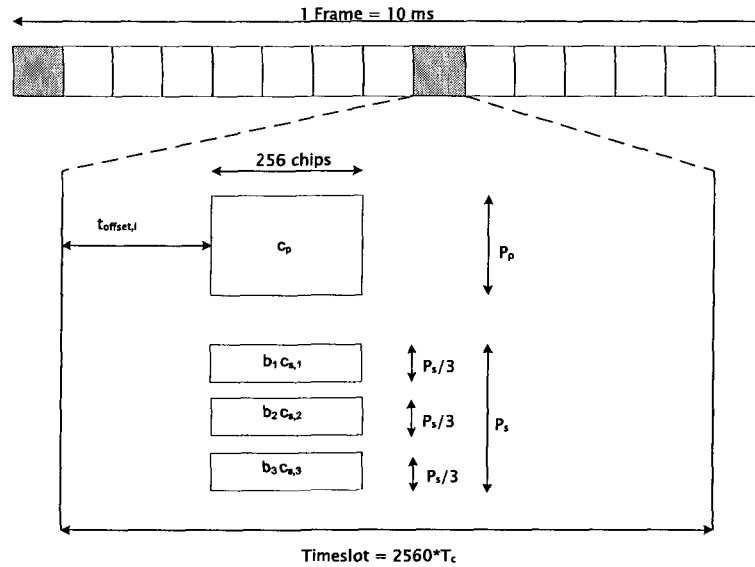
Figure 3.7: *Structure of the synchronisation channel* (SCH) [3GP01a].

The secondary codes $c_{s,j}$ of Figure 3.7 are constructed as follows. The 12 different codes c_n, $n = 0, 1, 3, 4, 5, 6, 8, 10, 12, 13, 14, 15$ of [3GP01c] are partitioned into four *secondary synchronisation code sets* with three codes each (Table 3.2). Depending on the current

Table 3.2: *Allocation of synchronisation codes to code sets* [3GP01c].

	Case 1	Case 2
Code set 1:	c_1, c_3, c_5	c_1, c_3, c_5
Code set 2:	c_{10}, c_{13}, c_{14}	c_{10}, c_{13}, c_{14}
Code set 3:	not used	c_0, c_6, c_{12}
Code set 4:	not used	c_4, c_8, c_{15}

synchronisation code allocation, one of the four code sets is used for the three secondary synchronisation codes $c_{s,j}$.

Since frame borders in UMTS/TDD are temporally aligned within the whole network, distinct time offsets $t_{\text{offset},i}$ of the SCH from the slot border are used to prevent the SCHs of different base stations from interfering. The actual value of $t_{\text{offset},i}$ is depending on the

code group i of the cell and is given as [3GP01a]

$$t_{\text{offset},i} = \begin{cases} 48iT_c & i < 16 \\ (720 + 48i)T_c & i \geq 16 \end{cases} \quad i = 0, \ldots, 31. \tag{3.1}$$

Note that the gap between $t_{\text{offset},15}$ and $t_{\text{offset},16}$ ensures that the SCH never overlaps the midamble in order not to impair channel estimation performance. Also the guard period is kept clear of the SCH for every value of i.

As mentioned above, each cell is assigned a certain code group that specifies a set of four scrambling codes, a set of four basic midambles, and the time offset of the SCH. Which one of the four codes is actually used depends on the cell parameter of the base station as shown in Table 3.3. This cell parameter is toggled from frame to frame depending on whether the system frame number (SFN) is even or odd (Table 3.4). This implies that the scrambling code and basic midamble are toggled from frame to frame, but since the code group does not change, the time offset of the SCH stays constant.

Table 3.3: *Mapping scheme for cell parameters, code groups, scrambling codes, midambles, and time offsets* [3GP01c].

| Cell Parameter | Code Group | Associated Codes | | t_{offset} |
		Scrambling Code	Midamble Code	
0	Group 0	Code 0	m_0	t_0
1		Code 1	m_1	
2		Code 2	m_2	
3		Code 3	m_3	
4	Group 1	Code 4	m_4	t_1
5		Code 5	m_5	
6		Code 6	m_6	
7		Code 7	m_7	
$\vdots$				
124	Group 31	Code 124	m_{124}	t_{31}
125		Code 125	m_{125}	
126		Code 126	m_{126}	
127		Code 127	m_{127}	

3.3 Synchronisation Procedure

The synchronisation parameters needed to read the BCH are the exact starting time of the first interleaved block of the BCH, and the scrambling code and basic midamble used by the base station. All this information is carried on the SCH as shown in Table 3.5 and Table 3.6 for the two synchronisation cases, respectively.[1]

Here, the QPSK symbols b_j and the used synchronisation code sets define the code group i of the cell, the value of $t_{\text{offset},i}$, the frame index (first or second frame in interleaving

---

[1]The last columns in Tables 3.5 and 3.6 contain the values of $t_{\text{offset},i}$ given in (3.1).

Table 3.4: *Alignment of cell parameter toggling and system frame number* (SFN) [3GP01c].

Initial Cell Parameter Assignment	Code Group	Cell Parameter used when SFN is even	Cell Parameter used when SFN is odd
0	Group 0	0	1
1	Group 0	1	0
2	Group 0	2	3
3	Group 0	3	2
4	Group 1	4	5
5	Group 1	5	4
6	Group 1	6	7
7	Group 1	7	6
$\vdots$			
124	Group 31	124	125
125	Group 31	125	124
126	Group 31	126	127
127	Group 31	127	126

Table 3.5: *Code allocation for synchronisation case 1* [3GP01c].

Code Group	Code Set	Frame 1			Frame 2			t_{offset}
0	1	c_1	c_3	c_5	c_1	c_3	$-c_5$	t_0
1	1	c_1	$-c_3$	c_5	c_1	$-c_3$	$-c_5$	t_1
2	1	$-c_1$	c_3	c_5	$-c_1$	c_3	$-c_5$	t_2
3	1	$-c_1$	$-c_3$	c_5	$-c_1$	$-c_3$	$-c_5$	t_3
4	1	jc_1	jc_3	c_5	jc_1	jc_3	$-c_5$	t_4
5	1	jc_1	$-jc_3$	c_5	jc_1	$-jc_3$	$-c_5$	t_5
6	1	$-jc_1$	jc_3	c_5	$-jc_1$	jc_3	$-c_5$	t_6
7	1	$-jc_1$	$-jc_3$	c_5	$-jc_1$	$-jc_3$	$-c_5$	t_7
8	1	jc_1	jc_5	c_3	jc_1	jc_5	$-c_3$	t_8
9	1	jc_1	$-jc_5$	c_3	jc_1	$-jc_5$	$-c_3$	t_9
10	1	$-jc_1$	jc_5	c_3	$-jc_1$	jc_5	$-c_3$	t_{10}
11	1	$-jc_1$	$-jc_5$	c_3	$-jc_1$	$-jc_5$	$-c_3$	t_{11}
12	1	jc_3	jc_5	c_1	jc_3	jc_5	$-c_1$	t_{12}
13	1	jc_3	$-jc_5$	c_1	jc_3	$-jc_5$	$-c_1$	t_{13}
14	1	$-jc_3$	jc_5	c_1	$-jc_3$	jc_5	$-c_1$	t_{14}
15	1	$-jc_3$	$-jc_5$	c_1	$-jc_3$	$-jc_5$	$-c_1$	t_{15}
16	2	c_{10}	c_{13}	c_{14}	c_{10}	c_{13}	$-c_{14}$	t_{16}
17	2	c_{10}	$-c_{13}$	c_{14}	c_{10}	$-c_{13}$	$-c_{14}$	t_{17}
...	...	...	...	...	...	...	...	...
20	2	jc_{10}	jc_{13}	c_{14}	jc_{10}	jc_{13}	$-c_{14}$	t_{20}
...	...	...	...	...	...	...	...	...
24	2	jc_{10}	jc_{14}	c_{13}	jc_{10}	jc_{14}	$-c_{13}$	t_{24}
...	...	...	...	...	...	...	...	...
31	2	$-jc_{13}$	$-jc_{14}$	c_{10}	$-jc_{13}$	$-jc_{14}$	$-c_{10}$	t_{31}

24

Table 3.6: *Code allocation for synchronisation case 2. CG stands for "code group" and CS for "code set"* [3GP01c].

CG	CS	Frame 1						Frame 2						t_{offset}
		Slot k			Slot $k+8$			Slot k			Slot $k+8$			
0	1	c_1	c_3	c_5	c_1	c_3	$-c_5$	$-c_1$	$-c_3$	c_5	$-c_1$	$-c_3$	$-c_5$	t_0
1	1	c_1	$-c_3$	c_5	c_1	$-c_3$	$-c_5$	$-c_1$	c_3	c_5	$-c_1$	c_3	$-c_5$	t_1
2	1	jc_1	jc_3	c_5	jc_1	jc_3	$-c_5$	$-jc_1$	$-jc_3$	c_5	$-jc_1$	$-jc_3$	$-c_5$	t_2
3	1	jc_1	$-jc_3$	c_5	jc_1	$-jc_3$	$-c_5$	$-jc_1$	jc_3	c_5	$-jc_1$	jc_3	$-c_5$	t_3
4	1	jc_1	jc_5	c_3	jc_1	jc_5	$-c_3$	$-jc_1$	$-jc_5$	c_3	$-jc_1$	$-jc_5$	$-c_3$	t_4
5	1	jc_1	$-jc_5$	c_3	jc_1	$-jc_5$	$-c_3$	$-jc_1$	jc_5	c_3	$-jc_1$	jc_5	$-c_3$	t_5
6	1	jc_3	jc_5	c_1	jc_3	jc_5	$-c_1$	$-jc_3$	$-jc_5$	c_1	$-jc_3$	$-jc_5$	$-c_1$	t_6
7	1	jc_3	$-jc_5$	c_1	jc_3	$-jc_5$	$-c_1$	$-jc_3$	jc_5	c_1	$-jc_3$	jc_5	$-c_1$	t_7
8	2	c_{10}	c_{13}	c_{14}	c_{10}	c_{13}	$-c_{14}$	$-c_{10}$	$-c_{13}$	c_{14}	$-c_{10}$	$-c_{13}$	$-c_{14}$	t_8
9	2	c_{10}	$-c_{13}$	c_{14}	c_{10}	$-c_{13}$	$-c_{14}$	$-c_{10}$	c_{13}	c_{14}	$-c_{10}$	c_{13}	$-c_{14}$	t_9
10	2	jc_{10}	jc_{13}	c_{14}	jc_{10}	jc_{13}	$-c_{14}$	$-jc_{10}$	$-jc_{13}$	c_{14}	$-jc_{10}$	$-jc_{13}$	$-c_{14}$	t_{10}
11	2	jc_{10}	$-jc_{13}$	c_{14}	jc_{10}	$-jc_{13}$	$-c_{14}$	$-jc_{10}$	jc_{13}	c_{14}	$-jc_{10}$	jc_{13}	$-c_{14}$	t_{11}
12	2	jc_{10}	jc_{14}	c_{13}	jc_{10}	jc_{14}	$-c_{13}$	$-jc_{10}$	$-jc_{14}$	c_{13}	$-jc_{10}$	$-jc_{14}$	$-c_{13}$	t_{12}
13	2	jc_{10}	$-jc_{14}$	c_{13}	jc_{10}	$-jc_{14}$	$-c_{13}$	$-jc_{10}$	jc_{14}	c_{13}	$-jc_{10}$	jc_{14}	$-c_{13}$	t_{13}
14	2	jc_{13}	jc_{14}	c_{10}	jc_{13}	jc_{14}	$-c_{10}$	$-jc_{13}$	$-jc_{14}$	c_{10}	$-jc_{13}$	$-jc_{14}$	$-c_{10}$	t_{14}
15	2	jc_{13}	$-jc_{14}$	c_{10}	jc_{13}	$-jc_{14}$	$-c_{10}$	$-jc_{13}$	jc_{14}	c_{10}	$-jc_{13}$	jc_{14}	$-c_{10}$	t_{15}
16	3	c_0	c_6	c_{12}	c_0	c_6	$-c_{12}$	$-c_0$	$-c_6$	c_{12}	$-c_0$	$-c_6$	$-c_{12}$	t_{16}
...	...	...	...	...	...	...	...	...	...	...	...	...	...	...
23	3	jc_6	$-jc_{12}$	c_0	jc_6	$-jc_{12}$	$-c_0$	$-jc_6$	jc_{12}	c_0	$-jc_6$	jc_{12}	$-c_0$	t_{23}
24	4	c_4	c_8	c_{15}	c_4	c_8	$-c_{15}$	$-c_4$	$-c_8$	c_{15}	$-c_4$	$-c_8$	$-c_{15}$	t_{24}
...	...	...	...	...	...	...	...	...	...	...	...	...	...	...
31	4	jc_8	$-jc_{15}$	c_4	jc_8	$-jc_{15}$	$-c_4$	$-jc_8$	jc_{15}	c_4	$-jc_8$	jc_{15}	$-c_4$	t_{31}

period), and, for synchronisation case 2, the slot index (first or second slot in frame). This information is extracted from the SCH in a two-step process. The first step uses the primary synchronisation code (which is the same for all cells in all UMTS/TDD networks) to determine the temporal location of the SCH. This is done by correlating the received signal with the primary synchronisation code. The peaks in the correlation sequence indicate the presence of the SCH. From the number of slots in a frame that contain primary synchronisation peaks, we can derive the synchronisation case.

The second step of the synchronisation procedure is based on the secondary synchronisation codes. Since the secondary synchronisation codes are transmitted temporally aligned with the primary code, we will perform secondary synchronisation at the temporal locations indicated by the primary synchronisation stage. Correlation of the received signal with the 12 possible secondary synchronisation codes yields the information which code set has been used, and, with the primary synchronisation code as a phase reference, the symbols b_j (cf. Figure 3.7) are obtained. Together with the synchronisation case, this gives information on the code group i, the time offset $t_{\text{offset},i}$, and the ordering of interleaving blocks via Table 3.5 or Table 3.6.

Figure 3.8 shows an example of the synchronisation procedure. Shaded in grey are
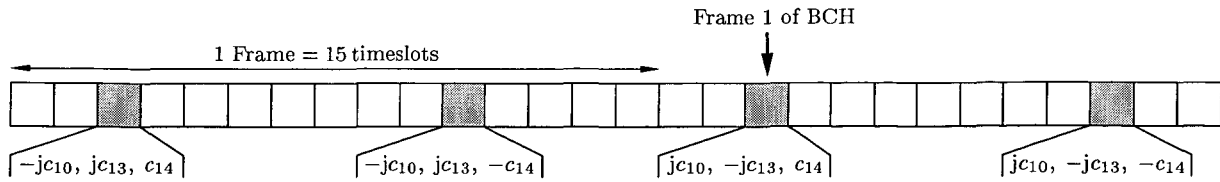
Figure 3.8: *Example of synchronisation procedure*.

the timeslots where a primary synchronisation code has been detected, while below, the results of secondary synchronisation are plotted. So e.g. in the first shaded timeslot, the codes c_{10}, c_{13}, and c_{14} (code set 2) have been detected and the symbols $-j$, j, and 1 have been extracted. Since the SCH is present four times within two frames, synchronisation case 2 is used and code allocation according to Table 3.6 is valid. Comparing the results of secondary synchronisation for the four shaded timeslots with the entries in Table 3.6, we see that the base station uses code group 11 (we highlighted this row in Table 3.6 for the reader's convenience). Moreover, the first interleaving block of the BCH lies lies in that timeslot, where the code combination jc_{10}, $-jc_{13}$, c_{14} (corresponding to the columns Frame 1, Slot k in Table 3.6) has been extracted. This is the case for the third shaded timeslot in our example. The time offset t_{11} that corresponds to $t_{\text{offset},11} = 528\,T_c$ in (3.1), finally determines that the slot border lies 528 chips ahead of the SCH.

As a concluding remark it has to be said that not exactly all the knowledge needed to detect the BCH is available at the end of the synchronisation procedure, since we know only the used code group but not which of the four different scrambling codes and basic midambles of this code group are used. However, this "one out of four" decision can easily be made after correlating the received signal with the four possible midambles. This correlation is part of the channel estimation stage.

26

Chapter 4

Synchronisation

One of the goals of the ANTIUM project is to demodulate and decode the broadcast channels (BCHs) of as many surrounding base stations of a UMTS/TDD network as possible (cf. Chapter 2). This is only possible if a synchronisation stage has located the BCHs within the received data and extracted the necessary parameters. In the following, we present synchronisation methods that are able to deal with strong co-channel interference, and we assess the performance of these methods by means of simulations.

The baseband model for the discrete-time signal vector received at the M antenna elements is given as

$$\mathbf{x}(n) = \sum_{k=1}^{K} \mathbf{x}_k(n) + \mathbf{n}(n) \quad \text{with} \quad \mathbf{x}_k(n) = \sum_{p=0}^{L-1} \mathbf{h}_{k,p}\, s_k(n-p)\,, \tag{4.1}$$

where K is the number of base stations and L is the maximum channel length. Since we only consider one timeslot at a time, we can omit the slot dependence of the channel vector $\mathbf{h}_{k,p}(n_s)$ in (2.4) and use a time-invariant vector $\mathbf{h}_{k,p}$ in (4.1).[1] The data signal of the kth base station is denoted as $s_k(n)$, while $\mathbf{n}(n)$ is a white Gaussian noise vector.

4.1 Primary Synchronisation

As explained in Chapter 3, the synchronisation procedure consists of primary and secondary synchronisation. In primary synchronisation, the aim is to detect the presence and temporal location of the primary synchronisation code c_p. The primary synchronisation stage will yield a decision statistic whose main peaks occur at these locations. Since c_p is the same for all base stations, a single decision statistic is sufficient to locate the primary synchronisation codes of all surrounding base stations.

We will now present three code detection algorithms that yield the desired decision statistic. These algorithms are all based on the generalised likelihood ratio test (GLRT) principle [Kay98] but differ by their signal model assumptions. Note that the use of these

---

[1] However, if we average over several slots, we have to take care of the changing channel.

detection algorithms is not restricted to the primary synchronisation stage, since they are able to detect an *arbitrary* known sequence in the received data vector. For instance, we will use them later in secondary synchronisation and channel estimation.

4.1.1 Spatial Detector

The first detection algorithm is based on a purely spatial model that assumes the channel to have only one path.

4.1.1.1 Derivation of the Spatial Detector

The primary synchronisation code has the length of $N = 256$ chips. In order to determine its presence at time n, we use the discrete-time receive vector $\mathbf{x}(n)$ in the time interval $[n, n + N - 1]$. The synchronisation code detection problem for one base station[1] can be formulated as a hypothesis test with the following two hypotheses [BR82, DS89]:

- Hypothesis $\mathcal{H}_0$ (absence of synchronisation code at time n):

$$\mathbf{x}(n + l) = \mathbf{w}(n + l), \quad \text{for } l = 0, \ldots, N-1;$$

- Hypothesis $\mathcal{H}_1$ (presence of synchronisation code at time n):

$$\mathbf{x}(n + l) = \mathbf{h}\, d(l) + \mathbf{w}(n + l), \quad \text{for } l = 0, \ldots, N-1.$$

For $\mathcal{H}_1$, we used the simplifying assumption of a one-tap channel modelled by the single $M \times 1$ vector $\mathbf{h}$, and neglected the other multipath contributions. Since we are not able to distinguish between the contributions of different base stations in the primary synchronisation stage, we have suppressed the base station index k of $\mathbf{h}$. The unknown channel vector $\mathbf{h}$ is assumed to be deterministic. The sequence $d(l)$ of length N serves as a wild-card for the known code that has to be detected. (In this section, $d(l)$ is the primary synchronisation code c_p.) Finally, noise $\mathbf{n}(n)$ and interference from other base stations are collected in the vector $\mathbf{w}(n)$ which is modelled as a zero-mean, stationary, temporally white, Gaussian-distributed random vector with correlation matrix

$$\mathrm{E}\left\{\mathbf{w}(n + n')\, \mathbf{w}^H(n)\right\} = \mathbf{R_w}\, \delta(n').$$

The spatial correlation matrix of the interference, $\mathbf{R_w}$, is unknown.

Let us stack the vectors within the time interval $[n, n + N - 1]$ into the augmented vectors

$$\mathbf{x}_n \triangleq \begin{bmatrix} \mathbf{x}(n) \\ \mathbf{x}(n + 1) \\ \vdots \\ \mathbf{x}(n + N - 1) \end{bmatrix}, \quad \mathbf{w}_n \triangleq \begin{bmatrix} \mathbf{w}(n) \\ \mathbf{w}(n + 1) \\ \vdots \\ \mathbf{w}(n + N - 1) \end{bmatrix}, \quad (4.2)$$

---

[1] The different time offsets of the synchronisation channels ensure that primary synchronisation codes of different base stations do not overlap completely. It is thus sufficient to consider only a single base station in the derivation of the spatial detector.

and define

$$\mathbf{d} \triangleq \begin{bmatrix} d(0) \\ d(1) \\ \vdots \\ d(N-1) \end{bmatrix}. \tag{4.3}$$

The total interference correlation matrix is block diagonal:

$$\mathbf{R} \triangleq \mathrm{E}\{\mathbf{w}_n \mathbf{w}_n^H\} = \begin{bmatrix} \mathbf{R_w} & & \mathbf{0} \\ & \ddots & \\ \mathbf{0} & & \mathbf{R_w} \end{bmatrix}. \tag{4.4}$$

Introducing the block diagonal channel matrix of size $NM \times N$

$$\mathbf{H} \triangleq \begin{bmatrix} \mathbf{h} & & \mathbf{0} \\ & \ddots & \\ \mathbf{0} & & \mathbf{h} \end{bmatrix} = \mathbf{I}_N \otimes \mathbf{h}, \tag{4.5}$$

the received signal can be formulated as

$$\mathbf{x}_n = \mathbf{w}_n \qquad \text{under } \mathcal{H}_0,$$
$$\mathbf{x}_n = \mathbf{H}\,\mathbf{d} + \mathbf{w}_n \qquad \text{under } \mathcal{H}_1.$$

Using the fact that $\mathbf{x}_n$ is Gaussian, the likelihood functions[1] under the two hypotheses can be compactly formulated as

$$f_0(\mathbf{x}_n) \triangleq f_0(\mathbf{x}_n; \mathbf{R}) = \frac{1}{\pi^{MN} \det \mathbf{R}} e^{-\mathbf{x}_n^H \mathbf{R}^{-1} \mathbf{x}_n},$$

$$f_1(\mathbf{x}_n) \triangleq f_1(\mathbf{x}_n; \mathbf{R}, \mathbf{H}) = \frac{1}{\pi^{MN} \det \mathbf{R}} e^{-(\mathbf{x}_n - \mathbf{H}\,\mathbf{d})^H \mathbf{R}^{-1} (\mathbf{x}_n - \mathbf{H}\,\mathbf{d})}.$$

With (4.2), (4.4), and (4.5) they can be rewritten as

$$f_0(\mathbf{x}_n) = f_0(\mathbf{x}; \mathbf{R_w}) = \frac{1}{\pi^{MN} (\det \mathbf{R_w})^N} e^{-\sum_{l=0}^{N-1} \mathbf{x}^H(n+l)\, \mathbf{R_w}^{-1}\, \mathbf{x}(n+l)} \tag{4.6}$$

$$f_1(\mathbf{x}_n) = f_1(\mathbf{x}; \mathbf{R_w}, \mathbf{h}) = \frac{1}{\pi^{MN} (\det \mathbf{R_w})^N} e^{-\sum_{l=0}^{N-1} [\mathbf{x}(n+l) - \mathbf{h}\,d(l)]^H \mathbf{R_w}^{-1} [\mathbf{x}(n+l) - \mathbf{h}\,d(l)]}. \tag{4.7}$$

To test which of the two hypotheses is true at time n, we compute the so called *log-likelihood ratio*

$$L(n) \triangleq \ln \frac{f_1(\mathbf{x}_n)}{f_0(\mathbf{x}_n)}.$$

---

[1] The indexed probability density function (pdf) $f(\mathbf{x}_n; \mathbf{R})$—as a function of $\mathbf{R}$, for fixed $\mathbf{x}_n$—is called the *likelihood function* [Kay93].

A high value of $L(n)$ indicates that $\mathcal{H}_1$ is likely (i.e., code $d(l)$ is present in time interval $[n, n+N-1]$), whereas in the absence of the code, a low value of $L(n)$ can be expected. The fact that $\mathbf{R_w}$ and $\mathbf{h}$ are unknown can be overcome by computing their maximum likelihood (ML) estimates and inserting them in $L(n)$. This approach is then referred to as *generalised* likelihood ratio test (GLRT) [Kay98].

We start with hypothesis $\mathcal{H}_0$, where only $\mathbf{R_w}$ has to be estimated. Taking the logarithm in (4.6) gives

$$\ln f_0(\mathbf{x}; \mathbf{R_w}) = -N \left[M \ln \pi + \ln \det \mathbf{R_w} + \frac{1}{N} \sum_{l=0}^{N-1} \mathbf{x}^H(n+l) \, \mathbf{R_w^{-1}} \, \mathbf{x}(n+l) \right],$$

where the third term can be reformulated as

$$\frac{1}{N} \sum_{l=0}^{N-1} \mathbf{x}^H(n+l) \, \mathbf{R_w^{-1}} \, \mathbf{x}(n+l) = \frac{1}{N} \sum_{l=0}^{N-1} \text{trace} \left\{ \mathbf{R_w^{-1}} \, \mathbf{x}(n+l) \, \mathbf{x}^H(n+l) \right\}$$

$$= \text{trace} \left\{ \mathbf{R_w^{-1}} \frac{1}{N} \sum_{l=0}^{N-1} \mathbf{x}(n+l) \, \mathbf{x}^H(n+l) \right\}.$$

With the abbreviation

$$\hat{\mathbf{R}}_{\mathbf{x}}(n) \triangleq \frac{1}{N} \sum_{l=0}^{N-1} \mathbf{x}(n+l) \, \mathbf{x}^H(n+l),$$

we get

$$\ln f_0(\mathbf{x}; \mathbf{R_w}) = -N \left[M \ln \pi + \ln \det \mathbf{R_w} + \text{trace} \left\{ \mathbf{R_w^{-1}} \hat{\mathbf{R}}_{\mathbf{x}}(n) \right\} \right]. \qquad (4.8)$$

Taking the derivative with respect to $\mathbf{R_w}$ gives [Sch91]

$$\frac{d}{d\mathbf{R_w}} \ln f_0(\mathbf{x}; \mathbf{R_w}) = -N \left[\left(\mathbf{R_w^{-1}} \right)^H + \left(-\mathbf{R_w^{-1}} \, \hat{\mathbf{R}}_{\mathbf{x}}(n) \, \mathbf{R_w^{-1}} \right)^H \right],$$

and since $\mathbf{R_w}$, $\mathbf{R_w^{-1}}$, and $\hat{\mathbf{R}}_{\mathbf{x}}(n)$ are Hermitian matrices we can simplify further to obtain

$$\frac{d}{d\mathbf{R_w}} \ln f_0(\mathbf{x}; \mathbf{R_w}) = -N \, \mathbf{R_w^{-1}} \left[\mathbf{R_w} - \hat{\mathbf{R}}_{\mathbf{x}}(n) \right] \mathbf{R_w^{-1}}. \qquad (4.9)$$

Setting the right hand side of (4.9) to zero yields the maximum-likelihood estimate of $\mathbf{R_w}$ under hypothesis $\mathcal{H}_0$ as

$$\hat{\mathbf{R}}_{\mathbf{w},0}(n) = \hat{\mathbf{R}}_{\mathbf{x}}(n). \qquad (4.10)$$

Inserting $\hat{\mathbf{R}}_{\mathbf{w},0}(n)$ into (4.8), we obtain the maximum (with respect to $\mathbf{R_w}$) log-likelihood function for $\mathcal{H}_0$ as

$$\ln f_0(\mathbf{x}_n)_{\text{ML}} = -N \left[M \ln \pi + \ln \det \hat{\mathbf{R}}_{\mathbf{x}}(n) + \text{trace} \left\{ \hat{\mathbf{R}}_{\mathbf{x}}^{-1}(n) \hat{\mathbf{R}}_{\mathbf{x}}(n) \right\} \right],$$

and by using (4.10) again, we finally get

$$\ln f_0(\mathbf{x}_n)_{\mathrm{ML}} = -N \left[M \ln \pi + \ln \det \hat{\mathbf{R}}_{\mathbf{w},0}(n) + M \right].$$

(4.11)

For $\mathcal{H}_1$, we estimate the unknown $\mathbf{h}$ first. The logarithm of (4.7) is given as

$$\ln f_1(\mathbf{x}; \mathbf{R}_{\mathbf{w}}, \mathbf{h}) = -N \Bigg[M \ln \pi + \ln \det \mathbf{R}_{\mathbf{w}} +$$
$$+ \frac{1}{N} \sum_{l=0}^{N-1} \left[\mathbf{x}(n+l) - \mathbf{h}\, d(l) \right]^H \mathbf{R}_{\mathbf{w}}^{-1} \left[\mathbf{x}(n+l) - \mathbf{h}\, d(l) \right] \Bigg].$$

(4.12)

Omitting the first two terms, which are independent of $\mathbf{h}$, we obtain

$$\ln f_1(\mathbf{x}; \mathbf{R}_{\mathbf{w}}, \mathbf{h}) \mathrel{\hat{=}} -\mathbf{h}^H \left[\sum_{l=0}^{N-1} d^*(l) \mathbf{R}_{\mathbf{w}}^{-1} d(l) \right] \mathbf{h} +$$
$$+ \mathbf{h}^H \sum_{l=0}^{N-1} d^*(l)\, \mathbf{R}_{\mathbf{w}}^{-1}\, \mathbf{x}(n+l) +$$
$$+ \left[\sum_{l=0}^{N-1} \mathbf{x}^H(n+l)\, \mathbf{R}_{\mathbf{w}}^{-1}\, d(l) \right] \mathbf{h} - \sum_{l=0}^{N-1} \mathbf{x}^H(n+l)\, \mathbf{R}_{\mathbf{w}}^{-1}\, \mathbf{x}(n+l).$$

The derivative with respect to $\mathbf{h}^*$ is [Sch91]

$$\frac{\mathrm{d}}{\mathrm{d}\mathbf{h}^*} \ln f_1(\mathbf{x}; \mathbf{R}_{\mathbf{w}}, \mathbf{h}) = -\mathbf{R}_{\mathbf{w}}^{-1} \left[\sum_{l=0}^{N-1} |d(l)|^2 \right] \mathbf{h} + \sum_{l=0}^{N-1} d^*(l)\, \mathbf{R}_{\mathbf{w}}^{-1}\, \mathbf{x}(n+l),$$

and setting $\frac{\mathrm{d}}{\mathrm{d}\mathbf{h}^*} \ln f_1(\mathbf{x}; \mathbf{R}_{\mathbf{w}}, \mathbf{h}) = 0$ gives the ML estimate of $\mathbf{h}$ as

$$\hat{\mathbf{h}}(n) = \frac{\mathbf{R}_{\mathbf{w}} \sum_{l=0}^{N-1} d^*(l)\, \mathbf{R}_{\mathbf{w}}^{-1}\, \mathbf{x}(n+l)}{\sum_{l=0}^{N-1} |d(l)|^2} = \frac{1}{\|d\|^2} \hat{\mathbf{r}}_{\mathbf{x}d}(n),$$

(4.13)

where

$$\|d\|^2 = \sum_{l=0}^{N-1} |d(l)|^2, \qquad \hat{\mathbf{r}}_{\mathbf{x}d}(n) = \sum_{l=0}^{N-1} \mathbf{x}(n+l)\, d^*(l).$$

Since $\hat{\mathbf{h}}(n)$ is independent of $\mathbf{R}_{\mathbf{w}}$, we can insert $\hat{\mathbf{h}}(n)$ into (4.12) and maximise with respect to $\mathbf{R}_{\mathbf{w}}$ in the same way as it was done in hypothesis $\mathcal{H}_0$. We obtain

$$\hat{\mathbf{R}}_{\mathbf{w},1}(n) = \frac{1}{N} \sum_{l=0}^{N-1} \left[\mathbf{x}(n+l) - \hat{\mathbf{h}}(n)\, d(l) \right] \left[\mathbf{x}(n+l) - \hat{\mathbf{h}}(n)\, d(l) \right]^H$$
$$= \hat{\mathbf{R}}_{\mathbf{x}}(n) + \hat{\mathbf{h}}(n)\, \hat{\mathbf{h}}^H(n) \frac{1}{N} \|d\|^2 - \frac{1}{N} \hat{\mathbf{h}}(n)\, \hat{\mathbf{r}}_{\mathbf{x}d}^H(n) - \frac{1}{N} \hat{\mathbf{r}}_{\mathbf{x}d}(n)\, \hat{\mathbf{h}}^H(n),$$

and by using (4.13)

$$\hat{\mathbf{R}}_{\mathbf{w},1}(n) = \hat{\mathbf{R}}_{\mathbf{x}}(n) - \frac{1}{N}\|d\|^2\,\hat{\mathbf{h}}(n)\,\hat{\mathbf{h}}^H(n). \tag{4.14}$$

Now that we have computed $\hat{\mathbf{h}}(n)$ and $\hat{\mathbf{R}}_{\mathbf{w},1}(n)$, the maximum log-likelihood function for $\mathcal{H}_1$ is given as

$$\ln f_1(\mathbf{x}_n)_{\mathrm{ML}} = -N\left[M\ln\pi + \ln\det\hat{\mathbf{R}}_{\mathbf{w},1}(n) + M\right].$$

As mentioned above, the hypothesis test will be based on the generalised likelihood *ratio* that is given as

$$L(n) = \ln\frac{f_1(\mathbf{x}_n)_{\mathrm{ML}}}{f_0(\mathbf{x}_n)_{\mathrm{ML}}} = -N\left[\ln\det\hat{\mathbf{R}}_{\mathbf{w},1}(n) - \ln\det\hat{\mathbf{R}}_{\mathbf{w},0}(n)\right], \tag{4.15}$$

where (4.11) has been used.

Although (4.15) looks quite concise already, it can be further simplified by inserting (4.10) and (4.14):

$$\begin{aligned}
L(n) = &-N\left[\ln\det\left\{\hat{\mathbf{R}}_{\mathbf{x}}(n) - \frac{1}{N}\|d\|^2\,\hat{\mathbf{h}}(n)\,\hat{\mathbf{h}}^H(n)\right\} - \ln\det\hat{\mathbf{R}}_{\mathbf{x}}(n)\right]\\
= &-N\left[\ln\det\left\{\hat{\mathbf{R}}_{\mathbf{x}}^{1/2}(n)\left(\mathbf{I}_M - \frac{1}{N}\|d\|^2\,\hat{\mathbf{R}}_{\mathbf{x}}^{-1/2}(n)\,\hat{\mathbf{h}}(n)\,\hat{\mathbf{h}}^H(n)\,\hat{\mathbf{R}}_{\mathbf{x}}^{-1/2}(n)\right)\hat{\mathbf{R}}_{\mathbf{x}}^{1/2}(n)\right\}\right.\\
&\left. - \ln\det\hat{\mathbf{R}}_{\mathbf{x}}(n)\right]\\
= &-N\ln\det\left\{\mathbf{I}_M - \frac{1}{N}\|d\|^2\,\hat{\mathbf{R}}_{\mathbf{x}}^{-1/2}(n)\,\hat{\mathbf{h}}(n)\,\hat{\mathbf{h}}^H(n)\,\hat{\mathbf{R}}_{\mathbf{x}}^{-1/2}(n)\right\}\\
= &-N\ln\det\left\{\mathbf{I}_M - \mathbf{G}\right\}, \tag{4.16}
\end{aligned}$$

with

$$\mathbf{G} \triangleq \frac{1}{N}\|d\|^2\,\hat{\mathbf{R}}_{\mathbf{x}}^{-1/2}(n)\,\hat{\mathbf{h}}(n)\,\hat{\mathbf{h}}^H(n)\,\hat{\mathbf{R}}_{\mathbf{x}}^{-1/2}(n).$$

With the abbreviations

$$\mathbf{b} \triangleq \hat{\mathbf{R}}_{\mathbf{x}}^{-1/2}(n)\,\hat{\mathbf{h}}(n),$$

$$c \triangleq \frac{1}{N}\|d\|^2,$$

we find that the matrix

$$\mathbf{G} = c\,\mathbf{b}\mathbf{b}^H$$

has an eigenvalue decomposition

$$\mathbf{G} = \lambda_0\mathbf{u}\mathbf{u}^H \tag{4.17}$$

with eigenvector

$$\mathbf{u} = \frac{\mathbf{b}}{\|\mathbf{b}\|}$$

and eigenvalue

$$
\begin{aligned}
\lambda_0 &= c \, \|\mathbf{b}\|^2 \\
&= \frac{1}{N} \|d\|^2 \, \mathbf{b}^H \mathbf{b} \\
&= \frac{1}{N} \|d\|^2 \, \hat{\mathbf{h}}^H(n) \, \hat{\mathbf{R}}_{\mathbf{x}}^{-1}(n) \, \hat{\mathbf{h}}(n).
\end{aligned} \tag{4.18}
$$

With λ_m denoting the eigenvalues of $\mathbf{G}$, the eigenvalues of $\mathbf{I}_M - \mathbf{G}$ are $1 - \lambda_m$. From (4.17) we see that all eigenvalues of $\mathbf{G}$ except λ_0 are zero and so the determinant in (4.16) can be expressed as

$$
\det\{\mathbf{I}_M - \mathbf{G}\} = \prod_{m=0}^{M-1} (1 - \lambda_m) = 1 - \lambda_0. \tag{4.19}
$$

With (4.18) and (4.19), the log-likelihood ratio is given as

$$
L(n) = -N \ln \left(1 - \frac{1}{N} \|d\|^2 \, \hat{\mathbf{h}}^H(n) \, \hat{\mathbf{R}}_{\mathbf{x}}^{-1}(n) \, \hat{\mathbf{h}}(n) \right),
$$

and inserting (4.13), we finally get

$$
L(n) = -N \ln \left(1 - \frac{1}{N\|d\|^2} \, \hat{\mathbf{r}}_{\mathbf{x}d}^H(n) \, \hat{\mathbf{R}}_{\mathbf{x}}^{-1}(n) \hat{\mathbf{r}}_{\mathbf{x}d}(n) \right).
$$

We could use the quantity $L(n)$ as a *decision statistic* for the presence of the sequence $d(l)$. Since the logarithm is a monotonic function, we will prefer the equivalent, simplified decision statistic

$$
c(n) = \frac{1}{N\|d\|^2} \, \hat{\mathbf{r}}_{\mathbf{x}d}^H(n) \, \hat{\mathbf{R}}_{\mathbf{x}}^{-1}(n) \, \hat{\mathbf{r}}_{\mathbf{x}d}(n) \tag{4.20}
$$

instead. Peaks in $c(n)$ will indicate the locations of the primary synchronisation code c_p.

Since the ANTIUM equipment records N_f succeeding frames and the SCH is transmitted every frame, we can improve the quality of the decision statistic $c(n)$ through averaging. The fact that the channel changes from slot to slot will not cause any problems, since $\mathbf{h}$ is re-estimated at each time instant n. We can hence expect the decision statistic $c(n)$ to be qualitatively periodic with the period of a frame duration $T_f = 38400\,\text{chips}$[1]. Averaging $c(n)$ over the N_f different recorded frames, we obtain

$$
\bar{c}(n) \triangleq \frac{1}{N_f} \sum_{m=0}^{N_f-1} c(n + mT_f). \tag{4.21}
$$

Figure 4.1 shows the influence of averaging on the decision statistic (4.20). Plotted here is the decision statistic $c(n)$ and below the averaged decision statistic $\bar{c}(n)$ for averaging over $N_f = 16$ frames. A peak in $c(n)$ or $\bar{c}(n)$ corresponds to the presence of the

---

[1]Qualitatively periodic in the sense that a peak of $c(n)$ at time n_0 will also be present at time $n_0 + T_f$.

synchronisation code c_p at time n. All base stations use the same primary synchronisation code, and hence the eight peaks in $\bar{c}(n)$ correspond to the codes c_p of eight different base stations. Due to the distinct offset times $t_{\text{offset},i}$, the code sequences start at different time instances n and the peaks in the decision statistic are temporally separated. Depending on the distance to the receiver and the current propagation channel, the signals coming from different base stations differ in power, which is reflected by the varying heights of the peaks.
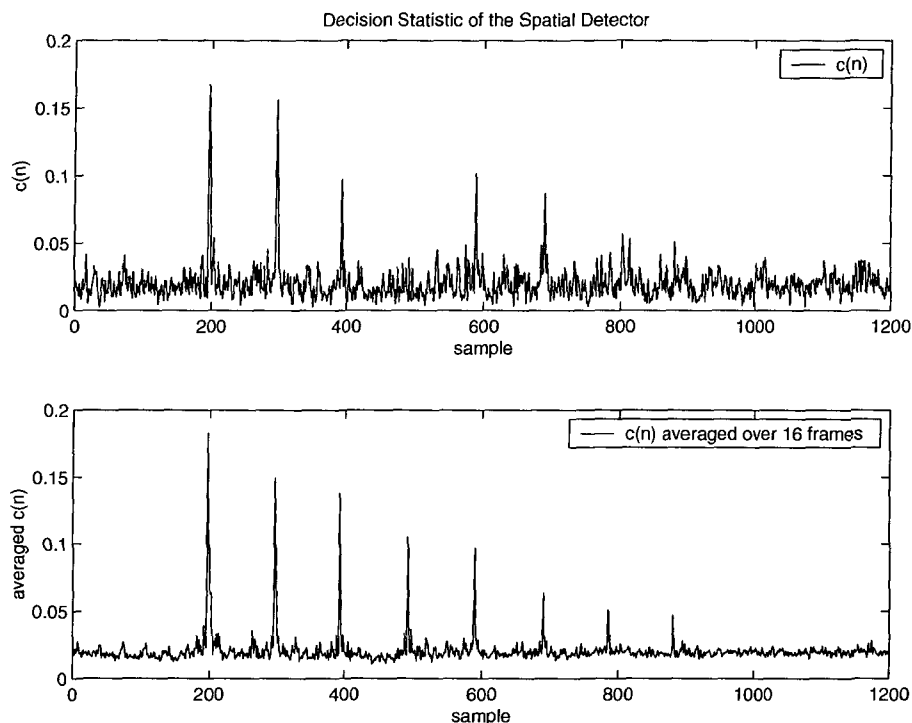
Figure 4.1: *Influence of averaging on the decision statistic of the spatial detector.*

The peaks of the stronger base stations are clearly visible in the original decision statistic $c(n)$, while the locations of the weaker base station's peaks cannot be detected. This is remedied by averaging, which causes also the location of the weakest peak to be discernible. Note further that the peak of the fourth base station is missing in the upper graph, while it is present in the averaged decision statistic below. This is due to the channel changing over time and base station four being in a deep fade in the frame considered for $c(n)$ in the upper graph. In conclusion, Figure 4.1 clearly shows that it is advantageous to use averaging over as many frames as possible in the synchronisation stage.[1]

---

[1] As the receiver moves, the absolute delays will change on a long-term basis. Averaging over changing delays will not enhance but rather degrade synchronisation performance. But since the ANTIUM equipment can only store a limited amount of data, the delays will stay effectively constant throughout the whole recorded data set.

4.1.1.2 False Alarm Probability and Threshold

As mentioned above, peaks in $\bar{c}(n)$ will indicate the presence of the code $d(l)$ in the time interval $[n, n + N - 1]$. In this context, we will call a value $\bar{c}(n_0)$ of the averaged decision statistic a peak if it exceeds a certain threshold η. To be able to choose this threshold η appropriately, we have to take a closer look at the properties of the averaged decision statistic $\bar{c}(n)$. Being calculated from random data $\mathbf{x}(n)$, the decision statistic $c(n)$ of (4.20) is itself a random process whose distribution at time n depends on whether hypothesis $\mathcal{H}_1$ or $\mathcal{H}_0$ is true. We will focus on the distribution under $\mathcal{H}_0$ in the following since it is analytically more tractable.

For Gaussian input data $\mathbf{x}(n)$ which is independent for different n, the sample correlation matrix $\hat{\mathbf{R}}_\mathbf{x}(n)$ is Wishart distributed [Wis67]. From [BR82, DS89] we further know that under $\mathcal{H}_0$, the decision statistic $c(n)$ is Beta distributed with parameters M and $N - M$:

$$c(n) \sim B(M, N - M) \qquad \text{for } c_p \text{ absent at time } n,$$

$$p_{c(n)}(x) = \frac{(N - 1)!}{(N - M - 1)!(M - 1)!} (1 - x)^{N - M - 1} x^{M - 1}. \tag{4.22}$$

To derive the distribution of the averaged decision statistic $\bar{c}(n)$, we consider the following approximations that are valid for $N \gg M$:

$$\frac{(N - 1)!}{(N - M - 1)!(M - 1)!} = \frac{(N - 1)(N - 2) \cdots (N - M)}{(M - 1)!} \approx \frac{N^M}{(M - 1)!},$$

$$(1 - x)^{N - M - 1} \approx (1 - x)^N = \left(1 - \frac{Nx}{N}\right)^N \approx e^{-Nx}.$$

It is now possible to approximate (4.22) by

$$p_{c(n)}(x) \approx \frac{N^M}{(M - 1)!} x^{M - 1} e^{-Nx},$$

which is a Gamma distribution with parameters M and $1/N$. This is a very accurate approximation in the context of ANTIUM, where $M = 5$ and $N = 256$.

Since the sample mean of K Gamma distributed random variables is again Gamma distributed according to

$$x_i \sim \Gamma(\alpha_i, \beta) \quad \Longrightarrow \quad \frac{1}{K} \sum_{i=1}^{K} x_i \sim \Gamma\left(\sum_{i=1}^{K} \alpha_i, \frac{\beta}{K}\right),$$

the approximate distribution of $\bar{c}(n)$ is Gamma with parameters MN_f and $\frac{1}{NN_f}$ like

$$\bar{c}(n) \sim \Gamma\left(MN_f, \frac{1}{NN_f}\right)$$

$$p_{\bar{c}(n)}(x) \approx \frac{(NN_f)^{MN_f}}{(MN_f - 1)!} x^{MN_f - 1} e^{-NN_f x}, \qquad \text{under } \mathcal{H}_0.$$

With this distribution we are able to compute a reasonable value for the threshold η. In case that hypothesis $\mathcal{H}_0$ holds at time n (code is absent), a detection error occurs if $\bar{c}(n)$ exceeds the threshold η. We would then decide for $\mathcal{H}_1$ and regard n as a synchronisation event (false alarm). The probability of a false alarm is thus given as

$$P_{\text{fa}} = \int_{\eta}^{\infty} p_{\bar{c}(n)}(x) \, dx = 1 - F_{\bar{c}(n)}(\eta), \qquad (4.23)$$

and by choosing $P_{\text{fa}} = 1\%$,[1] we can compute η depending on the averaging length N_f.

Figure 4.2 depicts the false alarm probability of the spatial detector versus the threshold for different averaging lengths. Both analytical and simulated results are shown. The simulated curves have been obtained by turning off the SCH and counting the times when $\bar{c}(n)$ exceeded the threshold. The close fit of the analytical and simulated curves indicates the good quality of the above-mentioned approximations. Note further that longer averaging will increase the slope of the curves and the synchronisation results will hence be more sensitive to variations of the threshold.
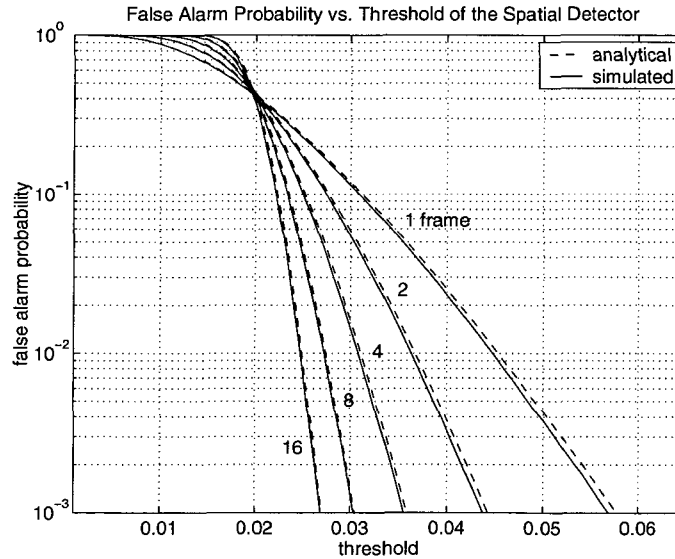
Figure 4.2: *False alarm probability* P_{fa} *of the spatial detector versus the threshold* η *for different averaging lengths* N_f. *The dashed lines represent the analytical results in* (4.23), *while the solid lines are simulation results.*

4.1.2 Heuristic Space-Time Detector

Multipath propagation was not considered by the spatial detector (4.20) and its averaged version (4.21). In the following, we will derive a simple *ad hoc* method for taking into account the temporal interference caused by multipath propagation.

---

[1] A moderate false alarm probability can be tolerated here since the primary synchronisation results will be verified later in the secondary synchronisation stage.

4.1.2.1 Derivation of the Heuristic Space-Time Detector

Let us stack successive samples of the received signal vector $\mathbf{x}(n)$ into the vector

$$
\tilde{\mathbf{x}}(n) \triangleq \begin{bmatrix} \mathbf{x}(n) \\ \mathbf{x}(n+1) \\ \vdots \\ \mathbf{x}(n+T_0-1) \end{bmatrix},
$$

where T_0 is the length of the temporal window considered. Formally substituting $\tilde{\mathbf{x}}(n)$ for $\mathbf{x}(n)$ in (4.20) yields the decision statistic

$$
c(n) = \frac{1}{N\|d\|^2}\,\hat{\mathbf{r}}_{\tilde{x}d}^{H}(n)\,\hat{\mathbf{R}}_{\tilde{\mathbf{x}}}^{-1}(n)\,\hat{\mathbf{r}}_{\tilde{x}d}(n),
$$

where $\hat{\mathbf{R}}_{\tilde{\mathbf{x}}}(n)$ and $\hat{\mathbf{r}}_{\tilde{x}d}(n)$ are given by

$$
\hat{\mathbf{R}}_{\tilde{\mathbf{x}}}(n) = \frac{1}{N}\sum_{l=0}^{N-1}\tilde{\mathbf{x}}(n+l)\,\tilde{\mathbf{x}}^{H}(n+l), \qquad \hat{\mathbf{r}}_{\tilde{x}d}(n) = \sum_{l=0}^{N-1}\tilde{\mathbf{x}}(n+l)\,d^{*}(l).
$$

This decision statistic is "heuristic" as it does not correspond to a GLRT with respect to the stacked signal vector $\tilde{\mathbf{x}}(n)$, but nevertheless this simple temporal extension proved to have good performance in simulations. As for the spatial case, averaging over different frames will improve the performance of the heuristic space-time detector.

4.1.2.2 False Alarm Probability and Threshold

Because of the stacking operation, which causes successive $\tilde{\mathbf{x}}(n)$ to have most of their entries in common, the $\tilde{\mathbf{x}}(n)$ are not independent of each other for different n and the correlation matrix $\hat{\mathbf{R}}_{\tilde{\mathbf{x}}}(n)$ is not Wishart distributed anymore. Therefore, the derivation of Section 4.1.1.2 cannot be applied to the decision statistic of the heuristic space-time detector and its averaged version. We thus have to use simulations to be able to come up with a suitable choice of the threshold.

Figure 4.3 shows the simulated false alarm probability of the heuristic space-time detector versus the threshold for different averaging lengths and three different lengths T_0 of the temporal window. As for the spatial detector, the slope of the curves increases with the averaging length. For fixed averaging length, a longer temporal window furthermore results in a more gentle decrease of the false alarm probability with the threshold.

4.1.3 Dispersive-Channel Detector

After this heuristic approach for considering multipath propagation, we will now develop a model that explicitly incorporates a time-dispersive channel. As in Section 4.1.1.1, a generalised likelihood ratio test (GLRT) based on this model will then yield a decision statistic for the presence of the synchronisation code.
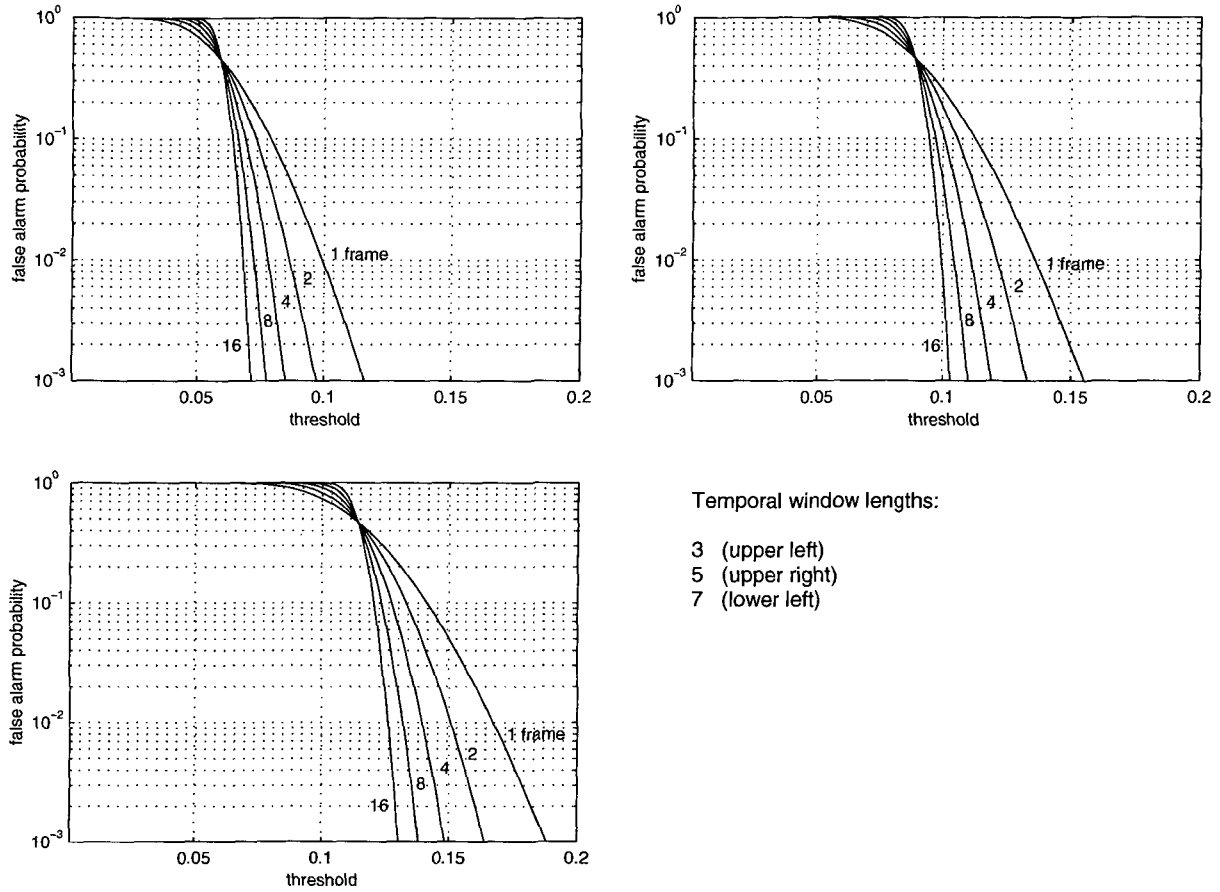
Figure 4.3: *Simulated false alarm probability* $\mathrm{P_{fa}}$ *of the heuristic space-time detector versus the threshold η for different averaging lengths N_f and different lengths T_0 of the temporal window.*

4.1.3.1 Derivation of the Dispersive-Channel Detector

Using a matrix-valued channel that contains all multipath contributions, the two hypotheses take the form of [And58]

- Hypothesis $\mathcal{H}_0$ (absence of synchronisation code at time n):

$$\mathbf{x}(n+l) = \mathbf{w}(n+l), \quad \text{for } l = 0, \ldots, N-1 \,;$$

- Hypothesis $\mathcal{H}_1$ (presence of synchronisation code at time n):

$$\mathbf{x}(n+l) = \mathbf{H}\,\mathbf{d}(l) + \mathbf{w}(n+l), \quad \text{for } l = 0, \ldots, N-1.$$

Here, the unknown $M \times L$ channel matrix is given as

$$\mathbf{H} = \begin{bmatrix} \mathbf{h}(0) & \mathbf{h}(1) & \cdots & \mathbf{h}(L-1) \end{bmatrix},$$

while the stacked code vector contains L succeeding values of $d(n)$ as[1]

$$\mathbf{d}(l) = \begin{bmatrix} d(l) \\ d(l-1) \\ \vdots \\ d(l-L+1) \end{bmatrix},$$

and L is the assumed channel length. If L is chosen greater than or equal to the maximum channel length, our model incorporates all multipath components present.

As in Section 4.1.1.1, we assume $\mathbf{w}(n)$ to be Gaussian with spatial correlation matrix $\mathbf{R_w}$ and temporally white.[2] The likelihood functions for a block of N successive samples $\mathbf{x}(n), \mathbf{x}(n+1), \ldots, \mathbf{x}(n+N-1)$ combined in the vector $\mathbf{x}_n$ (cf. Section 4.1.1.1) then become

$$f_0(\mathbf{x}_n) = f_0(\mathbf{x}; \mathbf{R_w}) = \frac{1}{\pi^{MN} \left(\det \mathbf{R_w}\right)^N} \, e^{-\sum\limits_{l=0}^{N-1} \mathbf{x}^H(n+l) \, \mathbf{R_w}^{-1} \, \mathbf{x}(n+l)}$$

$$f_1(\mathbf{x}_n) = f_1(\mathbf{x}; \mathbf{R_w}, \mathbf{H}) = \frac{1}{\pi^{MN} \left(\det \mathbf{R_w}\right)^N} \, e^{-\sum\limits_{l=0}^{N-1} [\mathbf{x}(n+l) - \mathbf{H}\,\mathbf{d}(l)]^H \, \mathbf{R_w}^{-1} \, [\mathbf{x}(n+l) - \mathbf{H}\,\mathbf{d}(l)]}. \quad (4.24)$$

For hypothesis $\mathcal{H}_0$, nothing changes compared to Section 4.1.1.1: The ML estimate of the correlation matrix $\mathbf{R_w}$ is again given as

$$\hat{\mathbf{R}}_{\mathbf{w},0}(n) = \hat{\mathbf{R}}_{\mathbf{x}}(n) = \frac{1}{N} \sum_{l=0}^{N-1} \mathbf{x}(n+l) \, \mathbf{x}^H(n+l), \quad (4.25)$$

while the maximum log-likelihood function can again be written as

$$\ln f_0(\mathbf{x}_n)_{\text{ML}} = -N \left[M \ln \pi + \ln \det \hat{\mathbf{R}}_{\mathbf{x}}(n) + \text{trace}\left\{ \hat{\mathbf{R}}_{\mathbf{x}}^{-1}(n) \hat{\mathbf{R}}_{\mathbf{x}}(n) \right\} \right]$$

$$= -N \left[M \ln \pi + \ln \det \hat{\mathbf{R}}_{\mathbf{w},0}(n) + M \right].$$

For $\mathcal{H}_1$, we again start by estimating the unknown $\mathbf{H}$. From (4.24),

$$\ln f_1(\mathbf{x}; \mathbf{R_w}, \mathbf{H}) = -N \left[M \ln \pi + \ln \det \mathbf{R_w} + \right.$$

$$\left. + \frac{1}{N} \sum_{l=0}^{N-1} [\mathbf{x}(n+l) - \mathbf{H}\,\mathbf{d}(l)]^H \, \mathbf{R_w}^{-1} \, [\mathbf{x}(n+l) - \mathbf{H}\,\mathbf{d}(l)] \right].$$

---

[1]We note that $d(n) = 0$ for $n < 0$.

[2]For temporally coloured $\mathbf{w}(n)$, there exists no analytical solution for the GLRT.

Omitting the first two terms (which are independent of $\mathbf{H}$), we obtain

$$\ln f_1(\mathbf{x}; \mathbf{R_w}, \mathbf{H}) \,\hat{=}\, -\sum_{l=0}^{N-1} \mathbf{d}^H(l)\, \mathbf{H}^H\, \mathbf{R_w^{-1}}\, \mathbf{H}\, \mathbf{d}(l) +$$
$$+ \sum_{l=0}^{N-1} \mathbf{d}^H(l)\, \mathbf{H}^H\, \mathbf{R_w^{-1}}\, \mathbf{x}(n+l) +$$
$$+ \sum_{l=0}^{N-1} \mathbf{x}^H(n+l)\, \mathbf{R_w^{-1}}\, \mathbf{H}\, \mathbf{d}(l) - \sum_{l=0}^{N-1} \mathbf{x}^H(n+l)\, \mathbf{R_w^{-1}}\, \mathbf{x}(n+l).$$

The derivative with respect to $\mathbf{H}$ is [Wei91]

$$\frac{\mathrm{d}}{\mathrm{d}\mathbf{H}} \ln f_1(\mathbf{x}; \mathbf{R_w}, \mathbf{H}) = -\mathbf{R_w^{-1}}\, \mathbf{H} \sum_{l=0}^{N-1} \mathbf{d}(l)\, \mathbf{d}^H(l) + \mathbf{R_w^{-1}} \sum_{l=0}^{N-1} \mathbf{x}(n+l)\, \mathbf{d}^H(l),$$

and setting $\frac{\mathrm{d}}{\mathrm{d}\mathbf{H}} \ln f_1(\mathbf{x}; \mathbf{R_w}, \mathbf{H}) = 0$ gives the ML estimate of $\mathbf{H}$ as

$$\hat{\mathbf{H}}(n) = \left(\sum_{l=0}^{N-1} \mathbf{x}(n+l)\, \mathbf{d}^H(l) \right) \left(\sum_{l=0}^{N-1} \mathbf{d}(l)\, \mathbf{d}^H(l) \right)^{-1} = \hat{\mathbf{R}}_{\mathbf{xd}}(n)\, \mathbf{D}^{-1}, \qquad (4.26)$$

where

$$\hat{\mathbf{R}}_{\mathbf{xd}}(n) \,\triangleq\, \sum_{l=0}^{N-1} \mathbf{x}(n+l)\, \mathbf{d}^H(l), \qquad \mathbf{D} \,\triangleq\, \sum_{l=0}^{N-1} \mathbf{d}(l)\, \mathbf{d}^H(l).$$

Again, we see that $\hat{\mathbf{H}}(n)$ is independent of $\mathbf{R_w}$. Thus, we can insert $\hat{\mathbf{H}}(n)$ into (4.24) and maximise with respect to $\mathbf{R_w}$. This gives

$$\hat{\mathbf{R}}_{\mathbf{w},1}(n) = \frac{1}{N} \sum_{l=0}^{N-1} \left[\mathbf{x}(n+l) - \hat{\mathbf{H}}(n)\, \mathbf{d}(l) \right] \left[\mathbf{x}(n+l) - \hat{\mathbf{H}}(n)\, \mathbf{d}(l) \right]^H$$
$$= \hat{\mathbf{R}}_{\mathbf{x}}(n) + \frac{1}{N}\, \hat{\mathbf{H}}(n)\, \mathbf{D}\, \hat{\mathbf{H}}(n) - \frac{1}{N}\, \hat{\mathbf{H}}(n)\, \hat{\mathbf{R}}_{\mathbf{xd}}^H(n) - \frac{1}{N}\, \hat{\mathbf{R}}_{\mathbf{xd}}(n)\, \hat{\mathbf{H}}^H(n),$$

and by using (4.26)

$$\hat{\mathbf{R}}_{\mathbf{w},1}(n) = \hat{\mathbf{R}}_{\mathbf{x}}(n) - \frac{1}{N}\, \hat{\mathbf{R}}_{\mathbf{xd}}(n)\, \mathbf{D}^{-1}\, \hat{\mathbf{R}}_{\mathbf{xd}}^H(n). \qquad (4.27)$$

Now that we have estimated $\hat{\mathbf{H}}(n)$ and $\hat{\mathbf{R}}_{\mathbf{w},1}(n)$, the maximum log-likelihood function for hypothesis $\mathcal{H}_1$ is given as

$$\ln f_1(\mathbf{x}_n)_{\mathrm{ML}} = -N \left[M \ln \pi + \ln \det \hat{\mathbf{R}}_{\mathbf{w},1}(n) + M \right],$$

while the generalised likelihood ratio can be written as

$$L(n) = \ln \frac{f_1(\mathbf{x}_n)_{\mathrm{ML}}}{f_0(\mathbf{x}_n)_{\mathrm{ML}}} = -N \left[\ln \det \hat{\mathbf{R}}_{\mathbf{w},1}(n) - \ln \det \hat{\mathbf{R}}_{\mathbf{w},0}(n) \right].$$

With (4.25) and (4.27), $L(n)$ becomes

$$L(n) = N \left[\ln \det \hat{\mathbf{R}}_\mathbf{x}(n) - \ln \det \left\{ \hat{\mathbf{R}}_\mathbf{x}(n) - \frac{1}{N} \hat{\mathbf{R}}_\mathbf{xd}(n) \, \mathbf{D}^{-1} \, \hat{\mathbf{R}}_\mathbf{xd}^{H}(n) \right\} \right] ,$$

which can be simplified to

$$L(n) = N \ln \det \left\{ \mathbf{I}_M - \frac{1}{N} \hat{\mathbf{R}}_\mathbf{xd}(n) \, \mathbf{D}^{-1} \, \hat{\mathbf{R}}_\mathbf{xd}^{H}(n) \, \hat{\mathbf{R}}_\mathbf{x}^{-1}(n) \right\}^{-1} . \tag{4.28}$$

In contrast to (4.16), the term $\mathbf{G} \triangleq \frac{1}{N} \hat{\mathbf{R}}_\mathbf{xd}(n) \, \mathbf{D}^{-1} \, \hat{\mathbf{R}}_\mathbf{xd}^{H}(n) \, \hat{\mathbf{R}}_\mathbf{x}^{-1}(n)$ is no rank-one matrix anymore and the steps of Section 4.1.1.1 involving the eigenvalue decomposition do not yield a simplified version of $L(n)$. The generalised likelihood ratio is a positive function and the argument of the logarithm is hence greater than one. Since the logarithm is a monotonic function, we obtain a final, simplified decision statistic as

$$c(n) = \det \left\{ \mathbf{I}_M - \frac{1}{N} \hat{\mathbf{R}}_\mathbf{xd}(n) \, \mathbf{D}^{-1} \, \hat{\mathbf{R}}_\mathbf{xd}^{H}(n) \, \hat{\mathbf{R}}_\mathbf{x}^{-1}(n) \right\}^{-1} - 1, \tag{4.29}$$

where the subtraction of one shifts the values of $c(n)$ such that they lie in the same range as the decision statistics of Sections 4.1.1 and 4.1.2. As in Section 4.1.1.1, we will use an averaged version of (4.29) for primary synchronisation, namely

$$\bar{c}(n) \triangleq \frac{1}{N_f} \sum_{m=0}^{N_f - 1} c(n + m T_f). \tag{4.30}$$

4.1.3.2 False Alarm Probability and Threshold

To derive the distribution of the averaged decision statistic $\bar{c}(n)$ in (4.30), we first consider $c(n)$ in (4.29). According to Lemma 8.4.1. of [And58], the term $\hat{\mathbf{R}}_\mathbf{xd}(n) \, \mathbf{D}^{-1} \, \hat{\mathbf{R}}_\mathbf{xd}^{H}(n)$ is central Wishart distributed,

$$\hat{\mathbf{R}}_\mathbf{xd}(n) \, \mathbf{D}^{-1} \, \hat{\mathbf{R}}_\mathbf{xd}^{H}(n) \sim W_M(L, \mathbf{R_w}),$$

and the sample correlation matrix $\hat{\mathbf{R}}_\mathbf{x}(n)$ is central Wishart distributed with the same correlation matrix $\mathbf{R_w}$ and N degrees of freedom

$$\hat{\mathbf{R}}_\mathbf{x}(n) \sim W_M(N, \mathbf{R_w}).$$

From [Rao65] we take the following result:

Let $\mathbf{S}_1 \sim W_M(N, \mathbf{R_w})$ and $\mathbf{S}_2 \sim W_M(L, \mathbf{R_w})$ be independent. Then if $N \geq M$, $\det \mathbf{S}_1 / \det\{\mathbf{S}_1 + \mathbf{S}_2\}$ is distributed as the product of M independent Beta variables with parameters

$$(N - M + 1, L), (N - M + 2, L), \dots, (N, L).$$

41

Since $c(n) + 1$ in (4.29) has the structure of $\det \mathbf{S}_1 / \det\{\mathbf{S}_1 + \mathbf{S}_2\}$ and all the assumptions hold, the distribution of $c(n)$ is given as that of a product of M independent Beta variables as explained above. For our parameter setting of $M = 5$, a closed-form expression of $p_{c(n)}(x)$ exists but is very cumbersome. Unfortunately, the cdf cannot be obtained in closed form and thus no threshold η can be computed analytically. The same holds for the averaged decision statistic $\bar{c}(n)$ of (4.30) and thus we again rely on simulations of the false alarm probability versus η to be able to choose an appropriate η.

Figure 4.4 shows the simulated false alarm probability of the dispersive-channel detector versus the threshold for different averaging lengths and three different assumed channel lengths L. As for the other detection algorithms, the slope of the curves increases with the averaging length. For fixed averaging length, a longer assumed channel length leads to a more gentle decrease of the false alarm probability with the threshold.
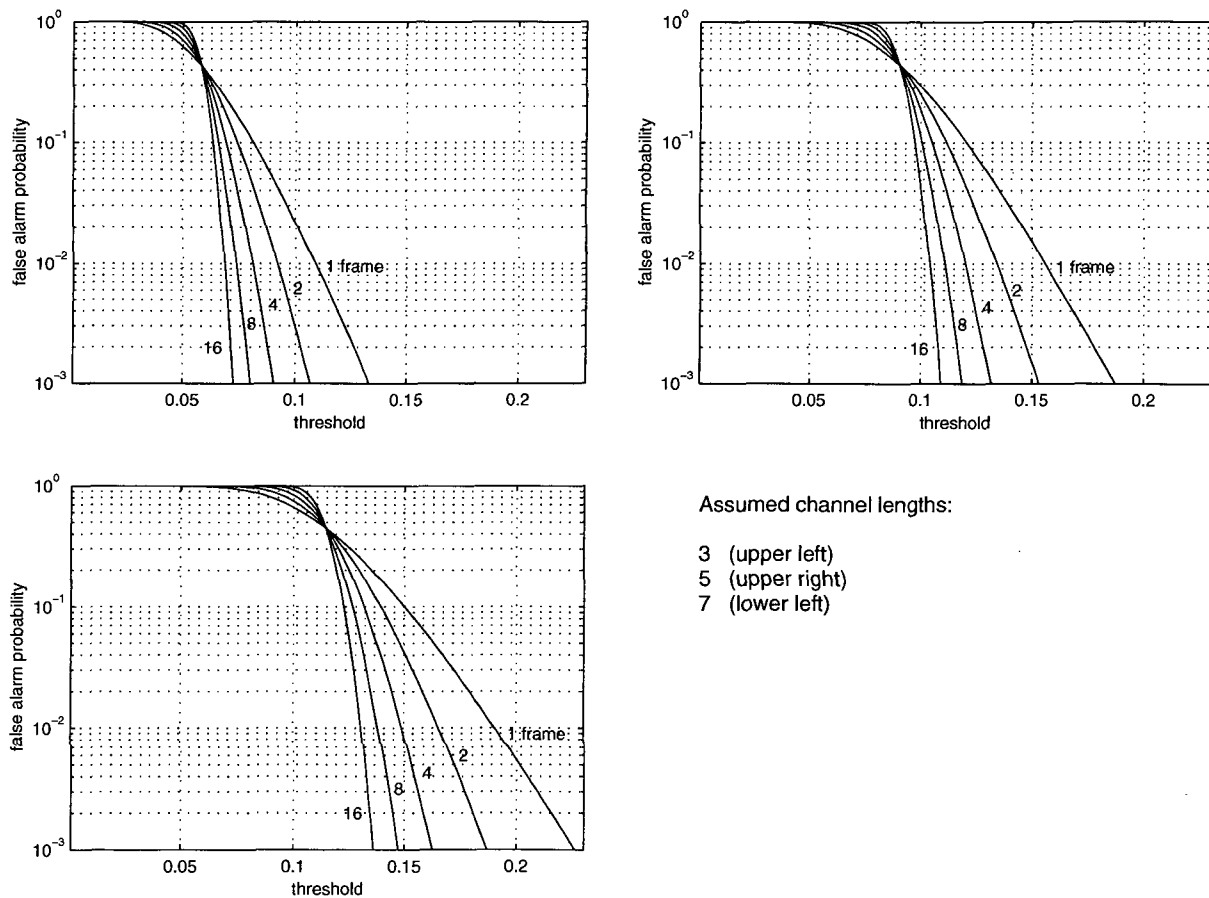

Figure 4.4: *Simulated false alarm probability* $\mathrm{P_{fa}}$ *of the dispersive-channel detector versus the threshold* η *for different averaging lengths* N_f *and different assumed channel lengths* L.

4.2 Secondary Synchronisation

Recall that the SCH consists of a primary and three secondary code sequences (cf. Figure 3.7). During primary synchronisation, the aim was to localise the primary synchronisation code c_p within the received data. We used the code c_p as a reference sequence $d(l)$ for one of the three detection algorithms and obtained a corresponding averaged decision statistic $\bar{c}(n)$. Since the same primary synchronisation code c_p is transmitted by all UMTS/TDD base stations, we encountered several peaks in $\bar{c}(n)$ caused by different base stations. The presence of a primary synchronisation code always implies the presence of secondary synchronisation codes, and we have to perform secondary synchronisation only at time instances n where a peak in $\bar{c}(n)$ occurred.

The goal of secondary synchronisation is now to extract the used synchronisation code set and the symbols b_j at each peak location, which yields, for the corresponding base station, knowledge of the code group, of the SCH time offset, and, via Table 3.5 or Table 3.6, of the ordering of BCH interleaving blocks. In principle, the symbols b_j could be demodulated, as described in Section 3.3, by correlating with the secondary synchronisation codes. For low SINR, however, this method will fail. In the following we present a more sophisticated approach that uses the three detection algorithms of the primary synchronisation stage to enable secondary synchronisation even for weak base stations. Although this method can be applied to synchronisation case 2 as well, we only considered synchronisation case 1 (SCH present in a single timeslot per frame) in the course of ANTIUM for the sake of simplicity.

4.2.1 Secondary Synchronisation for Strongest Base Station

A high peak in the primary synchronisation decision statistic $\bar{c}(n)$ indicates the presence of a strong synchronisation signal at time n. Since a strong signal is likely to have high SINR, and thus secondary synchronisation can be expected to be reliable, we will first perform secondary synchronisation at the time index n_0 of the highest peak of $\bar{c}(n)$.

According to Table 3.5, there exist 64 possible constellations of secondary synchronisation codes and weights b_j for a particular timeslot.[1] Since the SCH is the sum of the primary and the three weighted secondary codes

$$c_{\text{tot}} = c_p + \sum_{j=1}^{3} b_j \, c_{s,j} \, ,$$

the task of secondary synchronisation is to decide which of these 64 *total synchronisation codes* c_{tot} is present at time n_0. As for primary synchronisation, this is a code detection problem and we can re-use the detection algorithms of Section 4.1. Using the total synchronisation codes as reference sequences $d(l)$ for one of the three detection methods at time n_0, we obtain 64 decision values. The maximum of these decision values should

---

[1]These are needed to encode the 32 different code groups as well as two possibilities for the frame position in the interleaving period.

correspond to the total synchronisation code actually present. From the code set and the symbols b_j used to construct this specific total synchronisation code, we finally obtain the desired synchronisation parameters of the strongest base station.

In the following we will exploit the knowledge of the code group of the strongest base station in the synchronisation procedure for the weaker base stations. Since an erroneous result for the strongest base station will thus cause the synchronisation procedures for all weaker base stations to fail, it is necessary to carefully validate the correctness of the strongest base station's code group.

This *synchronisation validation* can be achieved as follows. According to Chapter 3, the code group of a base station determines the used scrambling code and midamble sequence. From secondary synchronisation at time n_0, we thus know which midamble is used by the strongest base station and where it is located in the received data sequence. We consider the synchronisation procedure of the strongest base station as successful if we are able to detect the correct midamble sequence at the correct temporal location with sufficient confidence. Since this is again a code detection problem, we will use the midamble as reference sequence for one of the three detection algorithms to obtain a decision value. "Sufficient confidence" in this context means that the decision value has to exceed a threshold η_m. In contrast to primary synchronisation, we will choose η_m quite high in order to achieve a low false alarm probability. Since there are four midambles in a code group, we will perform the above-mentioned validation process with all of them. Synchronisation is successfully validated if one of the four decision values exceeds the threshold.

In the case that validation fails because no decision value exceeds the threshold η_m, we perform the whole secondary synchronisation and midamble validation procedure at the position n_1 of the *second strongest* peak of $\bar{c}(n)$. This process is continued until synchronisation has been successful somewhere. However, the case that synchronisation does not even succeed for the strongest base station is very unlikely, in fact it never happened in our simulations.

4.2.2 Secondary Synchronisation for Weaker Base Stations

The detection-based secondary synchronisation algorithm presented above is not restricted to the strongest base station. We could in principle perform it at any time instant n_p corresponding to a primary synchronisation peak. But since we chose a relatively low primary synchronisation threshold in order to keep the detection probability high, the number of peaks will be quite large and a significant percentage of them will be false alarms. Performing secondary synchronisation on all of them would be a waste of effort that can easily be avoided: Because UMTS/TDD base stations are synchronous, we can discard some peaks *a priori* without having to perform secondary synchronisation at all.

Recall that all SCHs are transmitted in the same time slot. Since the slot borders of different base stations are temporally aligned upon transmission, the only difference in peak time n at the receiver is due to the time offsets $t_{\text{offset},i}$ and the run-time differences

of the signals.[1] After secondary synchronisation for the strongest base station, we know the temporal location of the SCH timeslot. We furthermore know beforehand that the 32 possible time offsets $t_{\text{offset},i}$ of the synchronisation codes differ by multiples of 48 chips (cf. (3.1)). Since base stations in adjacent cells never use the same time offset, we know that the synchronisation code peaks of weaker base stations have to be located multiples of 48 chips away from the peak of the strongest base station in $\bar{c}(n)$, apart from path-length dependent run-time differences. To account for these run-time differences, we search for the synchronisation code peaks in a certain time window around the expected locations. The size of this window depends on the cell size and the expected maximal runtime differences. For secondary synchronisation to a weaker base station, we then take only those peaks of the primary synchronisation decision statistic $\bar{c}(n)$ into account that *both* exceed the threshold η *and* are located within one of our time windows. Figure 4.5 shows the three cases possible:

1. Peak lies within time window and exceeds the threshold: Peak is accepted;

2. Peak lies within time window but is lower than the threshold: Peak is rejected;

3. Peak lies outside of time window: Peak is rejected regardless of its height.
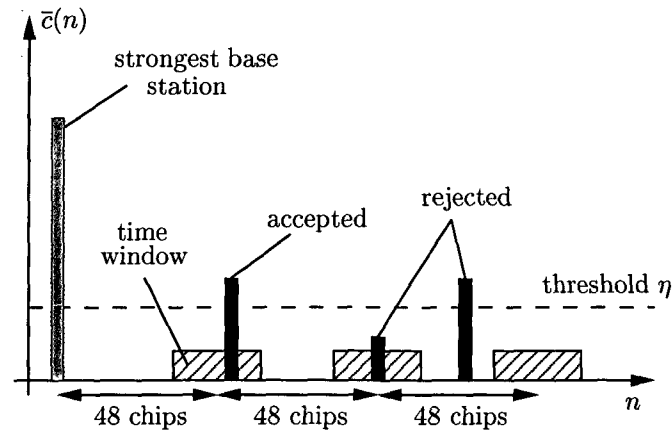

Figure 4.5: *Synchronisation for weaker base stations using time windows.*

On the "accepted" peak locations, we perform secondary synchronisation as explained in the previous section. In order to keep the false alarm probability low, we perform midamble code validation as previously described for the strongest base station also for the weaker base stations.

Figure 4.6 summarises the particular steps of the total synchronisation procedure. The upper part describes synchronisation for the strongest base station, while in the lower part

---

[1]Due to different path lengths, a timing variation of a few chips between the signals received from different base stations will be experienced. Here, a path length difference of about 78 m corresponds to a timing variation of one chip. However, the concept of time windows will fail in the presence of extremely long delays (strong distant reflections) or broken inter-base-station synchronisation.

the 32 different time windows are scanned for synchronisation channels of weaker base stations.
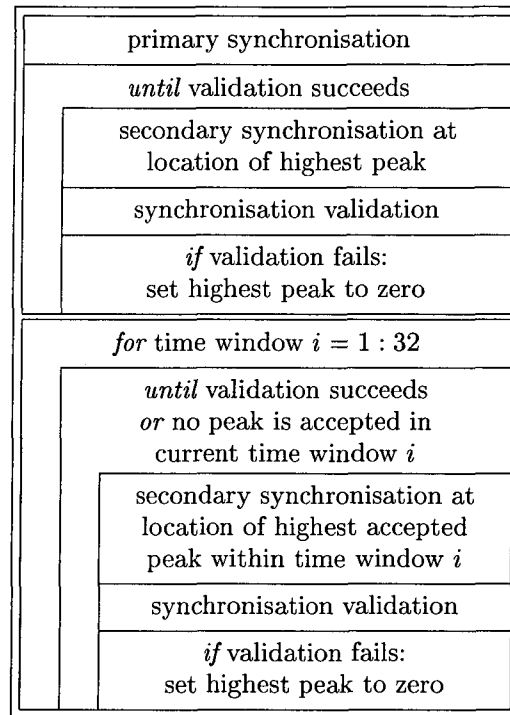

Figure 4.6: *Structure chart of the total synchronisation procedure.*

4.3 Simulation Results

To assess the performance of the synchronisation algorithms presented above, we conducted Monte Carlo simulations using the simulation scenarios described in Section 2.2.

The threshold values needed for primary synchronisation and for the midamble-based validation of secondary synchronisation were chosen according to Table 4.1 and Table 4.2, respectively. These values correspond to a false alarm probability of 1 % for primary synchronisation and 0.1 % for midamble validation. The threshold values for the different algorithms have been taken from Figures 4.2–4.4. Together with the false alarm probability of the secondary synchronisation stage,[1] the total false alarm rate for each time instant within a time window is about 0.15 ppm, which is sufficiently low for practical use.

Figures 4.7–4.12 show the percentage of successful synchronisation events for the total synchronisation procedure including primary and secondary synchronisation with midamble validation. We carried out 100 simulation rounds for each scenario and averaged

---

[1]In the absence of the SCH, the probability to detect the "correct" total synchronisation code is $P_{fa} = 1/64$.

Table 4.1: *Primary synchronisation threshold for a false alarm probability of* $P_{fa} = 1\%$..

Number of Averaged Frames		4	8	16
Spatial Detector		0.0308	0.0272	0.0248
Heuristic	$T_0 = 3$	0.0778	0.0722	0.0681
Space-Time	5	0.1110	0.1044	0.0994
Detector	7	0.1394	0.1318	0.1261
Dispersive-	$L = 3$	0.0808	0.0736	0.0685
Channel	5	0.1200	0.1108	0.1041
Detector	7	0.1488	0.1380	0.1303

Table 4.2: *Midamble threshold for validation of secondary synchronisation for a false alarm probability of* $P_{fa} = 0.1\%$.

Number of Averaged Frames		4	8	16
Spatial Detector		0.0185	0.0178	0.0175
Heuristic	$T_0 = 3$	0.0408	0.0401	0.0393
Space-Time	5	0.0578	0.0576	0.0564
Detector	7	0.0719	0.0715	0.0707
Dispersive-	$L = 3$	0.0459	0.0454	0.0437
Channel	5	0.0655	0.0650	0.0630
Detector	7	0.0815	0.0805	0.0789

$c(n)$ over 4, 8, and 16 frames. For each base station (characterised on the abscissa by its number and respective SINR value), the synchronisation score of the different algorithms is indicated by the height of seven bars. From the left, these bars correspond to the spatial detector (labeled *Spatial*), the heuristic space-time detector with temporal window lengths of $T_0 = 3$, 5, and 7 samples (labeled *HST*), and the dispersive-channel detector with assumed channel lengths of $L = 3$, 5, and 7 samples (labeled *DCD*).

Pedestrian Environment

Looking at the results for **scenario 1** (Figure 4.7), we see that the performance of the *spatial detection algorithm* for channel A is very good. Even for averaging over only 4 frames, we achieve a synchronisation score of over 80 % down to an SINR of −22 dB. If we average over 8 or even 16 frames, the performance improves nearly to the 100 % level. For channel B with its longer delay spread and significantly larger number of taps, we experience a performance degradation.[1] The synchronisation performance is now sufficiently good only down to an SINR of −18 dB if sufficient averaging is used. Indeed, for these weak base stations, the longer averaging time results in great performance improvements from around 50 % to over 90 % success. Note that the synchronisation score for base station 4 is worse than for base station 5 although the mean SINR is the

---

[1] Since the spatial detection method neglects multipath propagation, this behaviour could somehow be expected.

Figure 4.7: *Percentage of successful synchronisation events for the pedestrian environment, scenario 1.*

48

Figure 4.8: *Percentage of successful synchronisation events for the pedestrian environment, scenario 2.*

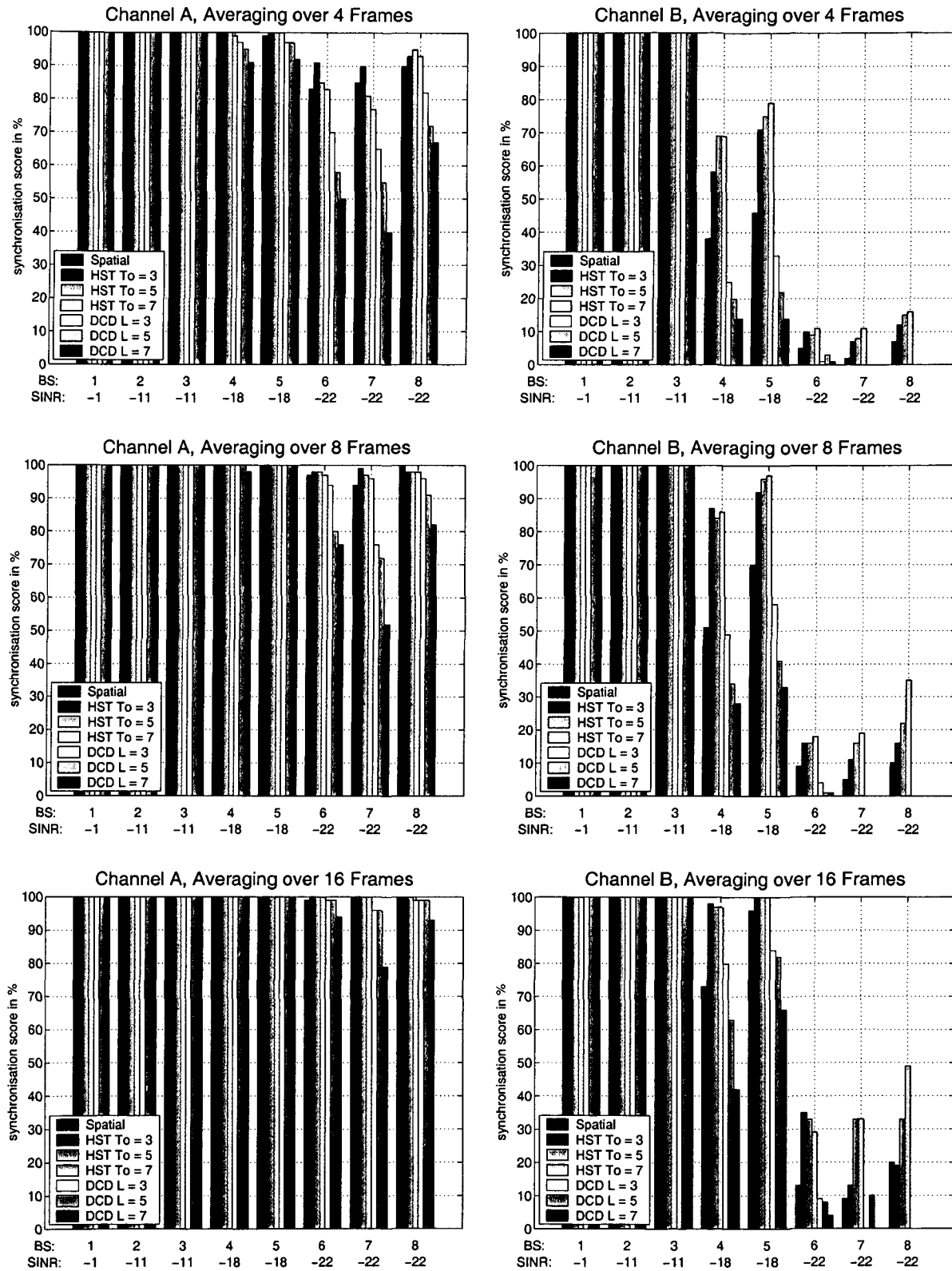Figure 4.9: *Percentage of successful synchronisation events for the pedestrian environment, scenario 3.*

Figure 4.10: *Percentage of successful synchronisation events for the indoor environment, scenario 1.*
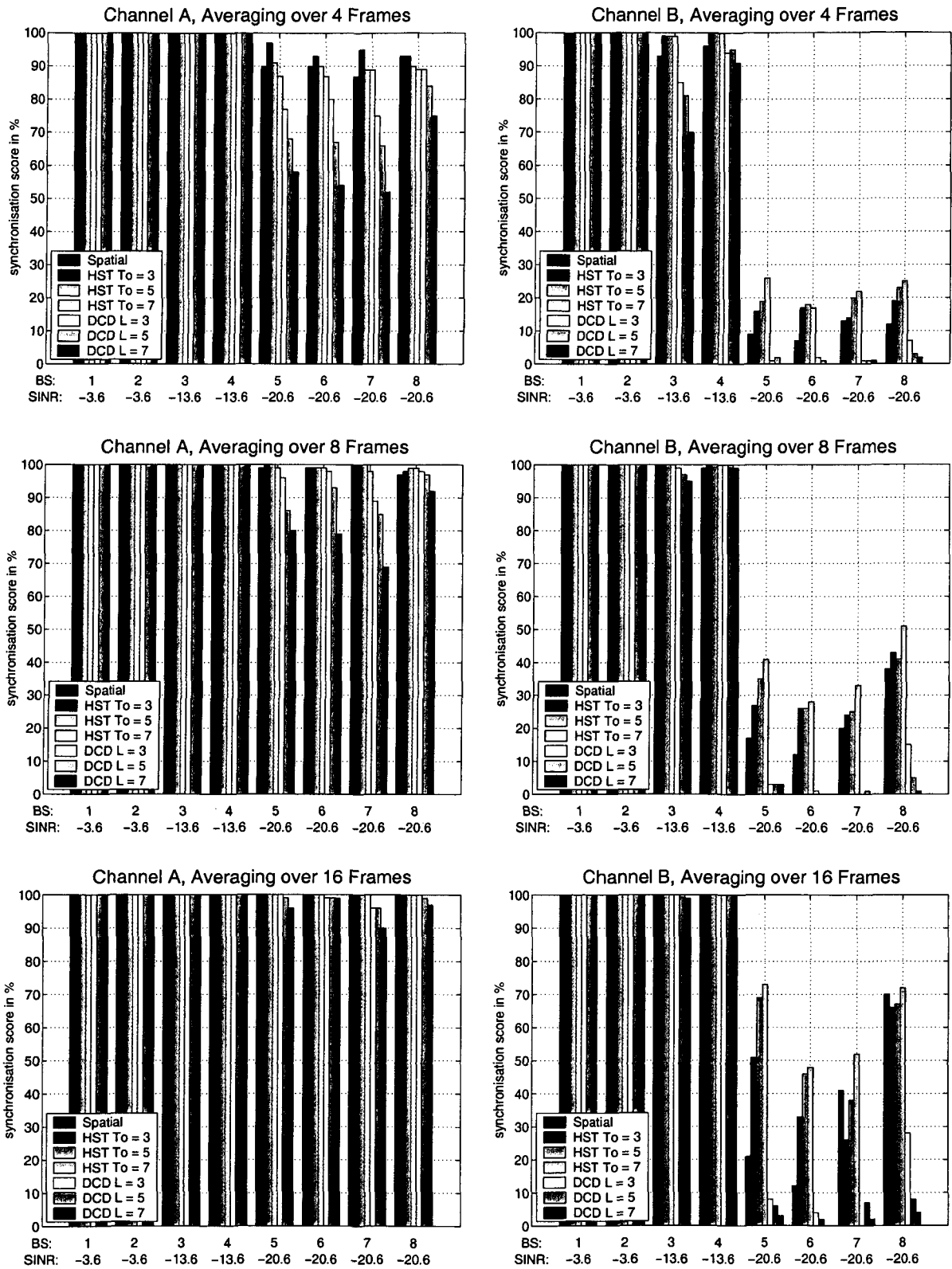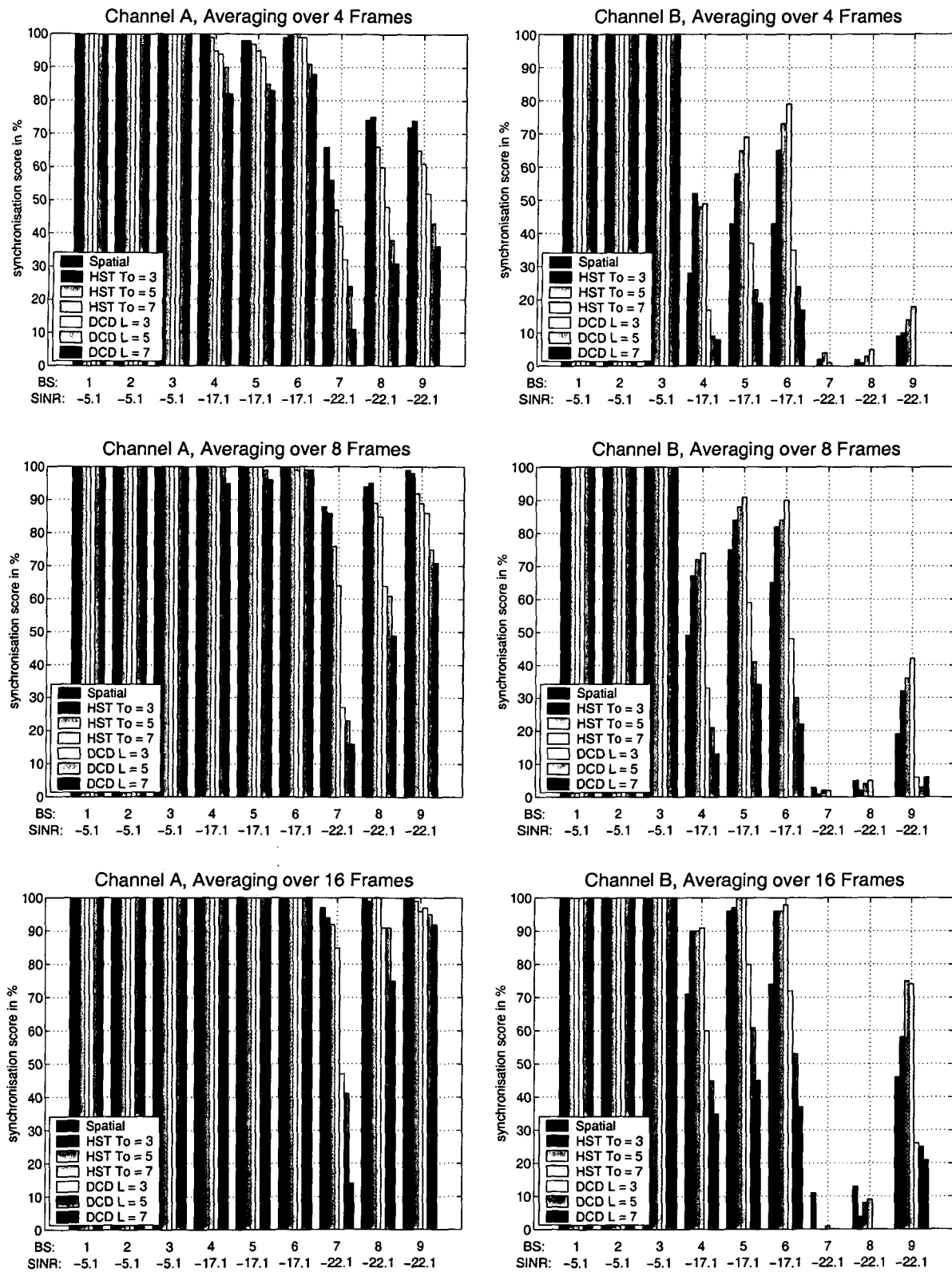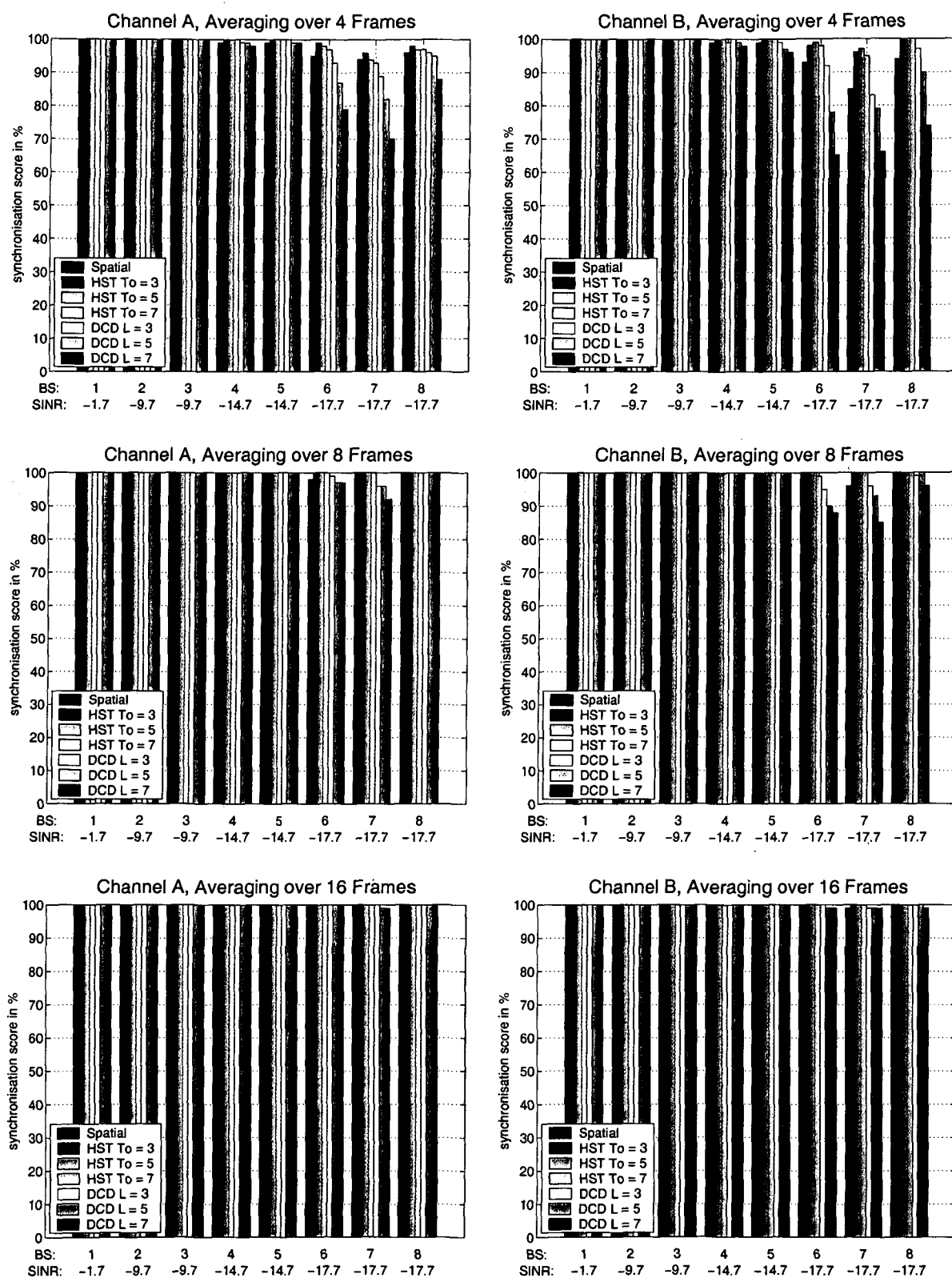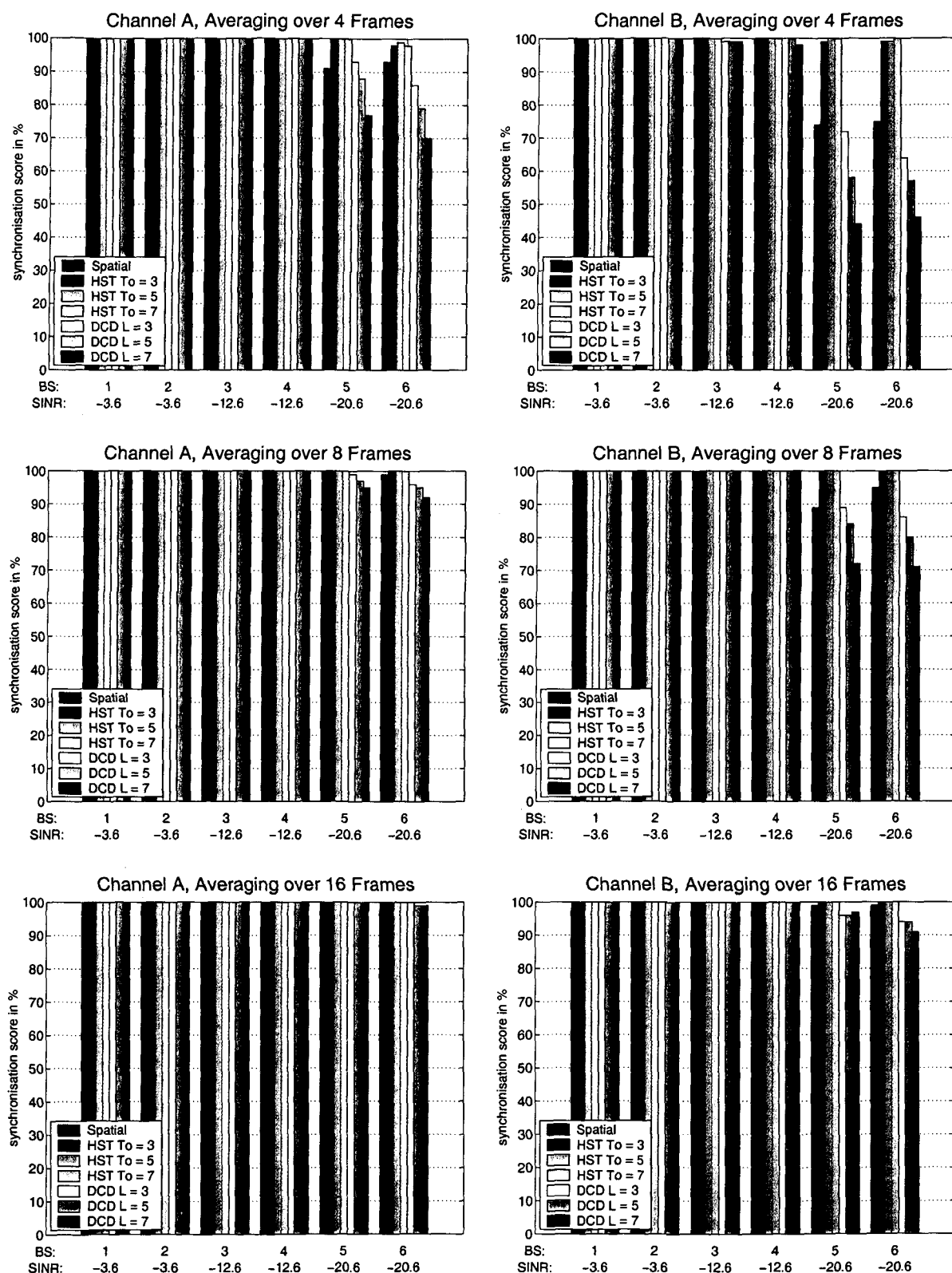
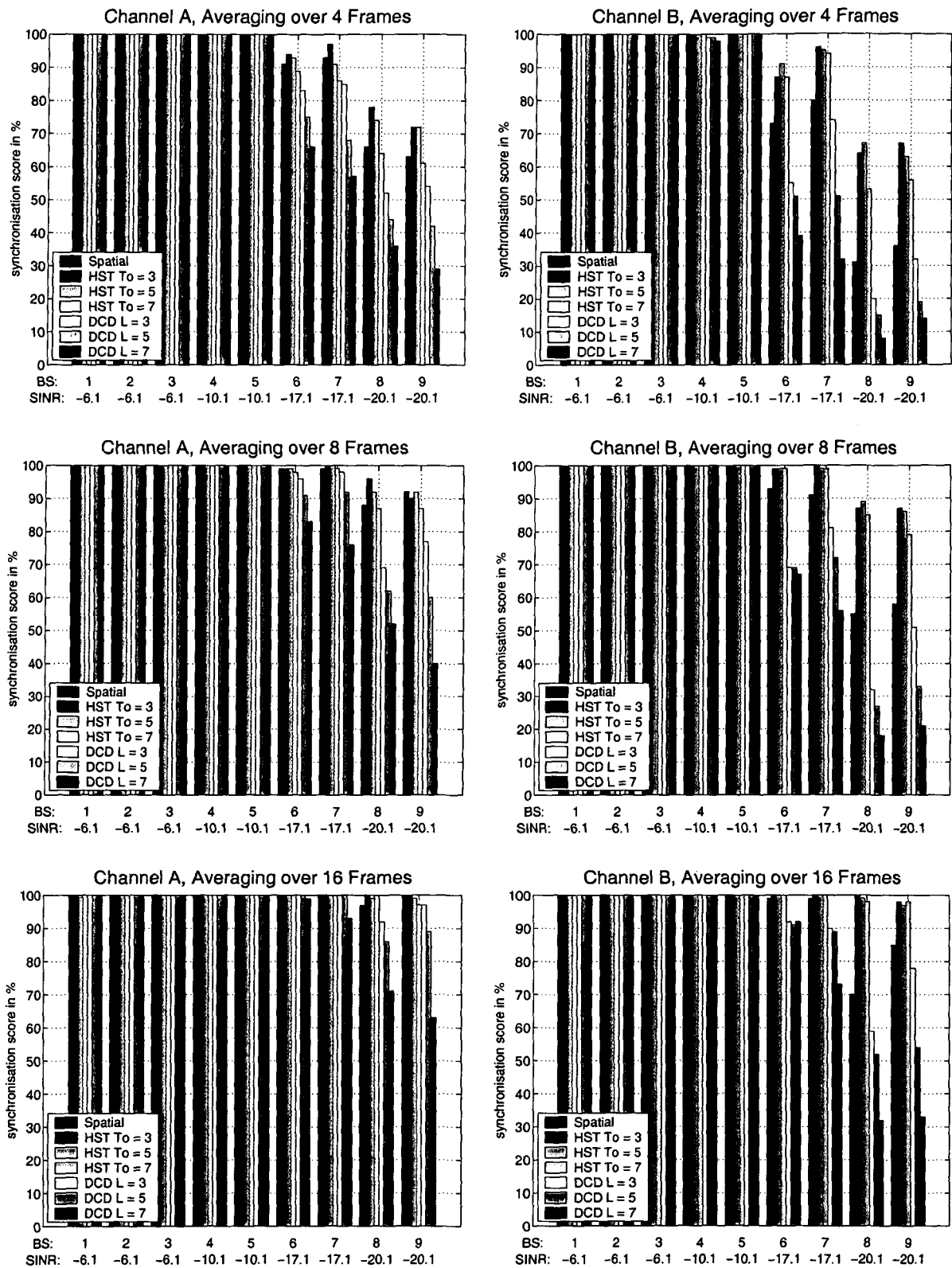Figure 4.11: *Percentage of successful synchronisation events for the indoor environment, scenario 2.*

Figure 4.12: *Percentage of successful synchronisation events for the indoor environment, scenario 3.*

same. This is due to the chosen code group allocation, which assigns code groups 2–9 to base stations 1–8. Since the SCH time offsets of two adjacent code groups differ by only 48 chips, while the synchronisation code length is 256 chips, base station 3, which is 7 dB stronger than base station 4, impairs the synchronisation process of base station 4. This behaviour is more severe for significant multipath propagation, where the good auto-correlation properties of the primary synchronisation code are partially lost.

The *heuristic space-time detector* has been simulated with three different temporal window lengths T_0. For the short channel A, the smallest window of $T_0 = 3$ samples is sufficient to achieve synchronisation scores of 100 % for averaging over 16 frames. Nevertheless, the longer time windows perform nearly equally well. For channel B, the advantage of a longer temporal window becomes obvious. For a window length of 7, the synchronisation score for the weakest base stations (SINR of −22 dB) is roughly doubled compared to the purely spatial method. But due to the hostile channel, the absolute performance is still only on the order of 50 %.

The *dispersive-channel detector* performs unexpectedly poor. The performance for both channels is in the range of the spatial detector or even worse. The best results are obtained with assumed channel length $L = 3$, while the performance drops for $L = 5$ and $L = 7$. A possible explanation for this behaviour is that the dispersive-channel detector is based on the most complex model of all methods. The unknown channel is matrix-valued, requiring the estimation of many parameters. It seems to be better to use a theoretically less accurate model that contains fewer parameters. These fewer parameters can then be estimated with higher accuracy, which leads to improved detection performance compared to a model with more, but less accurately estimated parameters.

For **scenario 2** (Figure 4.8), the results are similar to those for scenario 1. All three methods perform well for channel A when averaged over 8 or 16 frames. For channel B, the heuristic space-time detector is again superior, and with window length $T_0 = 7$, synchronisation scores of over 50 % can be obtained down to an SINR of −20 dB if averaging over 16 frames is used.

Scenario 3 (Figure 4.9) is the most challenging one. Especially for channel B, the weak base stations with an SINR of −22.1 dB cannot be detected reliably. But nevertheless, all methods except the dispersive-channel detector achieved good synchronisation performance down to an SINR of −17 dB.

Indoor Environment

In the indoor environment (Figures 4.10–4.12), the overall synchronisation results are very good. For **scenario 1** (Figure 4.10) with averaging over 16 frames, all algorithms nearly reach the 100 % level even for the weakest base stations (SINR = −17.7 dB) and for the longer channel B. But even if we average over only 8 frames, the performance of the spatial and the heuristic space-time detectors does not degrade. Only the dispersive-channel detector slightly falls short of the 100 % level, especially for assumed channel lengths of 5 and 7 samples. However, a synchronisation score of over 90 % is easily obtained in any case.

For *scenario 2* (Figure 4.11), the situation is very similar, since again all algorithms perform nearly perfectly. More specifically, the heuristic space-time detector performs best and requires only averaging over 4 frames, especially with a temporal window length of 7 samples.

In the most challenging *scenario 3* (Figure 4.12), the spatial detector and the dispersive-channel detector have problems to detect the weakest base stations with an SINR of -20.1 dB. The heuristic space-time detector, on the other hand, performs sufficiently well even for these weak base stations with all three temporal window lengths.

Conclusions

In conclusion, we can state that the synchronisation performance in the pedestrian environment is generally poorer than in the indoor environment. Nevertheless, reliable synchronisation is possible at least down to an SINR of about -18 dB for channel B, and even down to an SINR of -22 dB for channel A. We also see that averaging significantly improves the synchronisation performance of all three detection methods. Finally, the heuristic space-time detector shows the best performance of all presented methods, regardless of the temporal window length.

Chapter 5

Channel Estimation

After synchronisation to the surrounding base stations has been successful, the next step towards the decoding of the BCHs is channel estimation. In this chapter, we present a novel multiuser channel estimation scheme for the joint acquisition of the channel impulse responses of all base stations which were detected in the synchronisation stage.

The model for the discrete-time baseband signal vector $\mathbf{x}(n)$, collected at the M antenna elements of the receiver, is again given by (cf. (4.1))

$$\mathbf{x}(n) = \sum_{k=1}^{K} \mathbf{x}_k(n) + \mathbf{n}(n) \quad \text{with} \quad \mathbf{x}_k(n) = \sum_{p=0}^{L-1} \mathbf{h}_{k,p}\, s_k(n-p). \tag{5.1}$$

Here, the received contribution $\mathbf{x}_k(n)$ of the kth base station is resulting from a signal $s_k(n)$ transmitted via a multipath channel with taps $\mathbf{h}_{k,p}$, and $\mathbf{n}(n)$ is a Gaussian noise vector. K denotes the the number of base stations and L is the maximum length of all K channels. Reformulating the right-hand side of (5.1) in matrix notation, we obtain

$$\mathbf{x}_k(n) = \mathbf{H}_k\, \mathbf{s}_k(n), \tag{5.2}$$

where the $M \times L$ matrix

$$\mathbf{H}_k \triangleq \begin{bmatrix} \mathbf{h}_{k,0} & \dots & \mathbf{h}_{k,L-1} \end{bmatrix} \tag{5.3}$$

contains the channel taps of the kth base station.[1] The $L \times 1$ vector

$$\mathbf{s}_k(n) \triangleq \begin{bmatrix} s_k(n) \\ s_k(n-1) \\ \vdots \\ s_k(n-L+1) \end{bmatrix}$$

is composed of delayed versions of $s_k(n)$. Because the UMTS/TDD network is synchronised, the BCHs of all base stations are transmitted in the same timeslot and the

---

[1]If the channel of the kth base station has only $L_k < L$ taps, the remaining channel tap vectors $\mathbf{h}_{k,i}$, $i = L_k, \dots, L-1$ are zero.

midambles are temporally aligned. For channel estimation, it is hence sufficient to consider $\mathbf{x}(n)$ only in the time interval corresponding to the midambles, whose location is known from the synchronisation stage. For simplicity of notation, we will denote this interval as $[0, N-1]$, where $N = 512$ chips is the midamble length. Within this interval, our implicit assumption in (5.1), that the channel is time-invariant, is satisfied, since the channel $\mathbf{h}_{k,p}(n_s)$ in (2.4) only changes from slot to slot.

5.1 Midamble Estimation

As described in Chapter 3, UMTS/TDD uses eight midambles $m_k^{(l)}(n)$ ($l \in \{1,\ldots,8\}$) per base station [3GP01a]. These midambles are constructed from a single cell-specific basic midamble code that is known to the receiver from the synchronisation stage. The BCH always uses $m_k^{(1)}(n)$ and each data channel uses one of the six midambles $m_k^{(3)}(n),\ldots,m_k^{(8)}(n)$. The remaining midamble $m_k^{(2)}(n)$ is reserved for BCH transmit diversity, which will not be considered here. The *total midamble* transmitted by the kth base station is thus given by (see Figure 5.1)

$$m_k(n) \;=\; a_{\text{ref}}\, m_k^{(1)}(n) \;+\; \sum_{l \in \mathcal{L}_k} a_k^{(l)}\, m_k^{(l)}(n)\,, \tag{5.4}$$

where the index set $\mathcal{L}_k \subseteq \{3,\ldots,8\}$ specifies the midambles used by the data channels of the kth base station. Since the number of data channels present in the BCH timeslot is unknown, we do not know the index sets $\mathcal{L}_k$ *a priori*. The amplitude a_{ref} of the BCH midamble is fixed and known, whereas the amplitudes of the data channel midambles $a_k^{(l)}$ are unknown due to the effects of power control used for the associated data channels.
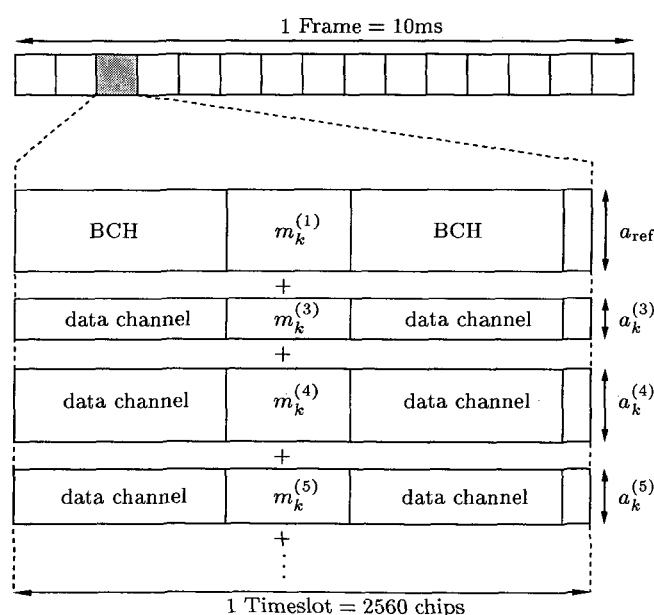

Figure 5.1: *Structure of a BCH timeslot (cf. Figure 3.6).*

58

With (5.4), the data model (5.1) for the midamble interval of the kth base station signal becomes

$$\mathbf{x}_k(n) = \sum_{p=0}^{L-1} \mathbf{h}_{k,p}\, m_k(n-p) \quad \text{with} \quad n = 0, \ldots, N-1. \tag{5.5}$$

Ideally, channel estimation would utilise the total midambles $m_k(n)$ in (5.5). Unfortunately, the composition of the $m_k(n)$ (i.e., the midamble index sets $\mathcal{L}_k$ and midamble amplitudes $a_k^{(l)}$) is unknown at the receiver. Using only the BCH midamble $m_k^{(1)}(n)$ (which is always present) with its known amplitude a_{ref} would be suboptimal, because the midambles of the data channels would act as interferers. Thus, prior to channel estimation, we will estimate the total midambles $m_k(n)$ by detecting the index sets $\mathcal{L}_k$ and estimating the amplitudes $a_k^{(l)}$.

5.1.1 Basic Midamble Estimation

The estimation of the midamble index sets $\mathcal{L}_k$ is a code detection problem similar to that of detecting the synchronisation codes in the synchronisation stage. We can thus use the same detection algorithms as in Chapter 4. Considering the spatial detector[1] (Section 4.1.1) with the lth midamble code of the kth base station, $m_k^{(l)}(n)$, as a reference sequence, we obtain the GLRT test statistic (cf. (4.20))

$$c_k^{(l)} = \frac{1}{N\|m_k^{(l)}\|^2}\, \hat{\mathbf{r}}_{\mathbf{x}m_k^{(l)}}^H\, \hat{\mathbf{R}}_{\mathbf{x}}^{-1}\, \hat{\mathbf{r}}_{\mathbf{x}m_k^{(l)}}, \tag{5.6}$$

where

$$\hat{\mathbf{R}}_{\mathbf{x}} = \frac{1}{N}\sum_{n=0}^{N-1}\mathbf{x}(n)\,\mathbf{x}^H(n),$$

$$\hat{\mathbf{r}}_{\mathbf{x}m_k^{(l)}} = \sum_{n=0}^{N-1}\mathbf{x}(n)\,m_k^{(l)*}(n). \tag{5.7}$$

The detected midamble set $\hat{\mathcal{L}}_k$ is now given as the set of indices $l \in \{3, \ldots, 8\}$ for which $c_k^{(l)}$ exceeds a certain threshold η. The choice of η is quite delicate because it corresponds to a tradeoff between high detection probability and low false alarm probability. If η is too low, we will detect midambles that are not being used; if it is too high, we will miss some midambles. As in the synchronisation stage, we will use a certain predefined level of false alarm probability to set η.

---

[1] The heuristic space-time detector performed better than the spatial detector in the synchronisation stage. But since the spatial detector also yields *amplitude estimates*, as shown below, we use it instead of the heuristic space-time detector for basic midamble estimation.

For estimation of the midamble amplitudes $a_k^{(l)}$, we propose a simple scheme that can be motivated as follows. Consider the case of a one-tap channel per base station (i.e., $L = 1$ or $\mathbf{H}_k = \mathbf{h}_{k,0} \triangleq \mathbf{h}_k$), orthogonal midamble sequences $m_k^{(l)}(n)$, and no noise. Then,

$$\mathbf{x}(n) = \sum_{k=1}^{K} \mathbf{h}_k \left[a_{\mathrm{ref}}\, m_k^{(1)} + \sum_{l \in \mathcal{L}_k} a_k^{(l)}\, m_k^{(l)} \right],$$

and thus (5.7) becomes

$$\hat{\mathbf{r}}_{\mathbf{x} m_k^{(l)}} = \| m_k^{(l)} \|^2\, a_k^{(l)}\, \mathbf{h}_k,$$

where $a_k^{(1)} \triangleq a_{\mathrm{ref}}$. Since the entries of $m_k^{(l)}(n)$ are powers of j, we have $\| m_k^{(l)} \|^2 = N$ and thus (5.6) can be written as

$$c_k^{(l)} = a_k^{(l)2}\, \mathbf{h}_k^H\, \hat{\mathbf{R}}_{\mathbf{x}}^{-1}\, \mathbf{h}_k.$$

We then obtain

$$\frac{c_k^{(l)}}{c_k^{(1)}} = \left(\frac{a_k^{(l)}}{a_{\mathrm{ref}}} \right)^2,$$

and hence

$$a_k^{(l)} = a_{\mathrm{ref}} \sqrt{\frac{c_k^{(l)}}{c_k^{(1)}}}. \tag{5.8}$$

In practice, the above-mentioned assumptions will be satisfied only approximately. Nevertheless, we can use the right-hand side of (5.8) as an estimate $\hat{a}_k^{(l)}$ of the amplitude $a_k^{(l)}$ of the lth midamble of the kth base station. In our simulations, we observed these amplitude estimates to be quite good (cf. Section 5.4).

Finally, with the detected midamble set $\hat{\mathcal{L}}_k$ and the corresponding amplitude estimates $\hat{a}_k^{(l)}$, an estimate of the total midamble of the kth base station (cf. (5.4)) is obtained as

$$\hat{m}_k(n) = a_{\mathrm{ref}}\, m_k^{(1)}(n) + \sum_{l \in \hat{\mathcal{L}}_k} \hat{a}_k^{(l)} m_k^{(l)}(n).$$

5.1.2 Maximum-Likelihood Midamble Estimation

The midamble estimation scheme presented above was based on very simplifying assumptions that do not necessarily hold in practice. In the following, we will derive a maximum-likelihood (ML) method for estimating the midamble amplitudes of the kth base station.

Let us assume for the moment that the channel impulse response of the kth base station $\mathbf{H}_k$ is known. We can reformulate (5.1) as

$$\mathbf{x}(n) = \mathbf{H}_k\, \mathbf{m}_k(n)\, a_{\mathrm{ref}} + \mathbf{H}_k\, \mathbf{M}_k(n)\, \mathbf{a}_k + \mathbf{w}(n). \tag{5.9}$$

Here, the $L \times 6$ matrix

$$\mathbf{M}_k(n) \triangleq \begin{bmatrix} m_k^{(3)}(n) & m_k^{(4)}(n) & \cdots & m_k^{(8)}(n) \\ m_k^{(3)}(n-1) & m_k^{(4)}(n-1) & \cdots & m_k^{(8)}(n-1) \\ \vdots & \vdots & & \vdots \\ m_k^{(3)}(n-L+1) & m_k^{(4)}(n-L+1) & \cdots & m_k^{(8)}(n-L+1) \end{bmatrix}$$

and the $L \times 1$ vector

$$\mathbf{m}_k(n) \triangleq \begin{bmatrix} m_k^{(1)}(n) \\ m_k^{(1)}(n-1) \\ \vdots \\ m_k^{(1)}(n-L+1) \end{bmatrix}$$

consist of current and delayed versions of the 6 possible data midambles and of the BCH midamble, respectively.[1] The 6×1 vector

$$\mathbf{a}_k \triangleq \begin{bmatrix} a_k^{(3)} \\ a_k^{(4)} \\ \vdots \\ a_k^{(8)} \end{bmatrix}$$

contains the unknown midamble amplitudes of the kth base station that will be estimated in the following, and $\mathbf{w}(n)$ summarises the interfering signals of the other $K-1$ base stations and noise. With the abbreviations

$$\mathbf{F}_k(n) \triangleq \mathbf{H}_k \, \mathbf{M}_k(n), \qquad \mathbf{y}_k(n) \triangleq \mathbf{x}(n) - \mathbf{H}_k \, \mathbf{m}_k(n) \, a_{\text{ref}},$$

we can formulate (5.9) as

$$\mathbf{y}_k(n) = \mathbf{F}_k(n) \, \mathbf{a}_k + \mathbf{w}(n) . \tag{5.10}$$

Stacking the real part $\mathbf{y}_{k,\text{Re}}(n)$ and the imaginary part $\mathbf{y}_{k,\text{Im}}(n)$ of $\mathbf{y}_k(n)$ into a real-valued $2M \times 1$ vector, we obtain the equivalent real-valued model of (5.10) as

$$\begin{bmatrix} \mathbf{y}_{k,\text{Re}}(n) \\ \mathbf{y}_{k,\text{Im}}(n) \end{bmatrix} = \begin{bmatrix} \mathbf{F}_{k,\text{Re}}(n) & -\mathbf{F}_{k,\text{Im}}(n) \\ \mathbf{F}_{k,\text{Im}}(n) & \mathbf{F}_{k,\text{Re}}(n) \end{bmatrix} \begin{bmatrix} \mathbf{a}_{k,\text{Re}} \\ \mathbf{a}_{k,\text{Im}} \end{bmatrix} + \begin{bmatrix} \mathbf{w}_{\text{Re}}(n) \\ \mathbf{w}_{\text{Im}}(n) \end{bmatrix} .$$

Since the unknown amplitude vector $\mathbf{a}_k$ is real-valued ($\mathbf{a}_{k,\text{Im}} = \mathbf{0}$), we can simplify the real-valued model to

$$\begin{bmatrix} \mathbf{y}_{k,\text{Re}}(n) \\ \mathbf{y}_{k,\text{Im}}(n) \end{bmatrix} = \begin{bmatrix} \mathbf{F}_{k,\text{Re}}(n) \\ \mathbf{F}_{k,\text{Im}}(n) \end{bmatrix} \mathbf{a}_{k,\text{Re}} + \begin{bmatrix} \mathbf{w}_{\text{Re}}(n) \\ \mathbf{w}_{\text{Im}}(n) \end{bmatrix} ,$$

or short

$$\tilde{\mathbf{y}}_k(n) = \tilde{\mathbf{F}}_k(n) \, \mathbf{a}_{k,\text{Re}} + \tilde{\mathbf{w}}(n). \tag{5.11}$$

---

[1]Note that $m_k^{(l)}(n) = 0$ for $n < 0$.

Because we only have to estimate the real part of $\mathbf{a}_k$ in (5.11), the number of unknowns is halved compared to (5.10), and we can expect the simplified real-valued model (5.11) to offer greater estimation accuracy than the complex-valued model (5.10). Assuming that the interference $\tilde{\mathbf{w}}(n)$ in (5.11) is temporally white and Gaussian with known spatial correlation matrix $\mathbf{R}_{\tilde{\mathbf{w}}}$ (i.e., $\mathrm{E}\{\tilde{\mathbf{w}}(n + n')\,\tilde{\mathbf{w}}^H(n)\} = \mathbf{R}_{\tilde{\mathbf{w}}}\,\delta(n')$), we obtain the likelihood function of $\tilde{\mathbf{y}}_k(n)$ as

$$f(\tilde{\mathbf{y}}_k; \mathbf{a}_k) = \frac{1}{\sqrt{(2\pi)^{2MN}(\det \mathbf{R}_{\tilde{\mathbf{w}}})^N}}\, e^{-\frac{1}{2}\sum_{n=0}^{N-1}\left[\tilde{\mathbf{y}}_k(n) - \tilde{\mathbf{F}}_k(n)\,\mathbf{a}_k\right]^T \mathbf{R}_{\tilde{\mathbf{w}}}^{-1}\left[\tilde{\mathbf{y}}_k(n) - \tilde{\mathbf{F}}_k(n)\,\mathbf{a}_k\right]}. \tag{5.12}$$

Setting the derivative of (5.12)[1] with respect to $\mathbf{a}_k$ equal to zero, we obtain the ML estimate of the midamble amplitudes as

$$\hat{\mathbf{a}}_{k,\mathrm{ML}} = \left[\sum_{n=0}^{N-1}\tilde{\mathbf{F}}_k^T(n)\,\mathbf{R}_{\tilde{\mathbf{w}}}^{-1}\,\tilde{\mathbf{F}}_k(n)\right]^{-1}\sum_{n=0}^{N-1}\tilde{\mathbf{F}}_k^T(n)\,\mathbf{R}_{\tilde{\mathbf{w}}}^{-1}\,\tilde{\mathbf{y}}_k(n). \tag{5.13}$$

As mentioned above, knowledge of the channel matrix $\mathbf{H}_k$ of the kth base station and the spatial interference correlation matrix $\mathbf{R}_{\tilde{\mathbf{w}}}$ is needed to compute $\hat{\mathbf{a}}_{k,\mathrm{ML}}$ in (5.13), but this knowledge is obviously not available prior to channel estimation. To break this deadlock, we use the basic midamble estimation algorithm of Section 5.1.1 in a first stage and perform channel estimation with the estimated midambles. The resulting channel estimate, together with an estimate of $\mathbf{R}_{\tilde{\mathbf{w}}}$ which is gained from the interference estimate

$$\hat{\mathbf{w}}(n) = \mathbf{x}(n) - \hat{\mathbf{H}}_k\,\mathbf{m}_k(n)\,a_{\mathrm{ref}} - \hat{\mathbf{H}}_k\,\mathbf{M}_k(n)\,\hat{\mathbf{a}}_k,$$

can then be used in a second stage by the ML midamble estimation algorithm to improve the midamble estimates. Finally, the channel is re-estimated using the improved midamble estimates.

5.2 MMSE Channel Estimation

Having estimated the midambles, we will now use them to perform the actual channel estimation step. In the following, we will develop a minimum-mean-square-error (MMSE) channel estimator that yields the channels of all base stations which were detected in the synchronisation stage.

For simplicity, we will estimate the channels associated to different antenna elements separately. This is theoretically optimal only if the fading for different antenna elements is uncorrelated. In practice, this will not always be the case[2] and the joint MMSE channel estimator over all antennas would then be superior. On the other hand, an MMSE channel estimator requires knowledge of the channel's second order moments, which are not

---

[1] Or equivalently the logarithm of (5.12).

[2] For instance in line-of-sight (LOS) situations.

available and have to be estimated. Thus, the joint-antenna MMSE estimator additionally requires estimation of the channel's cross-correlations for different antenna elements. The estimation errors resulting from this higher estimation effort must be expected to decrease the potential gain for correlated antennas that the joint-antenna MMSE channel estimation algorithm offers in theory.[1] Therefore, we choose the simpler approach and perform MMSE channel estimation separately for each antenna.

Channels of different base stations are statistically independent. Since their cross-correlations thus vanish, we do not have to estimate them and the above-mentioned problems do not exist. It is hence possible to jointly estimate all base station channels in a multiuser fashion. Let us partition the channel matrix $\mathbf{H}_k$ in (5.3) as

$$\mathbf{H}_k = \begin{bmatrix} \mathbf{g}_{k,1}^T \\ \vdots \\ \mathbf{g}_{k,M}^T \end{bmatrix}. \tag{5.14}$$

Here, the $L \times 1$ vector $\mathbf{g}_{k,i}$ contains the L taps of the channel impulse response corresponding to the kth base station and the ith antenna element. The multiuser (all k) input-output relation for the ith antenna element can then be formulated as

$$\mathbf{x}_i = \mathbf{C}\mathbf{h}_i + \mathbf{n}_i, \tag{5.15}$$

where the signal received at the ith antenna element is stacked into the $(N + L - 1) \times 1$ vector

$$\mathbf{x}_i \triangleq \begin{bmatrix} x_i(0) \\ x_i(1) \\ \vdots \\ x_i(N - 1 + L - 1) \end{bmatrix}. \tag{5.16}$$

Furthermore, the $LK \times 1$ vector

$$\mathbf{h}_i \triangleq \begin{bmatrix} \mathbf{g}_{1,i} \\ \vdots \\ \mathbf{g}_{K,i} \end{bmatrix} \tag{5.17}$$

contains the unknown channel impulse responses of all K base stations for the ith antenna. The $(N + L - 1) \times LK$ midamble matrix $\mathbf{C}$ is defined as

$$\tag{5.18}$$

---

where

$$\mathbf{m}_k \triangleq \begin{bmatrix} m_k(0) \\ m_k(1) \\ \vdots \\ m_k(N-1) \end{bmatrix}$$

is the total midamble vector of the kth base station (cf. (5.4)). Finally, $\mathbf{n}_i$ is a white Gaussian noise vector defined similarly to $\mathbf{x}_i$ in (5.16).

Assuming the channel impulse response vector $\mathbf{h}_i$ in (5.15) to be zero-mean Gaussian,[1] its MMSE estimate is [Sch91]

$$\hat{\mathbf{h}}_{i,\text{MMSE}} = \left(\mathbf{C}^H\mathbf{C} + \sigma^2\,\mathbf{R_h}^{-1}\right)^{-1}\mathbf{C}^H\mathbf{x}_i\,, \qquad (5.19)$$

where $\mathbf{R_h}$ denotes the covariance matrix of $\mathbf{h}_i$ (in practice, $\mathbf{R_h}$ does not depend on the antenna index i) and σ^2 is the noise variance. Note that via (5.17) and (5.14) we can convert the vectors $\hat{\mathbf{h}}_{i,\text{MMSE}}$ back into MMSE estimates $\hat{\mathbf{H}}_{k,\text{MMSE}}$ of the channel matrices $\mathbf{H}_k$ in (5.2).

Whereas an estimate $\hat{\mathbf{C}}$ of the midamble matrix $\mathbf{C}$ is achieved by using in (5.18) the estimated midambles obtained by one of the midamble estimation algorithms, $\mathbf{R_h}$ and σ^2 are *unknown* a priori. Therefore, we first calculate the least-squares (LS) channel estimate [Sch91]

$$\hat{\mathbf{h}}_{i,\text{LS}} = (\hat{\mathbf{C}}^H\hat{\mathbf{C}})^{-1}\hat{\mathbf{C}}^H\mathbf{x}_i\,, \qquad (5.20)$$

which does not require knowledge of $\mathbf{R_h}$ and σ^2.

If the second-order statistics of the channel do not change over time,[2] we can use the LS channel estimates $\hat{\mathbf{h}}_{i,\text{LS}}$ of the N_f recorded frames to estimate $\mathbf{R_h}$. Under the uncorrelated scattering assumption [Bel63], the elements of $\mathbf{h}_i$ (i.e. the channel taps) are uncorrelated and hence $\mathbf{R_h}$ is a diagonal matrix. An estimate of $\mathbf{R_h}$ is thus given by

$$\hat{\mathbf{R}}_\mathbf{h} = \begin{bmatrix} \widehat{\sigma_h^2}(1) & & 0 \\ & \ddots & \\ 0 & & \widehat{\sigma_h^2}(LK) \end{bmatrix},$$

where $\widehat{\sigma_h^2}(j)$ is the sample variance of the jth element of $\hat{\mathbf{h}}_{i,\text{LS}}$ computed over the M antenna elements and the N_f frames. Furthermore, an estimate $\widehat{\sigma^2}$ of the noise variance σ^2 is obtained as the sample variance computed from all elements of the noise vector estimates

$$\hat{\mathbf{n}}_i = \mathbf{x}_i - \hat{\mathbf{C}}\hat{\mathbf{h}}_{i,\text{LS}},$$

again using averaging over all antenna elements and recorded frames. With the estimates $\hat{\mathbf{C}}$, $\hat{\mathbf{R}}_\mathbf{h}$, and $\widehat{\sigma^2}$, we can finally compute the MMSE channel estimate $\hat{\mathbf{h}}_{i,\text{MMSE}}$ in (5.19) as

$$\hat{\mathbf{h}}_{i,\text{MMSE}} = \left(\hat{\mathbf{C}}^H\hat{\mathbf{C}} + \widehat{\sigma^2}\,\hat{\mathbf{R}}_\mathbf{h}^{-1}\right)^{-1}\hat{\mathbf{C}}^H\mathbf{x}_i\,. \qquad (5.21)$$

---

[1]This is the case e.g. for Rayleigh fading.

[2]This corresponds to the wide-sense-stationary assumption [Bel63].

The overall structure of the MMSE channel estimator is summarised in Figure 5.2. Note that for midamble estimation and the estimation of $\mathbf{R_h}$ and σ^2, all M antenna signals are used jointly, whereas LS and MMSE channel estimation are performed separately for each antenna element, using only the associated antenna signal $\mathbf{x}_i$.
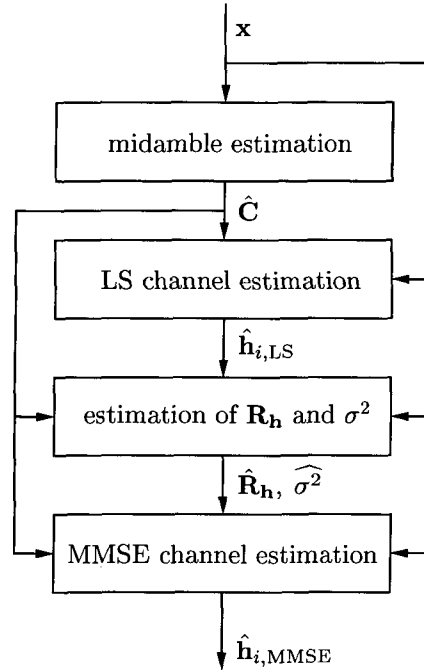

Figure 5.2: *Block diagram of the MMSE channel estimator.*

Figures 5.3 and 5.4 show simulation results obtained with the LS and MMSE channel estimators using basic midamble estimation (see Section 5.1.1) for $M = 5$ antenna elements and the simulation scenarios described in Section 2.2. As a performance measure, we use the normalised mean-square error (MSE) of the estimated channel impulse response matrices $\hat{\mathbf{H}}_k$. It is obtained by averaging channel estimation results over 100 simulation runs consisting of 16 transmitted frames each. For each base station (characterised on the abscissa by the number and respective SINR value), the normalised MSE is indicated by the height of two bars corresponding to (from the left) the LS and MMSE channel estimators.

The performance of the LS estimator turns out to be quite poor. Except for the strongest base stations in the indoor environment, where an MSE of around $-10\,$dB is obtained, the MSE is well above $0\,$dB.[1] Nevertheless, this accuracy level seems to be high enough to properly estimate the channel statistics, because the MMSE estimator (that uses the LS estimator for estimating $\mathbf{R_h}$ and σ^2) shows good estimation accuracy. In the indoor environment for channel A, the MSE of the MMSE estimator is below $-10\,$dB down to an SINR of about $-18\,$dB. For indoor channel B, the performance degrades significantly

---

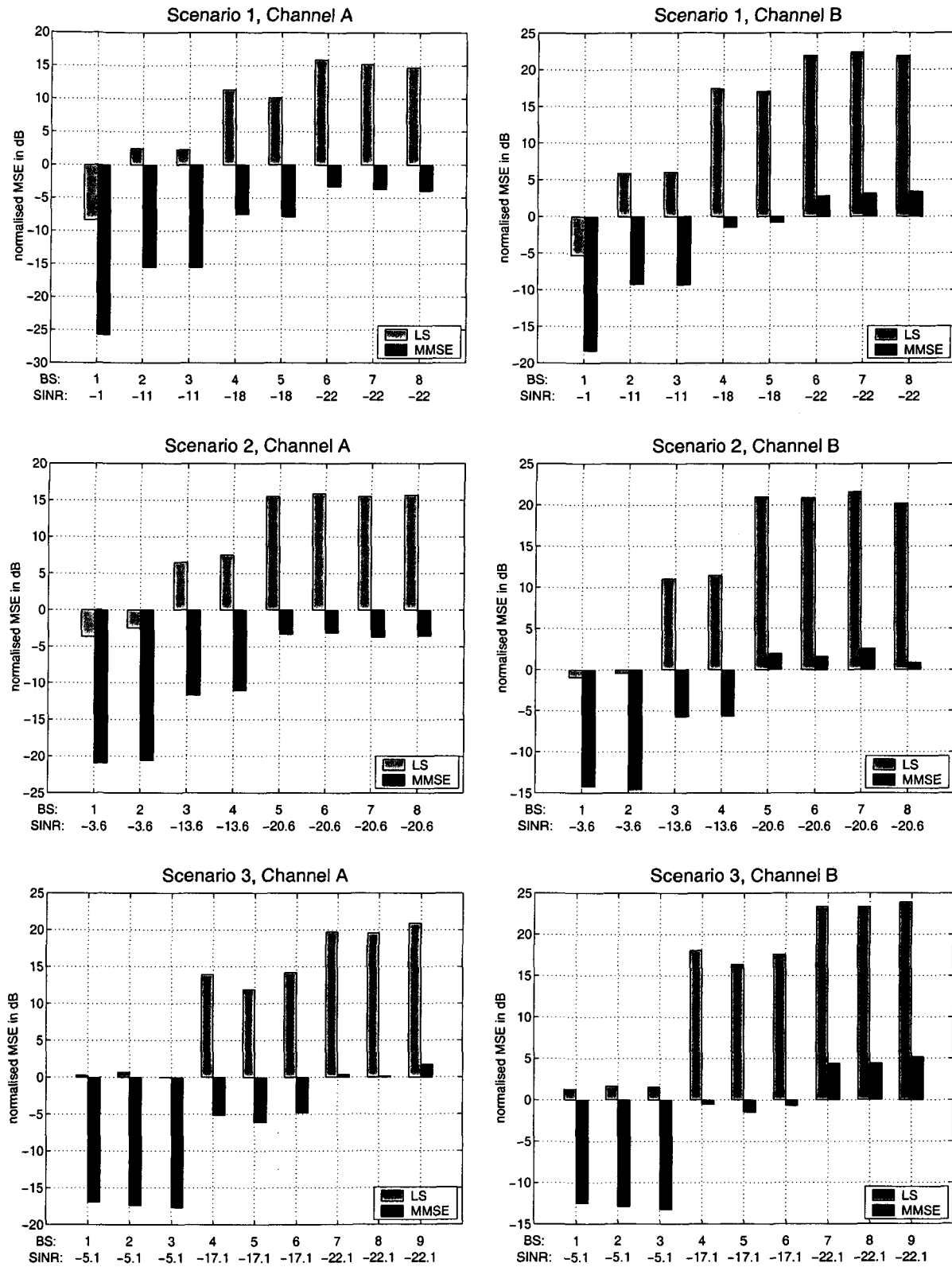[1]Note that this corresponds to an error level greater than 100 %.

65

Figure 5.3: *Normalised MSE in dB obtained with the LS and MMSE channel estimators for the pedestrian environment.*
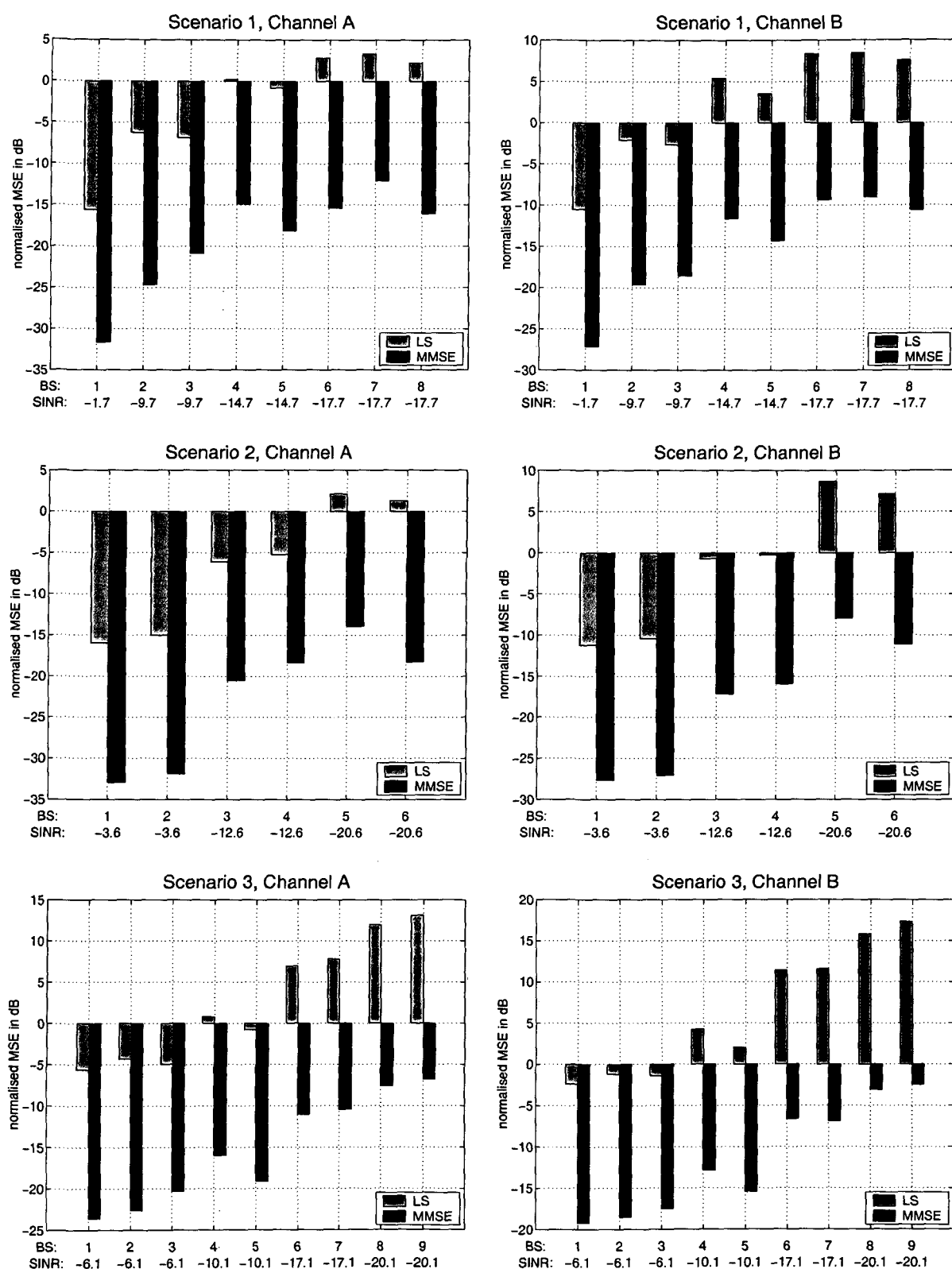
66

Figure 5.4: *Normalised MSE in dB obtained with the LS and MMSE channel estimators for the indoor environment.*

but the MSE still lies below $-2\,\mathrm{dB}$, even for the weakest base station in scenario 3. In the pedestrian environment, however, the performance of the MMSE channel estimator for weak base stations is not satisfactory anymore. While for channel A, the MSE is about $-3\,\mathrm{dB}$ for an SINR of about $-20\,\mathrm{dB}$, for channel B it is only in the range of $0\,\mathrm{dB}$ for an SINR of about $-20\,\mathrm{dB}$.

5.3 The SC-MMSE Channel Estimator

The results in Figures 5.3 and 5.4 showed that MMSE channel estimation for the weaker base stations sometimes does not perform well enough. Although we are performing multiuser channel estimation, the influence of the strong base stations impairs the channel estimation accuracy of the weak base stations.

To enhance channel estimation performance of the weak base stations, we propose to recursively apply the MMSE estimator within a successive interference cancellation scheme. This results in the novel *successive cancellation MMSE* (SC-MMSE) channel estimator that is depicted in Figure 5.5. Here, the shaded area marks the MMSE estimator of Figure 5.2 that is embedded in the successive interference cancellation loop. In every round of the successive scheme, only the MMSE channel estimate of the strongest base station is retained and used to reconstruct the midamble part of the strongest base station's signal. This estimated midamble part $\hat{\mathbf{x}}_{k_s}$ is then subtracted from the overall received vector $\mathbf{x}$. Because of the good accuracy of the channel estimate for the strongest base station, this cancellation step leads to an increased SINR for the weaker base stations and to improved midamble and channel estimation performance.

More specifically, we start by estimating the midambles of all K base stations by means of the basic midamble estimation algorithm (cf. Section 5.1.1) and construct the estimate $\hat{\mathbf{C}}$ of the midamble matrix $\mathbf{C}$. For every antenna element, we then jointly estimate the channels of all K base stations using the LS channel estimation method (5.20). After having estimated $\mathbf{R_h}$ and σ^2 from the LS channel estimates $\hat{\mathbf{h}}_{i,\mathrm{LS}}$ of all antenna elements and recorded frames, we calculate the MMSE channel estimates $\hat{\mathbf{h}}_{i,\mathrm{MMSE}}$ of all base stations (see (5.21)). As before, this MMSE estimation scheme is performed separately on the different antennas but jointly for all base stations. From the $\hat{\mathbf{h}}_{i,\mathrm{MMSE}}$, we now construct only the channel matrix $\hat{\mathbf{H}}_{k_s,\mathrm{MMSE}}$ of the strongest base station (whose index is denoted as k_s), while the channel estimates of the other base stations are discarded. The midamble part of the signal of the strongest base station is then reconstructed as

$$\hat{\mathbf{x}}_{k_s}(n) = \hat{\mathbf{H}}_{k_s,\mathrm{MMSE}}\,\hat{\mathbf{m}}_{k_s}(n),$$

where $\hat{\mathbf{m}}_{k_s}(n) \triangleq [\hat{m}_{k_s}(n),\ \hat{m}_{k_s}(n-1),\ \dots,\ \hat{m}_{k_s}(n-L+1)]^T$. The influence of the strongest base station is finally removed by subtracting $\hat{\mathbf{x}}_{k_s}(n)$ from the received signal $\mathbf{x}(n)$.

In the next round, the procedure is repeated with $\mathbf{x}(n)$ replaced by $\mathbf{x}(n) - \hat{\mathbf{x}}_{k_s}(n)$, from which the channels of the remaining $K-1$ base stations are estimated. Because of the improved SINR, these estimates should be more accurate than the respective esti-
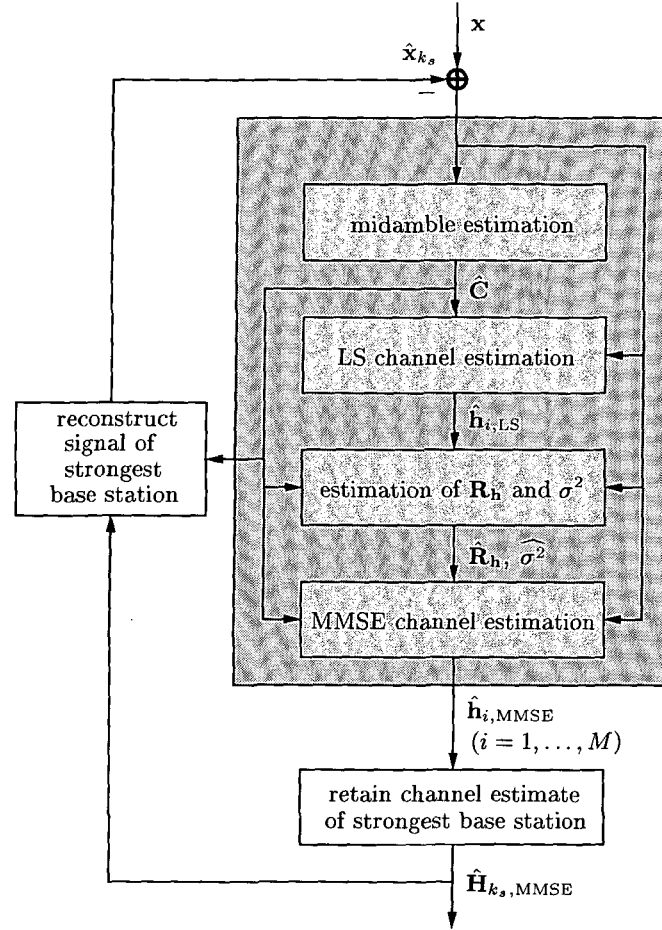
Figure 5.5: *Block diagram of the SC-MMSE channel estimator incorporating the MMSE channel estimator of Figure 5.2 (shaded area).*

mates obtained (but discarded) in the first round. This estimation-cancellation recursion continues until all channel estimates have been obtained.

After the SC-MMSE recursion using basic midamble estimation has terminated, we have estimates of the channels of all K base stations. With this knowledge, the SC-MMSE channel estimator can be repeated, this time using the ML midamble estimation scheme (cf. Section 5.1.2) instead of basic midamble estimation. This will lead to enhanced midamble estimation accuracy and, thus, improved channel estimation performance.

5.4 Simulation Results

Using the simulation scenarios of Section 2.2, we conducted Monte Carlo simulations to assess the performance of the SC-MMSE channel estimation scheme. Figures 5.6 and 5.7 show for each base station (characterised on the abscissa by the number and respective

SINR value) the normalised MSE obtained with the SC-MMSE channel estimator using either basic or ML midamble estimation. For comparison, we also included simulation results of the SC-MMSE channel estimator using the true midambles $m_k(n)$. For each scenario, we conducted 100 simulation rounds consisting of 16 frames each. The maximum channel length L, used by the channel estimation algorithms, was set to 7 chips for all scenarios. This value is sufficiently large for both indoor channels and for the pedestrian channel A. For pedestrian channel B, however, the true channel length exceeds L, which results in a systematic channel estimation error.

Pedestrian Environment

In the pedestrian environment (Figure 5.6), the basic SC-MMSE[1] estimates channel A nearly as accurately as the true SC-MMSE for all three scenarios. No great gains can hence be expected from the ML SC-MMSE, and indeed, somewhat surprisingly, its performance is even slightly poorer than that of the basic SC-MMSE. The MSE of all three methods is below $-4\,$dB down to an SINR of $-22\,$dB. For channel B, the true SC-MMSE performs best for the strongest base stations (SINR above $-10\,$dB), where the ML SC-MMSE loses from $4\,$dB (in scenarios 1 and 2) to $8\,$dB (in scenario 3). For the weaker base stations, the ML SC-MMSE shows comparable performance to the true SC-MMSE and achieves an MSE of around $-6\,$dB for an SINR of $-22\,$dB. The basic SC-MMSE performs worse than the ML SC-MMSE for all base stations, with its MSE being higher by 2 to 5 dB.

Indoor Environment

Figure 5.7 indicates that the relatively short indoor channels can be estimated with high accuracy. For channel A, the true SC-MMSE achieves an MSE of under $-20\,$dB for all base stations and even under $-30\,$dB for base stations with SINR above $-15\,$dB. But also for the basic SC-MMSE and the ML SC-MMSE, the MSE lies below $-20\,$dB for nearly all base stations. The ML SC-MMSE performs slightly better than the basic SC-MMSE: an MSE reduction of up to 2 dB is observed. For channel B, the ML SC-MMSE offers a performance improvement of up to about 3 dB only for scenario 3, in the other cases the performance of ML SC-MMSE and basic SC-MMSE is quite similar. Nevertheless, an MSE below $-15\,$dB is obtained by all three methods down to an SINR of $-20\,$dB.

Considering that the performance for the challenging scenario 3 is not significantly worse than for scenario 1, we can conclude that the SC-MMSE scheme is quite robust against strong interference. This can be attributed to the fact that we are using multiuser channel estimation in every stage of the successive interference cancellation scheme. Thus, the influence of interference on the current channel estimates is mitigated and the error that is passed on to the next stage is kept small.

---

[1]For simplicity, we will speak of the "basic SC-MMSE," the "ML SC-MMSE," and the "true SC-MMSE" instead of the SC-MMSE channel estimator using basic midamble estimation, ML midamble estimation, and true midambles, respectively.
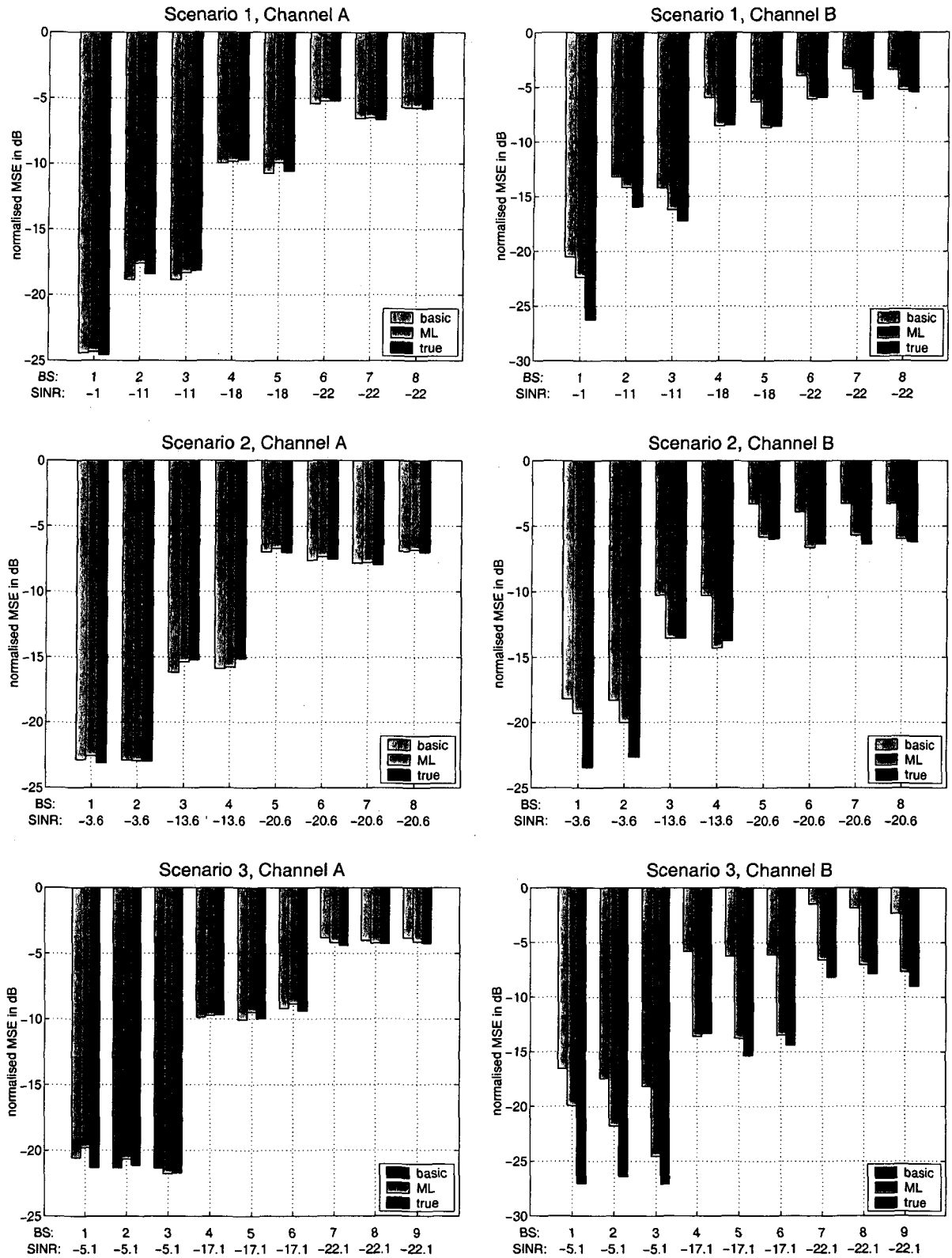
Figure 5.6: *Normalised MSE in dB obtained with the SC-MMSE channel estimator for the pedestrian environment.*
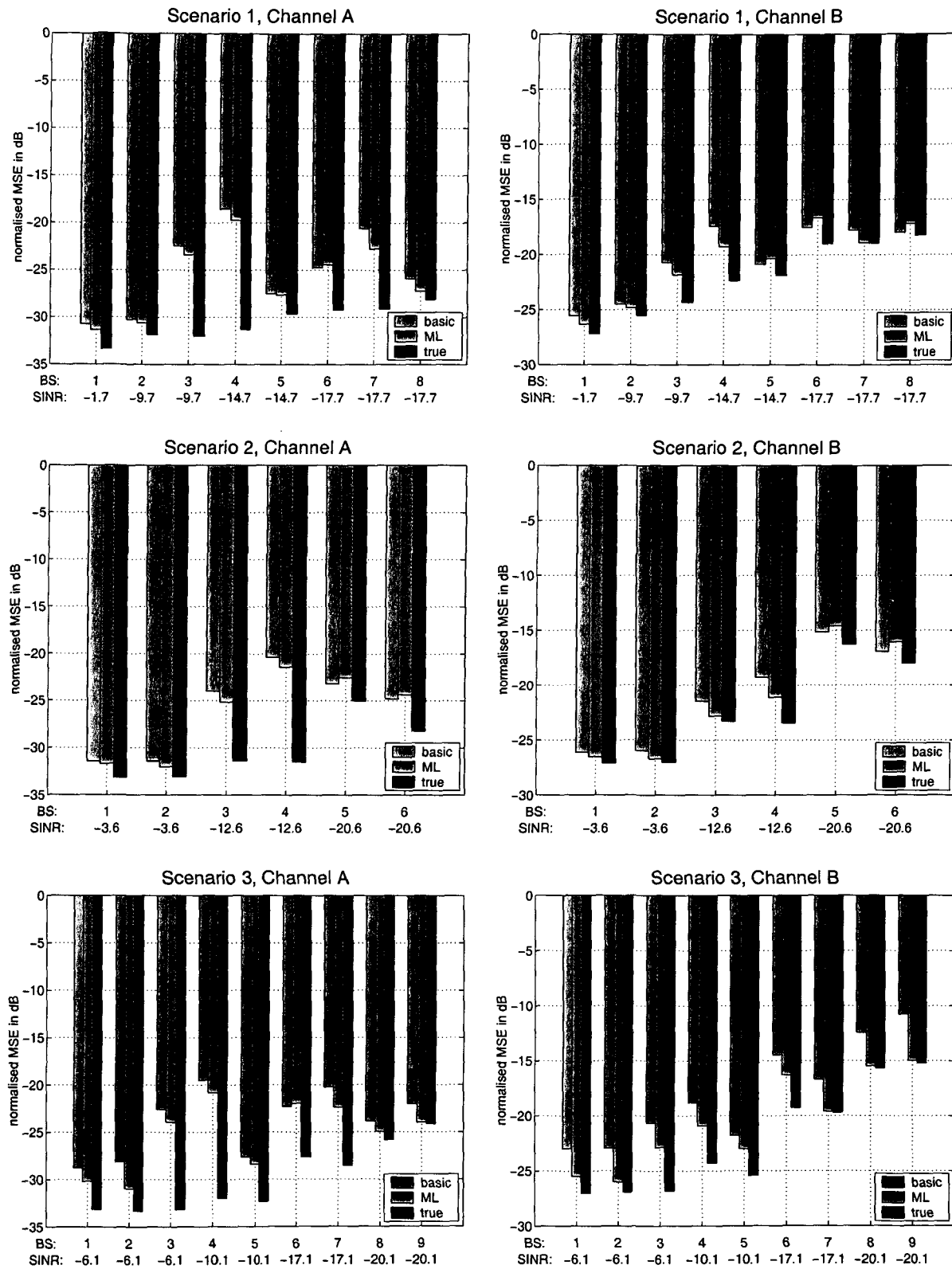
Figure 5.7: *Normalised MSE in dB obtained with the SC-MMSE channel estimator for the indoor environment.*

Conclusions

In conclusion, the basic SC-MMSE is sufficient in the indoor environment, where the MSE is below $-15\,\mathrm{dB}$ in nearly all cases. In the pedestrian environment, the performance of all methods is poorer for the weaker base stations, but for channel A the basic SC-MMSE still performs as well as the ML SC-MMSE. However, for channel B, the ML SC-MMSE is advantageous since it yields an MSE reduction of up to $7\,\mathrm{dB}$ for the weak base stations. Note further that the overall similarity of performance of the basic SC-MMSE and ML SC-MMSE on the one hand and the true SC-MMSE on the other hand indicates a high accuracy of the midamble estimates.

Chapter 6

Data Detection

After synchronisation and channel estimation have been performed, all prior knowledge needed to detect the BCH data transmitted by the K base stations is available. In this chapter, we present three different space-time detection algorithms that are based on the MMSE principle. Besides the conventional space-time MMSE detector, we will also use decision feedback techniques to mitigate the influence of co-channel interference. These detection techniques were developed by Harold Artés in the framework of the ANTIUM project. The article [AKH03] provided the basis of this chapter.

As mentioned previously, the BCHs of all base stations are transmitted in the same timeslot and it hence suffices to consider only this specific timeslot of the frame. Recall from Figure 3.3 (reproduced here in Figure 6.1 for the reader's convenience) that a timeslot consists of two data parts separated by a midamble and followed by a guard period. In

Data symbols 976 chips	Midamble 512 chips	Data symbols 976 chips	GP 96 CP

$$\longleftarrow \quad 2560^*T_c \quad \longrightarrow$$
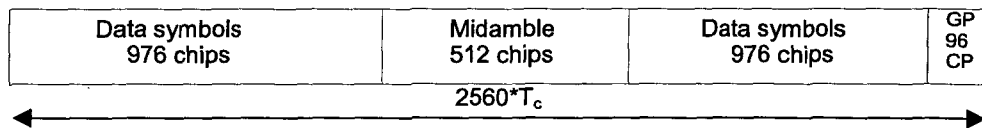
Figure 6.1: *Burst structure of burst type 1. GP denotes the guard period and CP the chip period* [3GP01a].

the timeslot of interest, the two data parts contain the BCH and up to 12 additional data channels. Each individual channel is spread using a unique spreading code with spreading factor $Q = 16$ [3GP01c]. The weighted sum of the spread channels is then scrambled with a base-station-specific scrambling code of length 16 chips [3GP01c], transmitted over a frequency-selective fading channel, and received by the M-element antenna array of the mobile receiver.

As in the previous chapters, the data model of the received signal is given as

$$\mathbf{x}(n) = \sum_{k=1}^{K} \mathbf{x}_k(n) + \mathbf{n}(n) \quad \text{with} \quad \mathbf{x}_k(n) = \sum_{p=0}^{L-1} \mathbf{h}_{k,p}\, s_k(n - p). \tag{6.1}$$

Here, the chip sequence $s_k(n)$ of base station k is the product of the total spreading codes[1] $c_k^{(l)}(m)$ and the data symbols $d_k^{(l)}(u)$ of the present data channels:

$$s_k(n) = c_k^{(1)}(m)\, d_k^{(1)}(u) + \sum_{l \in \mathcal{L}_k} a_k^{(l)} c_k^{(l)}(m)\, d_k^{(l)}(u),$$

where $m = [(n-1) \bmod Q] + 1$, the symbol time index u is given by $u = \lceil n/Q \rceil$, and the index set $\mathcal{L}_k \subseteq \{5, \ldots, 16\}$ denotes the set of active data channels for the kth base station.[2] The gain factors $a_k^{(l)}$ are due to power control of the corresponding data channels. Since the BCH is always transmitted with fixed reference power (no power control is used), we can normalise the gain factors such that $a_k^{(1)} = 1$.

Since the UMTS/TDD network is synchronised, data fields of all base stations are temporally aligned. In the detection stage it is thus sufficient to consider $\mathbf{x}(n)$ only in the time interval corresponding to the data fields, whose location is known from the synchronisation stage. We will cut out the midamble part in the following[3] and, for simplicity of notation, denote the time interval corresponding to the two data fields as $[1, NQ + L - 1]$. Here, $N = 122$ is the number of symbols in the two data fields, and L is the maximum channel length.

In the following we will reformulate (6.1) in a way such that the received chips $\mathbf{x}(n)$ of the data-field interval $[1, NQ + L - 1]$ depend on the input symbols $d_k^{(l)}(u)$, rather than on the input chips $s_k(n)$. In other words, we will include spreading and scrambling in the channel. Such a model, which maps the symbols of all data channels of all base stations onto the received signal, allows to *jointly* estimate all symbols by means of an equaliser.

Let $h_{k,p}^{(i)}$ denote the component of the impulse response vector $\mathbf{h}_{k,p}$ belonging to the ith antenna element. All the $h_{k,p}^{(i)}$ are known from the channel estimation stage. As in Chapter 5, L denotes the maximum length of all channels, i.e., $h_{k,p}^{(i)} = 0$ for all k, i if $p \notin \{0, \cdots, L-1\}$. Since we consider only one timeslot at a time and the channels are time-invariant during the transmission of one timeslot, we suppressed the time-dependence of $\mathbf{h}_{k,p}$ in (6.1). Including the total spreading code, the composite impulse response associated to the lth data channel, kth base station, and ith receive antenna is given by

$$g_k^{(l,i)}(m) \triangleq \sum_{p=0}^{L-1} h_{k,p}^{(i)} c_k^{(l)}(m - p). \tag{6.2}$$

Note that since $c_k^{(l)}(m) \neq 0$ only for $1 \leq m \leq Q$, the chip index m will be limited to $m = 1, \ldots, Q + L - 1$ in (6.2). Stacking the $g_k^{(l,i)}(m)$ of (6.2) into the $(Q + L - 1) \times 1$

---

[1] Since the spreading factor is equal to the scrambling code length, the total spreading code of the lth data channel of the kth base station is given by the product of the data-channel-specific spreading code and the base-station-specific scrambling code: $c_k^{(l)}(m) = c_{\mathrm{spr}}^{(l)}(m)\, c_{\mathrm{scr},k}(m)$.

[2] Index 1 corresponds to the BCH that is always present, while the indices 2, 3, and 4 are never used in the timeslot of interest.

[3] Hereby, we neglect the small influence of the midamble on the data parts due to multipath propagation.

vector

$$\mathbf{g}_k^{(l,i)} \triangleq \begin{bmatrix} g_k^{(l,i)}(1) \\ g_k^{(l,i)}(2) \\ \vdots \\ g_k^{(l,i)}(Q+L-1) \end{bmatrix}, \tag{6.3}$$

and stacking the symbols $d_k^{(l)}(u)$ of the two data fields into the $N \times 1$ vector

$$\mathbf{d}_k^{(l)} \triangleq \begin{bmatrix} d_k^{(l)}(1) \\ d_k^{(l)}(2) \\ \vdots \\ d_k^{(l)}(N) \end{bmatrix},$$

the whole signal component of the lth data channel from the kth base station, received at the ith antenna element[1] can be written as the $(NQ + L - 1) \times 1$ vector

$$\mathbf{x}_k^{(l,i)} \triangleq a_k^{(l)} \mathbf{G}_k^{(l,i)} \mathbf{d}_k^{(l)}. \tag{6.4}$$

Here, $\mathbf{G}_k^{(l,i)}$ is the $(NQ + L - 1) \times N$ block-Toeplitz channel matrix defined as

Denoting the signal component of $\mathbf{x}(n)$ received at the ith antenna element as $x^{(i)}(n)$ and using (6.4), the $NQ + L - 1 \times 1$ vector

$$\mathbf{x}^{(i)} \triangleq \begin{bmatrix} x^{(i)}(1) \\ x^{(i)}(2) \\ \vdots \\ x^{(i)}(NQ+L-1) \end{bmatrix}$$

can be written as

$$\mathbf{x}^{(i)} = \sum_{k=1}^{K} \left[\mathbf{G}_k^{(1,i)} \mathbf{d}_k^{(1)} + \sum_{l \in \mathcal{L}_k} a_k^{(l)} \mathbf{G}_k^{(l,i)} \mathbf{d}_k^{(l)} \right] + \mathbf{n}^{(i)}. \tag{6.5}$$

[1]Note that $l \in \mathcal{L}_k$, $k \in \{1, \ldots, K\}$, and $i \in \{1, \ldots, M\}$.

Here, $\mathbf{n}^{(i)}$ is a noise vector constructed from $\mathbf{n}(n)$ in (6.1) similarly to $\mathbf{x}^{(i)}$. Stacking all antenna signal vectors as

$$\mathbf{x} \triangleq \begin{bmatrix} \mathbf{x}^{(1)} \\ \mathbf{x}^{(2)} \\ \vdots \\ \mathbf{x}^{(M)} \end{bmatrix},$$

we can finally express the received signal of the whole timeslot as

$$\mathbf{x} = \mathbf{GAd} + \mathbf{n}. \tag{6.6}$$

Here, $\mathbf{G}$ is the $M(NQ + L - 1) \times N\big(K + \sum_{k=1}^{K} |\mathcal{L}_k|\big)$ total channel matrix defined as

$$\mathbf{G} \triangleq \begin{pmatrix} \mathbf{G}_1^{(1,1)} & \mathbf{G}_1^{(5,1)} & \cdots & \mathbf{G}_1^{(16,1)} & \cdots & \mathbf{G}_K^{(1,1)} & \mathbf{G}_K^{(5,1)} & \cdots & \mathbf{G}_K^{(16,1)} \\ \mathbf{G}_1^{(1,2)} & \mathbf{G}_1^{(5,2)} & \cdots & \mathbf{G}_1^{(16,2)} & \cdots & \mathbf{G}_K^{(1,2)} & \mathbf{G}_K^{(5,2)} & \cdots & \mathbf{G}_K^{(16,2)} \\ \vdots & \vdots & & \vdots & & \vdots & & & \\ \mathbf{G}_1^{(1,M)} & \mathbf{G}_1^{(5,M)} & \cdots & \mathbf{G}_1^{(16,M)} & \cdots & \mathbf{G}_K^{(1,M)} & \mathbf{G}_K^{(5,M)} & \cdots & \mathbf{G}_K^{(16,M)} \end{pmatrix}, \tag{6.7}$$

the amplitude matrix

$$\mathbf{A} \triangleq \mathrm{diag}\{1, a_1^{(5)}, \ldots, a_1^{(16)}, \ \ldots \ , 1, a_K^{(5)}, \ldots, a_K^{(16)}\} \otimes \mathbf{I}_N \tag{6.8}$$

($\otimes$ denotes the Kronecker product) is a diagonal matrix where each one of the entries $1, a_1^{(5)}, \ldots, a_1^{(16)}, \ \ldots \ , 1, a_K^{(5)}, \ldots, a_K^{(16)}$ is repeated N times on the main diagonal, and the vectors

$$\mathbf{d} \triangleq \begin{bmatrix} \mathbf{d}_1^{(1)} \\ \mathbf{d}_1^{(5)} \\ \vdots \\ \mathbf{d}_1^{(16)} \\ \vdots \\ \mathbf{d}_K^{(1)} \\ \mathbf{d}_K^{(5)} \\ \vdots \\ \mathbf{d}_K^{(16)} \end{bmatrix}, \qquad \mathbf{n} \triangleq \begin{bmatrix} \mathbf{n}^{(1)} \\ \mathbf{n}^{(2)} \\ \vdots \\ \mathbf{n}^{(M)} \end{bmatrix} \tag{6.9}$$

contain the data symbols of all channels of all base stations and the noise, respectively.

Equation (6.6) represents a space-time signal model since it contains the contributions of all antenna elements received during one timeslot. It should be noted that in the above definitions of $\mathbf{G}$, $\mathbf{A}$, and $\mathbf{d}$, *all* data channels are present whereas in practice only the entries corresponding to *active* data channels $l \in \mathcal{L}_k$ will appear.

6.1 Space-Time MMSE Receiver

A common space-time detection technique for extracting the data symbols in (6.6) is MMSE equalisation (e.g., [KKB96, Sch91]) followed by quantisation. The detected data vector is given as

$$\hat{\mathbf{d}} = Q\{\mathbf{F}_{\text{MMSE}}\,\mathbf{x}\}\,,$$

where $Q\{\cdot\}$ denotes componentwise quantisation according to the QPSK symbol alphabet and the MMSE filter-matrix $\mathbf{F}_{\text{MMSE}}$ is defined by

$$\mathbf{F}_{\text{MMSE}} \triangleq \arg\min_{\mathbf{F}} \mathrm{E}\Big\{\big\|\mathbf{F}\mathbf{x} - \mathbf{d}\big\|^2\Big\}\,.$$

One obtains [Sch91]

$$\mathbf{F}_{\text{MMSE}} = \mathbf{R}_{\mathbf{dx}}\,\mathbf{R}_{\mathbf{x}}^{-1} = \mathbf{A}^H\mathbf{G}^H\mathbf{R}_{\mathbf{x}}^{-1}. \tag{6.10}$$

Since we are only interested in the data part corresponding to the BCH, we will slightly reformulate the MMSE filter (6.10) such that it yields only the desired contributions. Let us introduce the $M(NQ + L - 1) \times NK$ matrix

$$\mathbf{G}_{\text{BCH}} \triangleq \begin{pmatrix} \mathbf{G}_1^{(1,1)} & \mathbf{G}_2^{(1,1)} & \cdots & \mathbf{G}_K^{(1,1)} \\ \mathbf{G}_1^{(1,2)} & \mathbf{G}_2^{(1,2)} & \cdots & \mathbf{G}_K^{(1,2)} \\ \vdots & & \vdots & \\ \mathbf{G}_1^{(1,M)} & \mathbf{G}_2^{(1,M)} & \cdots & \mathbf{G}_K^{(1,M)} \end{pmatrix}$$

which contains only the entries belonging to the BCHs of the K base stations. Using the fact that the gain factor matrix of the BCHs is the identity matrix $\mathbf{I}_{KN}$, the MMSE filter-matrix for the BCHs is then given as

$$\mathbf{F}_{\text{MMSE,BCH}} = \mathbf{G}_{\text{BCH}}^H\,\mathbf{R}_{\mathbf{x}}^{-1}.$$

The data vector which consists of the BCHs of all K base stations,

$$\mathbf{d}_{\text{BCH}} \triangleq \begin{bmatrix} \mathbf{d}_1^{(1)} \\ \mathbf{d}_2^{(1)} \\ \vdots \\ \mathbf{d}_K^{(1)} \end{bmatrix}\,,$$

can now be detected in the usual way as

$$\hat{\mathbf{d}}_{\text{BCH}} = Q\{\mathbf{F}_{\text{MMSE,BCH}}\,\mathbf{x}\} = Q\{\mathbf{G}_{\text{BCH}}^H\,\mathbf{R}_{\mathbf{x}}^{-1}\,\mathbf{x}\}.$$

Whereas $\mathbf{G}_{\text{BCH}}$ is known because the channel impulse responses and composite spreading codes of the BCHs are known, the correlation matrix of the received signal

$$\mathbf{R}_{\mathbf{x}} \triangleq \mathrm{E}\{\mathbf{x}\mathbf{x}^H\} = \mathbf{G}\mathbf{A}\mathbf{A}^H\mathbf{G}^H + \sigma_{\mathbf{n}}^2\mathbf{I} \tag{6.11}$$

79

is unknown *a priori* because the index sets $\mathcal{L}_k$ and the gain factors $a_k^{(l)}$ of the active data channels are not known. On the other hand, accurate knowledge of $\mathbf{R_x}$ is necessary because the data channels transmitted by the stronger base stations act as strong interferers for the BCHs of weaker base stations.

Therefore we have to estimate $\mathbf{R_x}$ from the observed $\mathbf{x}$. However, $\mathbf{R_x}$ corresponds to the received data of a whole timeslot and thus for a typical set of parameters ($M = 5$ antennas, $N = 122$ data symbols, spreading factor $Q = 16$, approximate channel length of 5 chips), its size is about 9800×9800. Because the channel is time-varying, a straightforward sample-mean estimation of $\mathbf{R_x}$ (which would require the data of at least 9800 timeslots) is impossible. At this point, we realise that the signal model (6.6) is quite convenient for deriving the MMSE filter (6.10), but not for estimating $\mathbf{R_x}$.

One possible solution is to re-formulate the input-output relation in a way such that the strong structure inherent in $\mathbf{R_x}$ is better exploited. We construct the vector

$$
\mathbf{x}'(u) \triangleq
\begin{bmatrix}
x^{(1)}\big((u-1)Q + 1\big) \\
\vdots \\
x^{(1)}(uQ) \\
\vdots \\
x^{(M)}\big((u-1)Q + 1\big) \\
\vdots \\
x^{(M)}(uQ)
\end{bmatrix}, \tag{6.12}
$$

where $x^{(i)}(n)$ denotes the signal received at the ith antenna element (cf. (6.1)). This vector of length QM contains all the chips of symbol time u received at the M antenna elements. Due to the stacking operation, the *cyclostationary* vector process $\mathbf{x}(n)$ is transformed into the equivalent *stationary* vector process $\mathbf{x}'(u)$ that has the matrix-valued correlation function $\mathbf{R_{x'}}(v) = \mathrm{E}\{\mathbf{x}'(u)\,\mathbf{x}'^H(u-v)\}$. Furthermore, the input-output relation on the symbol level can now be written as

$$
\mathbf{x}'(u) = \sum_{v=0}^{L'-1} \mathbf{G}'_{\mathrm{BCH}}(v)\mathbf{d}'_{\mathrm{BCH}}(u-v) + \mathbf{w}'(u), \tag{6.13}
$$

where we focused only on the symbols and the channels of the BCHs:

$$
\mathbf{d}'_{\mathrm{BCH}}(u) \triangleq
\begin{bmatrix}
d_1^{(1)}(u) \\
d_2^{(1)}(u) \\
\vdots \\
d_K^{(1)}(u)
\end{bmatrix}, \qquad
\mathbf{G}'_{\mathrm{BCH}}(u) \triangleq
\begin{bmatrix}
g_1^{(1,1)}(uQ+1) & \cdots & g_K^{(1,1)}(uQ+1) \\
\vdots & & \vdots \\
g_1^{(1,1)}\big((u+1)Q\big) & \cdots & g_K^{(1,1)}\big((u+1)Q\big) \\
\vdots & & \vdots \\
g_1^{(1,M)}(uQ+1) & \cdots & g_K^{(1,M)}(uQ+1) \\
\vdots & & \vdots \\
g_1^{(1,M)}\big((u+1)Q\big) & \cdots & g_K^{(1,M)}\big((u+1)Q\big)
\end{bmatrix}.
$$

The symbols of the other data channels together with the noise are collected in the interference term $\mathbf{w}'(u)$ that is defined similarly to $\mathbf{x}'(u)$ in (6.12), and finally $L' = \lceil L/Q \rceil$ denotes the channel length in units of symbol periods. Because the length of $\mathbf{x}'(u)$ is only $QM = 80$, the matrices $\mathbf{R}_{\mathbf{x}'}(v)$ can now be estimated using the $N = 122$ data symbols of one timeslot. Although correlation estimation is in principle possible for the symbol level model (6.13), simulations will show that these estimates are not always very accurate.

6.2 Space-Time Decision Feedback Receivers

In this section, we will develop an alternative approach to the problem of determining $\mathbf{R}_{\mathbf{x}}$. Instead of *estimating* $\mathbf{R}_{\mathbf{x}}$ from the received signal, we will explicitly *calculate* $\mathbf{R}_{\mathbf{x}}$ based on the expression (6.11). Calculation of $\mathbf{R}_{\mathbf{x}}$ requires detection of the sets $\mathcal{L}_k$ of active data channels for all base stations (in order to determine $\mathbf{G}$) and estimation of the gain factor matrix $\mathbf{A}$. Thus, we face a similar problem as in midamble estimation in the channel estimation stage (cf. Section 5.1), because although the sub-matrices $\mathbf{G}_k^{(l,i)}$ are known, it is unknown which of them are actually contained in $\mathbf{G}$ and what their corresponding amplitudes are.[1] Unfortunately, the midamble index sets and midamble amplitudes estimated in the channel estimation stage are of no use in the detection stage since one midamble is used by up to two data channels. Because detection is most reliable for the strongest base station, we propose a decision feedback (DFB) receiver that initially takes only the strongest base station into account.

6.2.1 DFB/MMSE Receiver

This DFB receiver works as follows. Starting with the strongest base station, we detect $\mathcal{L}_k$ (which allows us to construct the corresponding $\mathbf{G}$), estimate $\mathbf{A}$, and construct the correlation matrix $\mathbf{R}_{\mathbf{x}}$. With this knowledge we can extract the corresponding BCH and the user data from the overall received signal $\mathbf{x}$ by MMSE filtering followed by quantisation. Then we reconstruct the signal component corresponding to the strongest base station and subtract it from $\mathbf{x}$. The whole procedure is repeated for the second strongest base station and so on. This results in an enhanced SINR which improves the calculation of $\mathbf{R}_{\mathbf{x}}$ for the weak base stations in the successive stages. This recursive DFB (or interference cancellation) scheme is illustrated in Figure 6.2.

More specifically, denoting the index of the strongest base station as k_s, we model the received signal in the first round as (cf. (6.6))

$$\mathbf{x} = \mathbf{G}_{k_s}\mathbf{A}_{k_s}\mathbf{d}_{k_s} + \mathbf{w}. \tag{6.14}$$

Here, $\mathbf{G}_{k_s}$, $\mathbf{A}_{k_s}$, and $\mathbf{d}_{k_s}$ contain only those entries $\mathbf{G}_k^{(l,i)}$, $a_k^{(l)}$, and $\mathbf{d}_k^{(l)}$ of $\mathbf{G}$, $\mathbf{A}$, and $\mathbf{d}$ (cf. (6.7), (6.8), and (6.9)) that correspond to the BCH and the active data channels of

---

[1]We only know that the sub-matrices $\mathbf{G}_k^{(1,i)}$ corresponding to the BCHs are always present in $\mathbf{G}$ and that their amplitudes are equal to one.
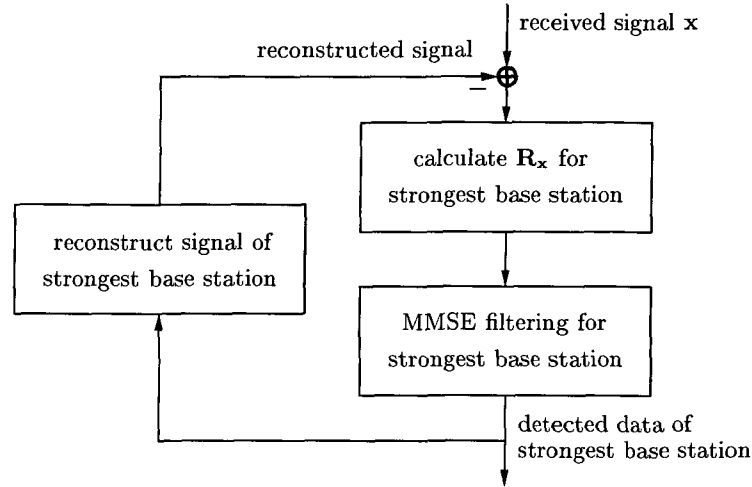
Figure 6.2: *Decision feedback detection scheme.*

base station k_s. The vector $\mathbf{w}$ summarises the noise and the interference from all other base stations; it will be modeled white for simplicity. The MMSE filter for the model (6.14) is (cf. (6.10))

$$\mathbf{F}_{\mathrm{MMSE},k_s} = \mathbf{A}_{k_s}^H \mathbf{G}_{k_s}^H \mathbf{R}_{\mathbf{x}}^{-1},$$

where the correlation matrix of the received data $\mathbf{x}$ is given as

$$\mathbf{R}_{\mathbf{x}} = \mathbf{G}_{k_s} \mathbf{A}_{k_s} \mathbf{A}_{k_s}^H \mathbf{G}_{k_s}^H + \sigma_{\mathbf{w}}^2 \mathbf{I}. \tag{6.15}$$

In order to construct $\mathbf{R}_{\mathbf{x}}$, we have to compute the estimates $\hat{\mathbf{G}}_{k_s}$ and $\hat{\mathbf{A}}_{k_s}$ (this will be discussed in Sections 6.2.3 and 6.2.4) and insert them in (6.15). With the resulting correlation-matrix estimate $\hat{\mathbf{R}}_{\mathbf{x}}$, the MMSE matrix filter of the strongest base station is obtained as

$$\mathbf{F}_{\mathrm{MMSE},k_s} = \hat{\mathbf{A}}_{k_s}^H \hat{\mathbf{G}}_{k_s}^H \hat{\mathbf{R}}_{\mathbf{x}}^{-1} = \hat{\mathbf{A}}_{k_s}^H \hat{\mathbf{G}}_{k_s}^H \left(\hat{\mathbf{G}}_{k_s} \hat{\mathbf{A}}_{k_s} \hat{\mathbf{A}}_{k_s}^H \hat{\mathbf{G}}_{k_s}^H + \widehat{\sigma_{\mathbf{w}}^2} \mathbf{I} \right)^{-1}. \tag{6.16}$$

Here, $\widehat{\sigma_{\mathbf{w}}^2}$ is an estimate of the interference-plus-noise variance. The detected data in the first round is now given by

$$\hat{\mathbf{d}}_{k_s} = \mathrm{Q}\{\mathbf{y}_{k_s}\},$$

where

$$\mathbf{y}_{k_s} = \mathbf{F}_{\mathrm{MMSE},k_s} \mathbf{x} = \hat{\mathbf{A}}_{k_s}^H \hat{\mathbf{G}}_{k_s}^H \left(\hat{\mathbf{G}}_{k_s} \hat{\mathbf{A}}_{k_s} \hat{\mathbf{A}}_{k_s}^H \hat{\mathbf{G}}_{k_s}^H + \widehat{\sigma_{\mathbf{w}}^2} \mathbf{I} \right)^{-1} \mathbf{x}. \tag{6.17}$$

Having computed $\hat{\mathbf{d}}_{k_s}$, the BCH detection for the strongest base stations is finished and we can remove the contribution of base station k_s from the overall received signal: The signal component corresponding to $\hat{\mathbf{d}}_{k_s}$ is reconstructed according to the model (6.14) and subtracted from the overall received signal

$$\tilde{\mathbf{x}} = \mathbf{x} - \hat{\mathbf{G}}_{k_s} \hat{\mathbf{A}}_{k_s} \hat{\mathbf{d}}_{k_s}. \tag{6.18}$$

The DFB procedure is now repeated using the "cleaned" $\tilde{\mathbf{x}}$ instead of $\mathbf{x}$ and the second strongest base station instead of the strongest one, and so on.

6.2.2 DFB/DFB Receiver

The DFB/MMSE scheme discussed above used decision feedback from base station to base station to improve the calculation of $\mathbf{R_x}$ for the weaker base stations, but data detection itself was performed by means of a conventional MMSE filter. A possible performance gain can be achieved by replacing this MMSE filter with a DFB equaliser. In the following, we derive the DFB step by step from the MMSE to highlight the close relation between both methods [KKB96].

Let us consider a modified version of the MMSE filter which is equivalent to (6.16) and can be obtained by applying the matrix inversion lemma [GV96]:

$$\mathbf{F}_{\text{MMSE},k_s} = \left(\hat{\mathbf{A}}_{k_s}^H \hat{\mathbf{G}}_{k_s}^H \hat{\mathbf{G}}_{k_s} \hat{\mathbf{A}}_{k_s} + \widehat{\sigma_{\text{w}}^2}\mathbf{I}\right)^{-1} \hat{\mathbf{A}}_{k_s}^H \hat{\mathbf{G}}_{k_s}^H. \tag{6.19}$$

The (inverse of the) first term of (6.19) is positive definite and hence can be split up according to a Cholesky factorisation as

$$\hat{\mathbf{A}}_{k_s}^H \hat{\mathbf{G}}_{k_s}^H \hat{\mathbf{G}}_{k_s} \hat{\mathbf{A}}_{k_s} + \widehat{\sigma_{\text{w}}^2}\mathbf{I} = \mathbf{L}^H\mathbf{L}, \tag{6.20}$$

where $\mathbf{L}$ is an upper-triangular matrix with real-valued entries along the main diagonal [GV96]. Inserting (6.20) into (6.19), we obtain

$$\mathbf{y}_{k_s} = \mathbf{F}_{\text{MMSE},k_s}\,\mathbf{x} = \mathbf{L}^{-1}\mathbf{L}^{-H}\hat{\mathbf{A}}_{k_s}^H \hat{\mathbf{G}}_{k_s}^H\mathbf{x}. \tag{6.21}$$

Let us introduce a normalised version of $\mathbf{L}$ as

$$\tilde{\mathbf{L}} = \text{diag}\{\mathbf{L}\}^{-1}\mathbf{L},$$

where $\text{diag}\{\mathbf{L}\}$ denotes a diagonal matrix containing the main-diagonal elements of $\mathbf{L}$. The matrix $\tilde{\mathbf{L}}$ has all ones along the main diagonal and thus corresponds to a monic filter. We can now rewrite (6.21) as

$$\left(\tilde{\mathbf{L}} + \mathbf{I} - \mathbf{I}\right)\mathbf{y}_{k_s} = \text{diag}\{\mathbf{L}\}^{-2}\tilde{\mathbf{L}}^{-H}\hat{\mathbf{A}}_{k_s}^H \hat{\mathbf{G}}_{k_s}^H\,\mathbf{x}$$

or equivalently

$$\mathbf{y}_{k_s} = \text{diag}\{\mathbf{L}\}^{-2}\tilde{\mathbf{L}}^{-H}\hat{\mathbf{A}}_{k_s}^H \hat{\mathbf{G}}_{k_s}^H\,\mathbf{x} - \left(\tilde{\mathbf{L}} - \mathbf{I}\right)\mathbf{y}_{k_s}. \tag{6.22}$$

Here, the matrix $\tilde{\mathbf{L}} - \mathbf{I}$ is strictly upper triangular, i.e., the main diagonal and all lower diagonals are filled with zero entries. We see that (6.22) implies a recursive (in the vector index j) rule to compute $\mathbf{y}_{k_s}$ since the jth component y_j on the left hand side only depends on the entries $(y_{j+1}, \ldots, y_J)$ on the right hand side. We start with the last entry y_J that does not depend on any other y_j and can be computed from $\mathbf{x}$, $\mathbf{L}$, $\hat{\mathbf{A}}_{k_s}$, and $\hat{\mathbf{G}}_{k_s}$ alone. This y_J is then used to compute y_{J-1}; next, y_J and y_{J-1} are used to compute y_{J-2}, and so on. The fact that we have to start the recursion with the "last" data symbol y_J causes no problems since the whole timeslot is available for detection (due to the off-line processing performed by the ANTIUM equipment).

Up to now, this recursive procedure is completely equivalent to the conventional MMSE filter (6.17). The only modification that remains to be made to change it into a DFB scheme is to use *quantised versions* $Q\{y_{j+1}\}, \ldots, Q\{y_J\}$ of the previously computed entries to calculate y_j in every recursion step.

6.2.3 Detection of Data Channels

Both DFB receivers assumed knowledge of the channel matrix $\mathbf{G}_{k_s}$ to calculate the correlation matrix $\mathbf{R_x}$ (or, in the case of the DFB/DFB receiver, quantities equivalent to $\mathbf{R_x}$). We will now propose methods for estimating the index set $\mathcal{L}_{k_s}$ of the strongest base station which is needed to construct $\mathbf{G}_{k_s}$. For simplicity, we will denote the strongest base station as k instead of k_s in the following.

Recall that the symbol-level vector $\mathbf{x}'(u)$ in (6.12) contains, among other things, the contributions of all active data channels $l \in \mathcal{L}_k$ from the strongest base station k at symbol time u. We assume for simplicity that $\mathbf{A} = \mathbf{I}$, i.e., no power control is used.[1] Then, the model for the data channels of the strongest base station can be written as

$$\mathbf{x}'(u) = \sum_{l \in \mathcal{L}_k} d_k^{(l)}(u) \tilde{\mathbf{g}}_k^{(l)} + \mathbf{w}'(u) \qquad \text{for} \quad u = 1, \ldots, N. \tag{6.23}$$

Here, the truncated—without intersymbol interference (ISI)—channel vector

$$\tilde{\mathbf{g}}_k^{(l)} \triangleq \begin{bmatrix} \tilde{\mathbf{g}}_k^{(l,1)} \\ \tilde{\mathbf{g}}_k^{(l,2)} \\ \vdots \\ \tilde{\mathbf{g}}_k^{(l,M)} \end{bmatrix}$$

consists of the M vectors $\tilde{\mathbf{g}}_k^{(l,i)}$ of length Q whose elements equal the first Q elements of $\mathbf{g}_k^{(l,i)}$, i.e., $\left(\tilde{\mathbf{g}}_k^{(l,i)}\right)_n = \left(\mathbf{g}_k^{(l,i)}\right)_n$ for $n = 1, \ldots, Q$, where $\mathbf{g}_k^{(l,i)}$ was defined in (6.3). Finally, $\mathbf{w}'(u)$ accounts for the BCH, the contributions of weaker base stations, the ISI from neighbouring CDMA symbols, and the noise. For simplicity, we will model $\mathbf{w}'(u)$ as being white, uncorrelated, and complex Gaussian.

In order to detect the presence of the data channels in (6.23) by means of a hypothesis test, we need a separate hypothesis for every possible combination of data channels. Since there are up to 12 parallel data channels in a timeslot, we have[2] $\sum_{j=0}^{12} \binom{12}{j} = 4096$ different hypotheses. Additionally, the 122 transmit symbols per data channel act as nuisance parameters.[3] Obviously, this composite hypothesis test is quite difficult to solve directly.

To derive suboptimal but computationally affordable detectors, we additionally assume that the vectors $\tilde{\mathbf{g}}_k^{(l)}$ for different $l \in \mathcal{L}_k$ are orthogonal such that the presence of each data channel can be detected individually rather than jointly. For each of the 12 possible data channels, we now have a *binary* hypothesis test (data channel is present or not present) with only 122 nuisance parameters. This test is much easier to develop.

---

[1]The detector to be developed also works in the presence of power control if the threshold is suitably adjusted (cf. Section 6.2.3.3).

[2]In a BCH timeslot, 12 different spreading codes can be used by data channels. In the case that j data channels are present, there are $\binom{12}{j}$ possible spreading code allocations.

[3]Depending on the hypothesis, we have $122j$ (with $j = 0, \ldots, 12$) nuisance parameters in total.

6.2.3.1 Incoherent Matched Filter

A simple way for obtaining a detection statistic $\Lambda_k^{(l)}$ for the binary hypothesis test corresponding to the lth data channel is to apply the so-called *incoherent matched filter* [Kay98]:

$$\Lambda_k^{(l)} = \sum_{u=1}^{N} \left| T_k^{(l)}(u) \right|^2, \quad \text{with } T_k^{(l)}(u) \triangleq \mathbf{x}'^H(u)\tilde{\mathbf{g}}_k^{(l)}. \tag{6.24}$$

The detected index set $\hat{\mathcal{L}}_k$ is then defined as the set of indices $l \in \{5, \ldots, 16\}$ for which $\Lambda_k^{(l)}$ exceeds a certain threshold η. The choice of this threshold will be discussed later.

However, it has to be mentioned that the incoherent matched filter is designed for the case where the distribution of the unknown nuisance parameters $d_k^{(l)}(u)$ is circularly symmetric (i.e., rotationally invariant) complex Gaussian. The $d_k^{(l)}(u)$ do not conform to this assumption: they are taken from a QPSK alphabet, and thus are discrete random variables whose distribution is invariant only to rotations by multiples of j. We can hence expect the incoherent matched filter to be suboptimal in our case.

6.2.3.2 Detector Based on Maximal Invariant Statistic

To overcome the inherent suboptimality of the incoherent matched filter, we now propose a detector that is invariant to rotations of the nuisance parameters $d_k^{(l)}(u)$ by multiples of j. Consider the statistic

$$T_k'^{(l)}(u) \triangleq \left| T_k^{(l)}(u) \right| e^{j \arg \bmod \{T_k^{(l)}(u)\}},$$

where $T_k^{(l)}(u) = \mathbf{x}'^H(u)\tilde{\mathbf{g}}_k^{(l)}$ as before and

$$\arg \bmod \{c\} \triangleq \left[(\arg\{c\} + \pi/4) \text{ modulo } \pi/2 \right] - \pi/4,$$

i.e., the phase of the complex number c is wrapped to the interval $[-\pi/4, \pi/4)$. It can be shown that $T_k'^{(l)}(u)$ constitutes a *maximal invariant statistic* [Sch91], which means that $T_k'^{(l)}(u)$ is invariant to multiplications of $d_k^{(l)}(u)$ by powers of j and $\{T_k'^{(l)}(u)\}_{u=1,\ldots,N}$ contains all information relevant to our detection problem

Figure 6.3 a shows the probability density function (pdf) of the statistic $T_k^{(l)}(u)$. Under hypothesis $\mathcal{H}_0$ (signal *not* present), the pdf of $T_k^{(l)}(u)$ is a 2-D Gaussian centered at the origin. Under hypothesis $\mathcal{H}_1$ (signal *present*), the pdf of $T_k^{(l)}(u)$ (conditional on the data symbol) is a 2-D Gaussian located about 1, j, -1, or $-j$ that is labeled $\mathcal{H}_1^{(1)}$ through $\mathcal{H}_1^{(4)}$ in Figure 6.3 a. The dashed arrows show how the phase of $T_k^{(l)}(u)$ is wrapped to the fundamental phase interval $[-\pi/4, \pi/4)$ during the transition from $T_k^{(l)}(u)$ to $T_k'^{(l)}(u)$. Note, however, that only the pdf parts outside the sector $[-\pi/4, \pi/4)$ are transferred into $[-\pi/4, \pi/4)$; the "tails" of the pdf components $\mathcal{H}_1^{(2)}$, $\mathcal{H}_1^{(3)}$, and $\mathcal{H}_1^{(4)}$ that are located inside $[-\pi/4, \pi/4]$ are left unchanged.

Ignoring these pdf tails, which is justified if the SINR is sufficiently high, we obtain the approximate conditional pdf of $T_k'^{(l)}(u)$ depicted in Figure 6.3 b. This approximate
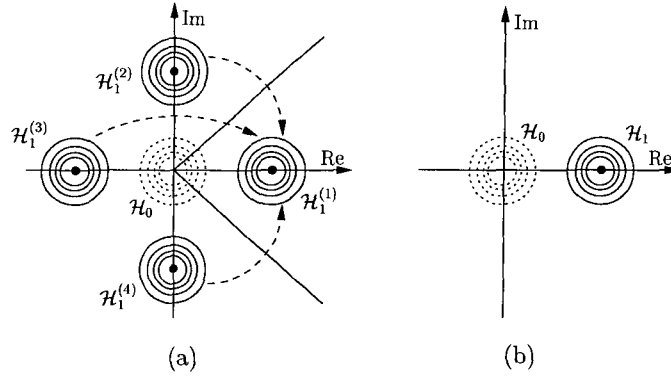
Figure 6.3: *Illustration of the maximal invariant statistic* $T_k'^{(l)}(u)$: (a) *conditional* pdf *of* $T_k^{(l)}(u)$, (b) *approximate conditional* pdf *of* $T_k'^{(l)}(u)$ *for high SINR. The dashed arrows in* (a) *show how the phase of* $T_k^{(l)}(u)$ *is wrapped to the fundamental phase interval* $[-\pi/4, \pi/4]$ *when* $T_k^{(l)}(u)$ *is converted to* $T_k'^{(l)}(u)$.

pdf corresponds to the standard problem of detecting a known signal in white Gaussian noise. For this latter problem, the appropriate detection statistic is given by [Kay98]

$$\Lambda_{k,\text{inv}}^{(l)} = \sum_{u=1}^{N} \text{Re}\{T_k'^{(l)}(u)\}.$$

6.2.3.3 Receiver Operating Characteristics and Choice of Threshold

Figure 6.4 a shows the receiver operating characteristics (ROCs) of the two detection statistics $\Lambda_k^{(l)}$ and $\Lambda_{k,\text{inv}}^{(l)}$ for a flat Rayleigh fading channel (note that there is no ISI) with 8 active and 4 inactive data channels, one base station, and white Gaussian noise with two different SNR values. For SNR $= -35$ dB, both ROCs are indistinguishable from 1 and thus both detection statistics yield detection probability $\approx 100\,\%$ even at false alarm probabilities smaller than $1\,\%$. For SNR $= -40$ dB, the ROCs still are roughly equal (interestingly enough, $\Lambda_k^{(l)}$ performs better than $\Lambda_{k,\text{inv}}^{(l)}$) but the detection probability is lower than 1, i.e., there now is a clear tradeoff between low false alarm probability and high detection probability.

For an analysis of the influence of the threshold η on the detection results, it is advantageous to normalise the detection statistics $\Lambda_k^{(l)}$ and $\Lambda_{k,\text{inv}}^{(l)}$ in such a way that in the absence of noise and interference they are one under $\mathcal{H}_1$. Neglecting the noise/interference term $\mathbf{w}'(u)$, we find that (cf. (6.23), (6.24))

$$T_k^{(l)}(u) = \mathbf{x}'^H(u)\tilde{\mathbf{g}}_k^{(l)} = \left[\sum_{l'\in\mathcal{L}_k} d_k^{(l')}(u)\tilde{\mathbf{g}}_k^{(l')}\right]^H \tilde{\mathbf{g}}_k^{(l)}.$$

The spreading codes $c_k^{(l)}(m)$ of different data channels are orthogonal. If no ISI is present, also the truncated channel vectors $\tilde{\mathbf{g}}_k^{(l,i)}$ (which are in this case equal to the composite
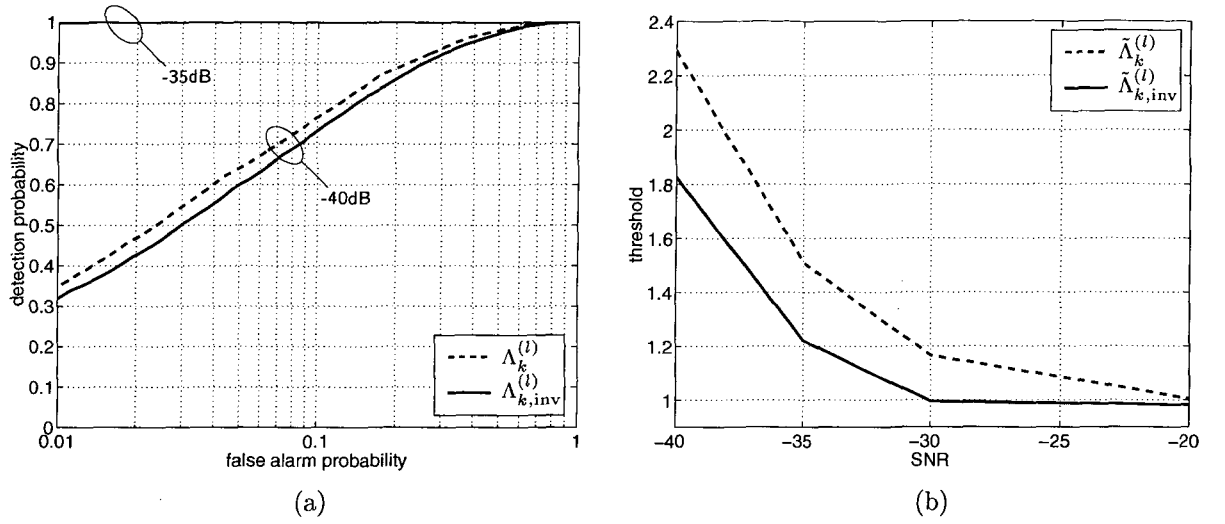
Figure 6.4: *Analysis of the detection statistics* $\Lambda_k^{(l)}$ *and* $\Lambda_{k,\text{inv}}^{(l)}$ *and their normalised versions* $\tilde{\Lambda}_k^{(l)}$ *and* $\tilde{\Lambda}_{k,\text{inv}}^{(l)}$: (a) *ROCs,* (b) *threshold vs. SNR for a detection probability of* 90%.

channel vectors $\mathbf{g}_k^{(l,i)}$) are hence orthogonal,[1] i.e., $\tilde{\mathbf{g}}_k^{(l')H} \tilde{\mathbf{g}}_k^{(l)} = 0$ for $l' \neq l$. Thus, if the lth data channel is not present in $\mathbf{x}'(u)$, ($l \notin \mathcal{L}_k$, corresponding to hypothesis $\mathcal{H}_0$), $T_k^{(l)}(u) \equiv 0$ and the detection statistics $\Lambda_k^{(l)}$ and $\Lambda_{k,\text{inv}}^{(l)}$ vanish. For $\mathcal{H}_1$ ($l \in \mathcal{L}_k$), we find that

$$T_k^{(l)}(u) = \left[\sum_{l' \in \mathcal{L}_k} d_k^{(l')}(u) \tilde{\mathbf{g}}_k^{(l')} \right]^H \tilde{\mathbf{g}}_k^{(l)} = d_k^{(l)}(u) \, \|\tilde{\mathbf{g}}_k^{(l)}\|^2. \tag{6.25}$$

Since the elements of $c_k^{(l)}(m)$ are powers of j and, for $L = 1$, $\tilde{\mathbf{g}}_k^{(l,i)} = \mathbf{g}_k^{(l,i)}$ and $g_k^{(l,i)}(m) = h_{k,0}^{(i)} c_k^{(l)}(m)$, (6.25) can be simplified as

$$T_k^{(l)}(u) = d_k^{(l)}(u) \, \|\tilde{\mathbf{g}}_k^{(l)}\|^2 = d_k^{(l)}(u) \, Q \sum_{i=1}^{M} |h_{k,0}^{(i)}|^2 = d_k^{(l)}(u) \, Q \, P_k, \tag{6.26}$$

with the abbreviation $P_k = \sum_{i=1}^{M} |h_{k,0}^{(i)}|^2$. The elements of $d_k^{(l)}(u)$ are also powers of j and hence we obtain

$$\Lambda_k^{(l)} = \sum_{u=1}^{N} |T_k^{(l)}(u)|^2 = \sum_{u=1}^{N} \left| d_k^{(l)}(u) \, Q \, P_k \right|^2 = N Q^2 P_k^2.$$

With (6.26), the maximal invariant statistic becomes $T_k'^{(l)}(u) = Q P_k$ and the detection statistic based on the maximal invariant statistic is given by

$$\Lambda_{k,\text{inv}}^{(l)} = N Q P_k.$$

---

[1]This requires the channels $h_{k,p}^{(i)}$ to have only one tap ($L = 1$). Due to the convolution in (6.2), orthogonality is lost in the case of $L > 1$.

Therefore, normalised detection statistics that are equal to one under $\mathcal{H}_1$ in the noise/interference-free case can be defined as

$$\tilde{\Lambda}_k^{(l)} \triangleq \sqrt{\frac{\Lambda_k^{(l)}}{NQ^2P_k^2}} = \frac{\sqrt{\Lambda_k^{(l)}/N}}{QP_k} \quad \text{and} \quad \tilde{\Lambda}_{k,\text{inv}}^{(l)} \triangleq \frac{\Lambda_{k,\text{inv}}^{(l)}}{NQP_k}.$$

Figure 6.4 b shows the threshold η for the normalised statistics versus the SNR for a detection probability of 90%. Here, $\tilde{\Lambda}_{k,\text{inv}}^{(l)}$ has a slight advantage over $\tilde{\Lambda}_k^{(l)}$ because its threshold is less dependent on the SNR, and thus easier to choose. Note that $\tilde{\Lambda}_k^{(l)}$ and $\tilde{\Lambda}_{k,\text{inv}}^{(l)}$ are normalised to one only in the noise/interference-free case and that for dominant noise/interference, higher values of $\tilde{\Lambda}_k^{(l)}$ and $\tilde{\Lambda}_{k,\text{inv}}^{(l)}$ are possible.

Even though power control has been disregarded so far, the detection statistics $\Lambda_k^{(l)}$ and $\Lambda_{k,\text{inv}}^{(l)}$ can also be used in the presence of power control if the threshold is suitably adjusted. In a UMTS/TDD network, we have $0.1 \leq a_k^{(l)} \leq 1$, corresponding to power control dynamics of 20 dB. It can be shown that under ideal conditions (one base station, no noise, no ISI), the normalised detection statistics $\tilde{\Lambda}_k^{(l)}$ and $\tilde{\Lambda}_{k,\text{inv}}^{(l)}$ under hypothesis $\mathcal{H}_1$ are equal to $a_k^{(l)}$. For a certain threshold, a data channel with small amplitude $a_k^{(l)}$ thus has a lower false alarm probability than a data channel with large $a_k^{(l)}$. Great care has to be taken to balance the false alarm probabilities of differently powered data channels when choosing the threshold.

With the threshold η, the detected index set of the strongest base station $\hat{\mathcal{L}}_k$ consists of those indices l, where $\tilde{\Lambda}_k^{(l)} > \eta$ (or respectively $\tilde{\Lambda}_{k,\text{inv}}^{(l)} > \eta$). Having obtained $\hat{\mathcal{L}}_k$, we know which sub-matrices $\mathbf{G}_k^{(l,i)}$ are contained in $\mathbf{G}_k$ and are able to construct the estimate $\hat{\mathbf{G}}_k$.

Finally, we note that in our simulations we observed very little difference between the data detection performance of the two normalised detection statistics and that differences only occurred at very low SINR values. We thus used the simpler detection statistic $\tilde{\Lambda}_k^{(l)}$ of the incoherent matched filter for the simulations in Section 6.3.

6.2.4 Estimation of Gain Factors

To actually compute $\mathbf{R_x}$ according to (6.15), it remains to estimate the diagonal gain factor matrix $\mathbf{A}_k$ or, more precisely, the gain factors $a_k^{(l)}$ for all $l \in \hat{\mathcal{L}}_k$. Because under ideal conditions (one base station, no noise, no ISI) $a_k^{(l)}$ equals $\tilde{\Lambda}_k^{(l)}$ and $\tilde{\Lambda}_{k,\text{inv}}^{(l)}$ as mentioned above, we suggest to initially use the estimate $\hat{a}_k^{(l)} = \tilde{\Lambda}_k^{(l)}$ or $\hat{a}_k^{(l)} = \tilde{\Lambda}_{k,\text{inv}}^{(l)}$ for detection of the data vector $\mathbf{d}_k$ of the strongest base station. For the subsequent subtraction step (6.18), however, a more accurate estimate should be used. Indeed, once that $\hat{\mathbf{d}}_k$ and $\hat{\mathbf{G}}_k$ are available, we can use the expression (6.14) and compute the least-squares estimate of the gain factor matrix as

$$\hat{\mathbf{A}}_k = \arg\min_{\mathbf{A}} \left\| \mathbf{x} - \hat{\mathbf{G}}_k \mathbf{A} \hat{\mathbf{d}}_k \right\|^2. \tag{6.27}$$

Setting the derivative of $\left\| \mathbf{x} - \hat{\mathbf{G}}_k \mathbf{A} \hat{\mathbf{d}}_k \right\|^2$ with respect to $\mathbf{A}^*$ equal to zero, we obtain the equation

$$\left(\hat{\mathbf{G}}_k^H \hat{\mathbf{G}}_k \mathbf{A} \hat{\mathbf{d}}_k \right) \hat{\mathbf{d}}_k^H = \left(\hat{\mathbf{G}}_k^H \mathbf{x} \right) \hat{\mathbf{d}}_k^H. \tag{6.28}$$

Since $\hat{\mathbf{G}}_k^H \hat{\mathbf{G}}_k \mathbf{A} \hat{\mathbf{d}}_k$ and $\hat{\mathbf{G}}_k^H \mathbf{x}$ are column vectors and $\hat{\mathbf{d}}_k^H$ is a row vector, (6.28) is equivalent to

$$\hat{\mathbf{G}}_k^H \hat{\mathbf{G}}_k \mathbf{A} \hat{\mathbf{d}}_k = \hat{\mathbf{G}}_k^H \mathbf{x}$$

and further to

$$\mathbf{A} \hat{\mathbf{d}}_k = \hat{\mathbf{G}}_k^\# \mathbf{x},$$

where $\hat{\mathbf{G}}_k^\#$ is the pseudo-inverse of $\hat{\mathbf{G}}_k$. Reformulating the diagonal matrix $\mathbf{A}$ as a column vector $\mathbf{a}$ and the column vector $\hat{\mathbf{d}}_k$ as a diagonal matrix $\hat{\mathbf{D}}_k$, and using the identity $\mathbf{A} \hat{\mathbf{d}}_k = \hat{\mathbf{D}}_k \mathbf{a}$, the least-squares estimate of the gain factor vector $\mathbf{a}$ becomes

$$\hat{\mathbf{a}}_k = \hat{\mathbf{D}}_k^{-1} \hat{\mathbf{G}}_k^\# \mathbf{x}.$$

The particular entries $\hat{a}_k^{(l)}$ corresponding to the data channels ($l \in \{5, \ldots, 16\}$) can then be derived from $\hat{\mathbf{a}}_k$ as

$$\hat{a}_k^{(l)} = \frac{1}{N} \sum_{j=(l-4)N}^{(l-3)N-1} \left(\hat{\mathbf{a}}_k \right)_j, \qquad l = 5, \ldots, 16.$$

6.3 Simulation Results

We used the scenarios defined in Section 2.2 to assess the performance of the three presented detection schemes through Monte Carlo simulations. Figures 6.5 and 6.6 show the percentage of successful detection events (i.e., error-free decoding of the BCH) obtained with the different detection schemes. For each base station (characterised on the abscissa by its number and respective SINR value[1]), the detection score of the different algorithms is indicated by the height of three bars. From the left, these bars correspond to the conventional space-time MMSE receiver that estimates $\mathbf{R_x}$ directly from the received signal $\mathbf{x}$ (discussed in Section 6.1; labeled *MMSE*), the DFB receiver using a space-time MMSE filter for every base station (discussed in Section 6.2.1; labeled *DFB/MMSE*), and the modified DFB receiver where the space-time MMSE filter is replaced by a DFB equaliser (discussed in Section 6.2.2; labeled *DFB/DFB*).

Pedestrian Environment

In the pedestrian environment (Figure 6.5), the conventional MMSE receiver performs poorly or even extremely poorly in almost all cases. Especially for channel B in scenario

---

[1]Note that for the definition of the SINR, the entire received signal corresponding to the base station of interest is considered as the desired signal, i.e., the data channels of this base station transmitted in parallel to the BCH are not considered as interference.
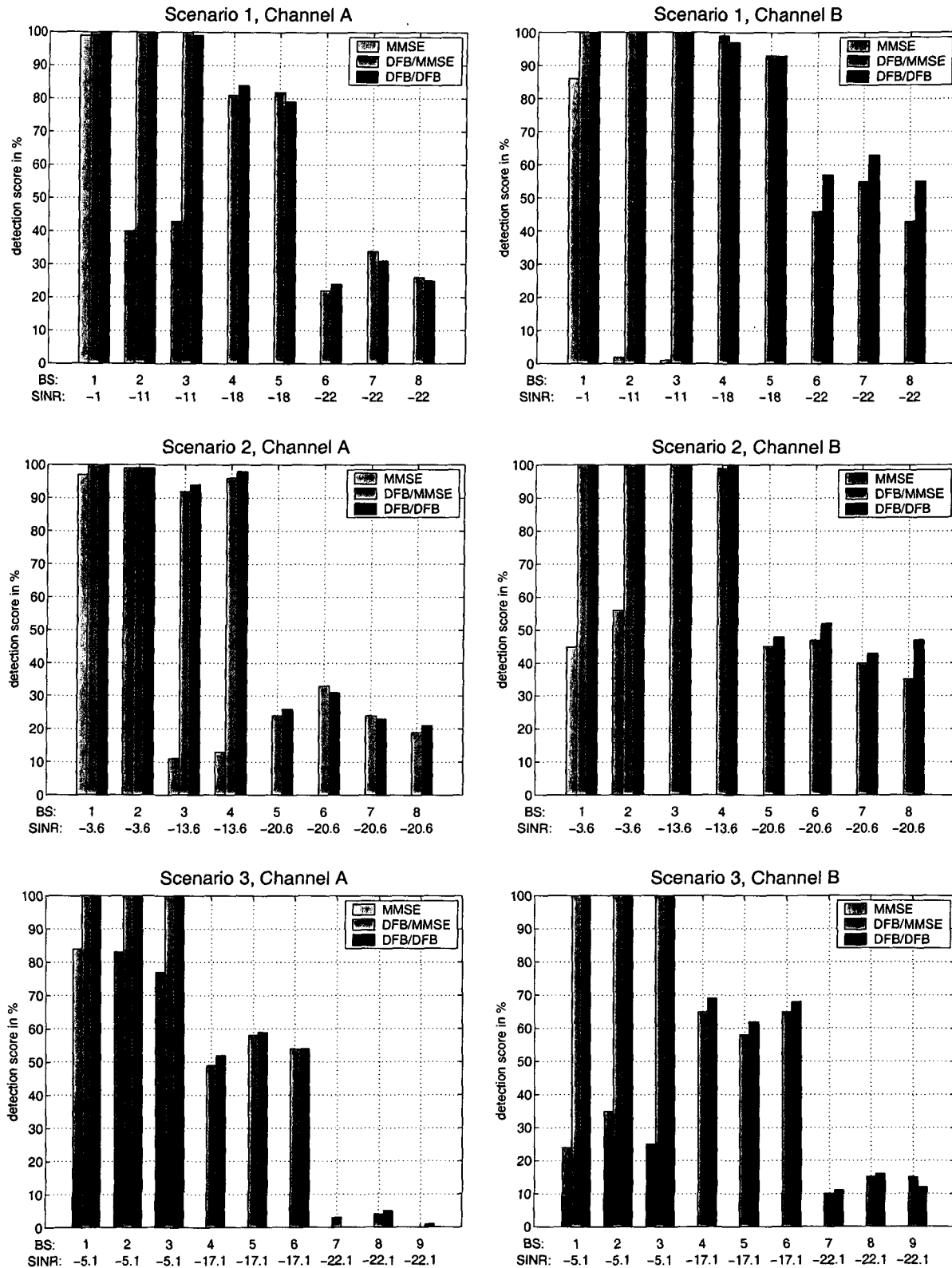
Figure 6.5: *Percentage of successful detection events for the pedestrian environment.*
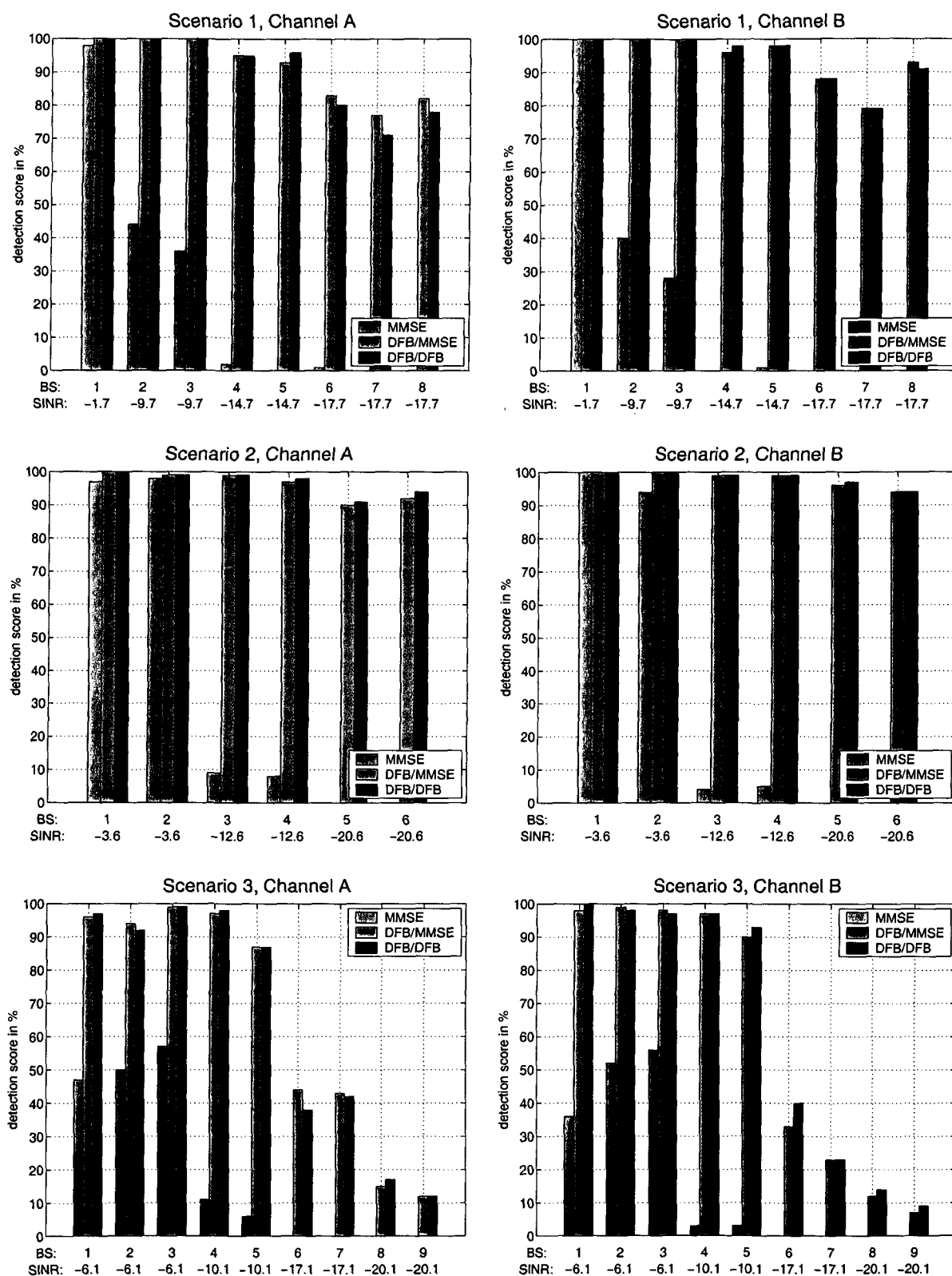
Figure 6.6: *Percentage of successful detection events for the indoor environment.*

3, the detection percentage does not exceed 35 % even for the strongest base stations. That this behaviour is due to the insufficient accuracy of the estimates of the correlation matrix $\mathbf{R_x}$ becomes clear as we consider the good performance of the DFB/MMSE scheme using a calculated rather than estimated version of $\mathbf{R_x}$.

For channel A, a detection percentage of over 80 % down to an SINR of −18 dB in scenario 1, and over 50 % down to an SINR of −17 dB in scenario 3 indicates the superiority of the DFB/MMSE scheme. However, the weakest base stations with SINR below −20 dB can only be detected in around 20 . . . 30 % of the cases in scenarios 1 and 2, while in scenario 3 detection of the weakest base stations is altogether impossible.

For channel B, the results are better than for channel A. The DFB/MMSE scheme now achieves a detection score of over 90 % for an SINR down to −18 dB in scenario 1, and around 60 % at −17 dB in scenario 3. Also for the weaker base stations, the performance is improved; we now reach detection scores of around 40 . . . 50 % in scenarios 1 and 2 and around 10 % in scenario 3. The performance in scenario 3 is generally lower than in the other scenarios, but this is not surprising in view of the fact that in scenario 3 the receiver is located at the border of three cells and thus there are impinging three equally strong signals. This situation is not favourable for DFB receivers that work best if all base stations have different powers.

The performance of the DFB/DFB scheme is slightly better, but on the whole comparable to that of the DFB/MMSE scheme. In scenario 1, the detection score for channel A is above 80 % down to an SINR of −18 dB. The more challenging scenarios 2 and 3 again result in a performance degradation, with detection scores dropping to about 55 % for an SINR of −17 dB. As for the DFB/MMSE receiver, the detection performance is better for the longer channel B. This is because channel B offers a greater amount of diversity that can be exploited by the receiver. However, in the channel estimation stage (cf. Section 5.4) we saw that especially the pedestrian channel B is very difficult to estimate and thus we can expect a tradeoff between channel estimation performance and detection performance when connecting the two stages. This will be verified in Chapter 7.

Indoor Environment

In the indoor environment (Figure 6.6), the situation is quite similar to the pedestrian environment. Again, the performance of the conventional MMSE detector is unsatisfactory for all base stations except the strongest ones. The DFB/MMSE equaliser, on the other hand, achieves a detection score of over 80 % down to an SINR of −17 dB in scenario 1. In scenario 2, scores of over 90 % down to an SINR of −20 dB are achieved, while in the most challenging scenario 3 the detection score drops to around 40 % (for channel A) and 20 . . . 30 % (for channel B) at an SINR of −17 dB. The performance of the DFB/DFB detector in the indoor environment is virtually equal to that of the DFB/MMSE equaliser.

As in the pedestrian environment, the performance of the DFB/MMSE and DFB/DFB schemes is better for the longer channel B, but the difference is not that large any more. This is because the channel lengths do not differ very much in the indoor environment. Indeed, channel B is just one tap longer than channel A, whereas in the pedestrian envi-

ronment channel B had 8 taps instead of only 3 for channel A. The additional diversity gain of channel B is hence very small in the indoor environment, and thus the performance improvements are only moderate.

Chapter 7

Performance of the Overall System

In Chapters 4–6, we presented various algorithms for synchronisation, channel estimation, and data detection, and rated their performance in simulations. However, these three receiver stages are not independent of each other since the channel estimation stage requires synchronisation information and the detection stage additionally has to be provided with channel impulse responses. In the simulations of Chapters 5 and 6, we assumed perfect results of the preceding stages, i.e., the channel estimation stage used the exact timing and code group of all base stations present, and the detector additionally disposed of perfect channel estimates.

In order to evaluate the performance of the overall receiver, including the effects of imperfect synchronisation and channel estimation on the detection stage, we conducted joint simulations of all three stages. Based on the simulation results of Chapters 4–6, we selected the "best" algorithm for each stage. These "best" algorithms are the *heuristic space-time detector* with a window length of $T_0 = 7$ samples for synchronisation,[1] the *SC-MMSE channel estimator with ML midamble estimation* for channel estimation, and finally the *DFB/DFB equaliser* for data detection. As in Chapters 4–6, we performed Monte Carlo simulations consisting of 100 simulation rounds with 16 frames each, using the scenarios defined in Section 2.2.

After channel estimation, an additional stage was included that removes the SCHs of all base stations detected by the synchronisation stage. Using the channel estimates and the extracted synchronisation codes, this task can be performed quite accurately. The purpose of this "cleaning stage" is to prevent the SCHs from impairing the interference cancellation performance of the subsequent DFB/DFB equaliser.

Figures 7.1–7.6 show the results of these simulations versus the SINRs of the different base stations. The graphs on the left hand side of each figure contain three bars per base station whose heights indicate the obtained scores in percent. From the left, these bars correspond to the synchronisation scores, the data detection scores, and, for comparison, the data detection scores of Chapter 6, where ideal synchronisation and channel estimation stages were used. Finally, the graphs on the right hand side plot the normalised MSE of the channel estimation stage averaged over all those timeslots where the corresponding

---

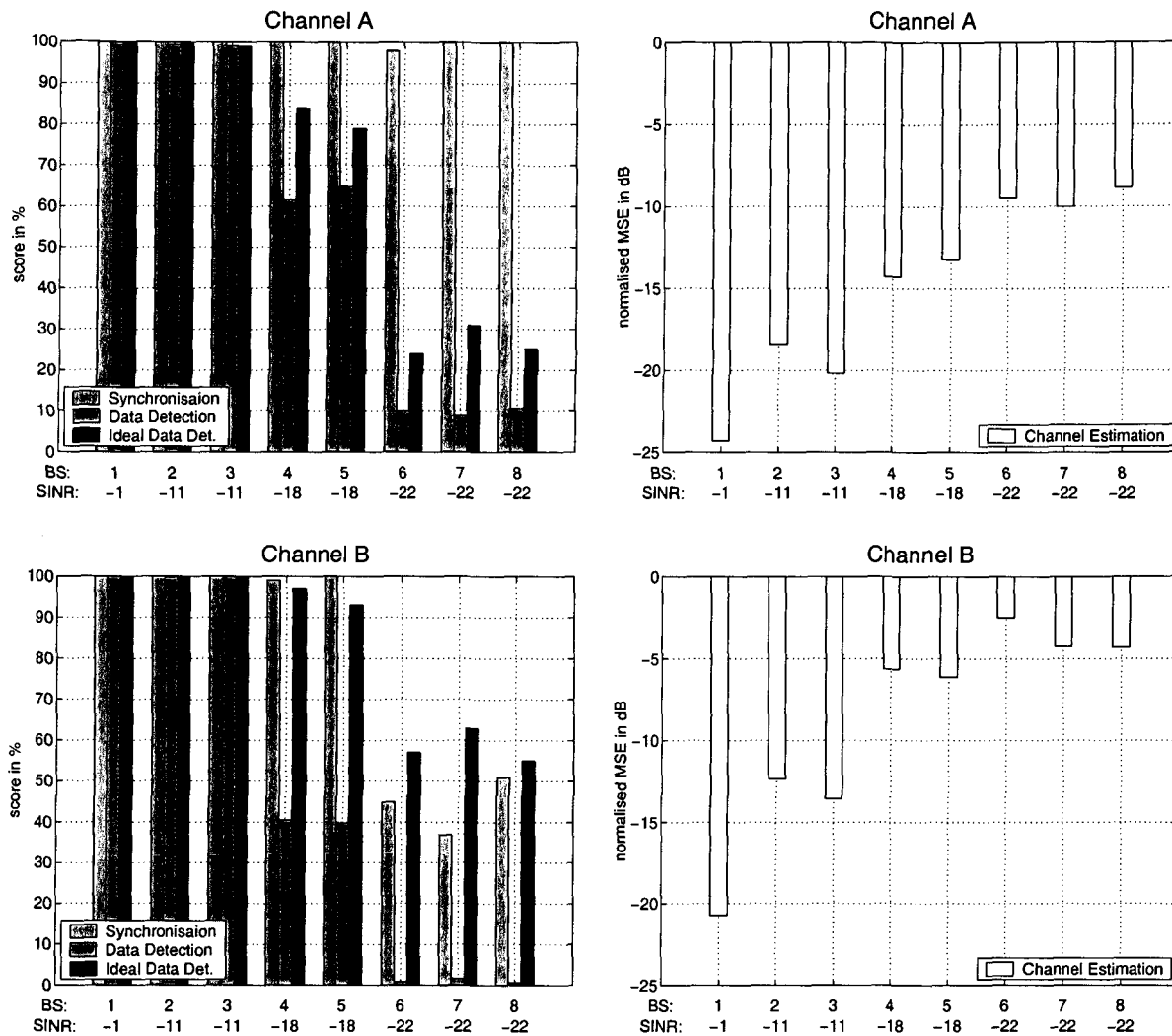[1] Averaging over 16 frames was used for synchronisation.

Figure 7.1: *Overall system simulation results for the pedestrian environment, scenario 1.*

base station could be detected by the synchronisation stage.

Pedestrian Environment

The synchronisation results in the pedestrian environment are similar to the results obtained in Chapter 4 (cf. Figures 4.7–4.9) since the synchronisation stage requires no prior knowledge.

For channel A, also the performance of the channel estimation stage shows no great difference from the ideal case of Chapter 5 (cf. Figure 5.6). This is not surprising since the synchronisation stage performs almost ideally in these cases. However, for channel B the accuracy of channel estimation drops slightly. For the weaker base stations this is caused by the imperfect synchronisation stage that is not always able to detect all base stations. The loss in channel estimation performance is then caused by the multiuser structure
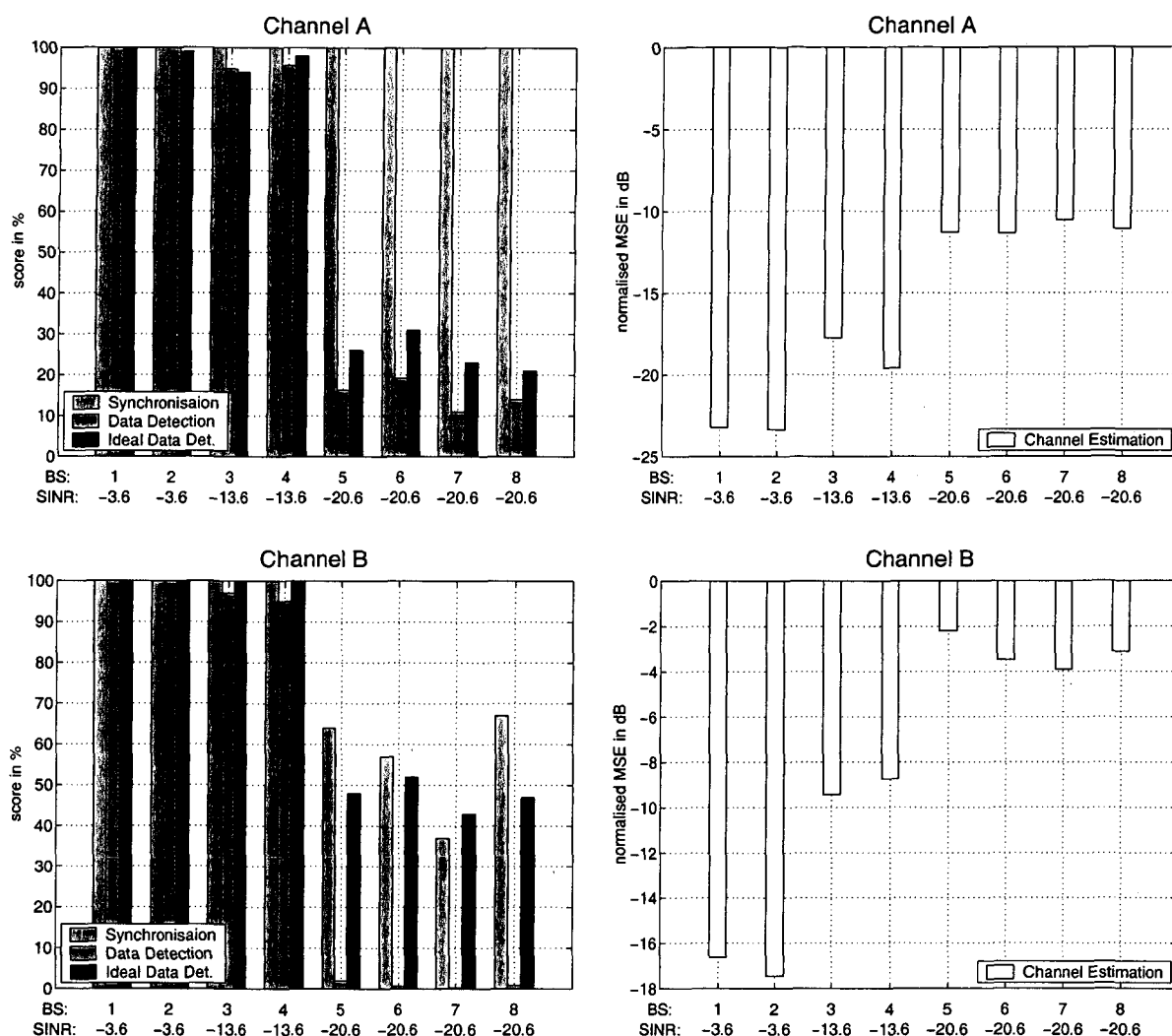
Figure 7.2: *Overall system simulation results for the pedestrian environment, scenario 2.*

of the channel estimation method, which includes the midambles of all base stations in a joint model. If some base stations are missing in this model, the channel estimation performance for the other base stations—especially the weaker ones—is reduced. However, since strong base stations are not likely being missed by synchronisation, this effect is quite small.

To understand the behaviour of the detection stage in the nonideal case, we will study the results a little bit more in detail. In **scenario 1**, the detection performance for both channels is similar to the ideal case down to an SINR of -11 dB. At -18 dB, however, the detection score for channel A is reduced from about 80 % (ideal case) to about 60 %. This significant reduction takes place although the MSE of the channel estimation stage is around -13 dB. For the weakest base stations with an SINR of -22 dB, a similar loss is experienced: the detection score drops from about 30 % to about 10 %. The channel estimation MSE here is about -10 dB. For channel B, at an SINR of -18 dB, the detection
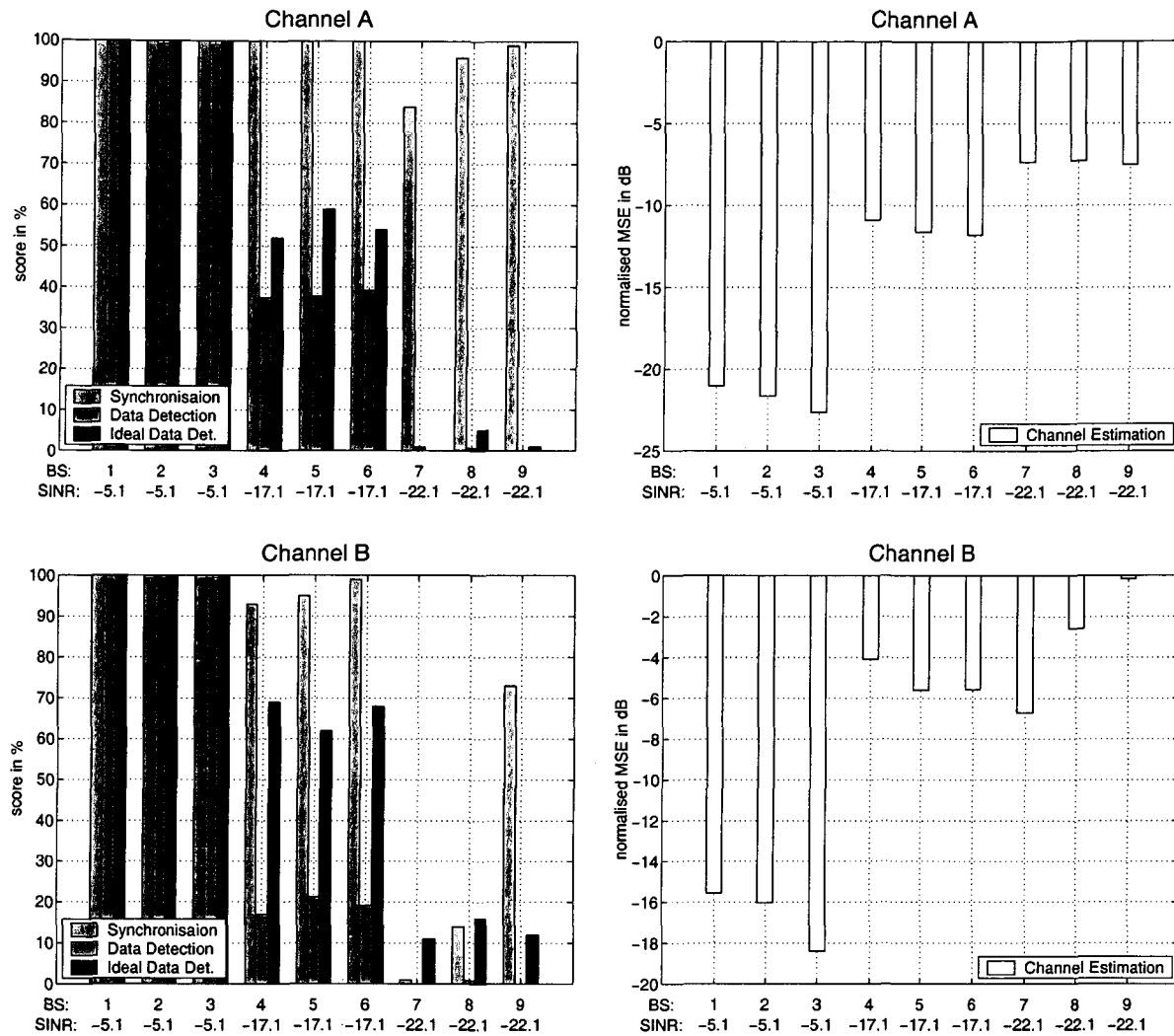
Figure 7.3: *Overall system simulation results for the pedestrian environment, scenario 3.*

score decreases by 55 % from about 95 % to 40 %, since the channel is only estimated with an MSE of about −6 dB. For an SINR of −22 dB, where channel estimation accuracy has dropped to an MSE of −4 dB, detection is virtually impossible.

For **scenario 2**, nearly ideal performance is achieved down to an SINR of −13 dB, although channel estimation accuracy is partly only moderate, the MSE being −9 dB for channel B at an SINR of −13 dB. At an SINR of −20 dB, we lose about 10 % for channel A (with channel estimation MSE of −11 dB), while for channel B, where the MSE is −3 dB, detection fails completely.

In **scenario 3**, the situation is similar, as we do not experience a performance degradation for the strongest base stations. This is due to the sufficiently accurate channel estimates that have an MSE below −15 dB. At an SINR of −17 dB, however, we find that for channel A where the MSE is −11 dB, the performance drops by about 15 . . . 20 %. Channel B even experiences a decrease of 40 . . . 50 % because of the high MSE of −5 dB.
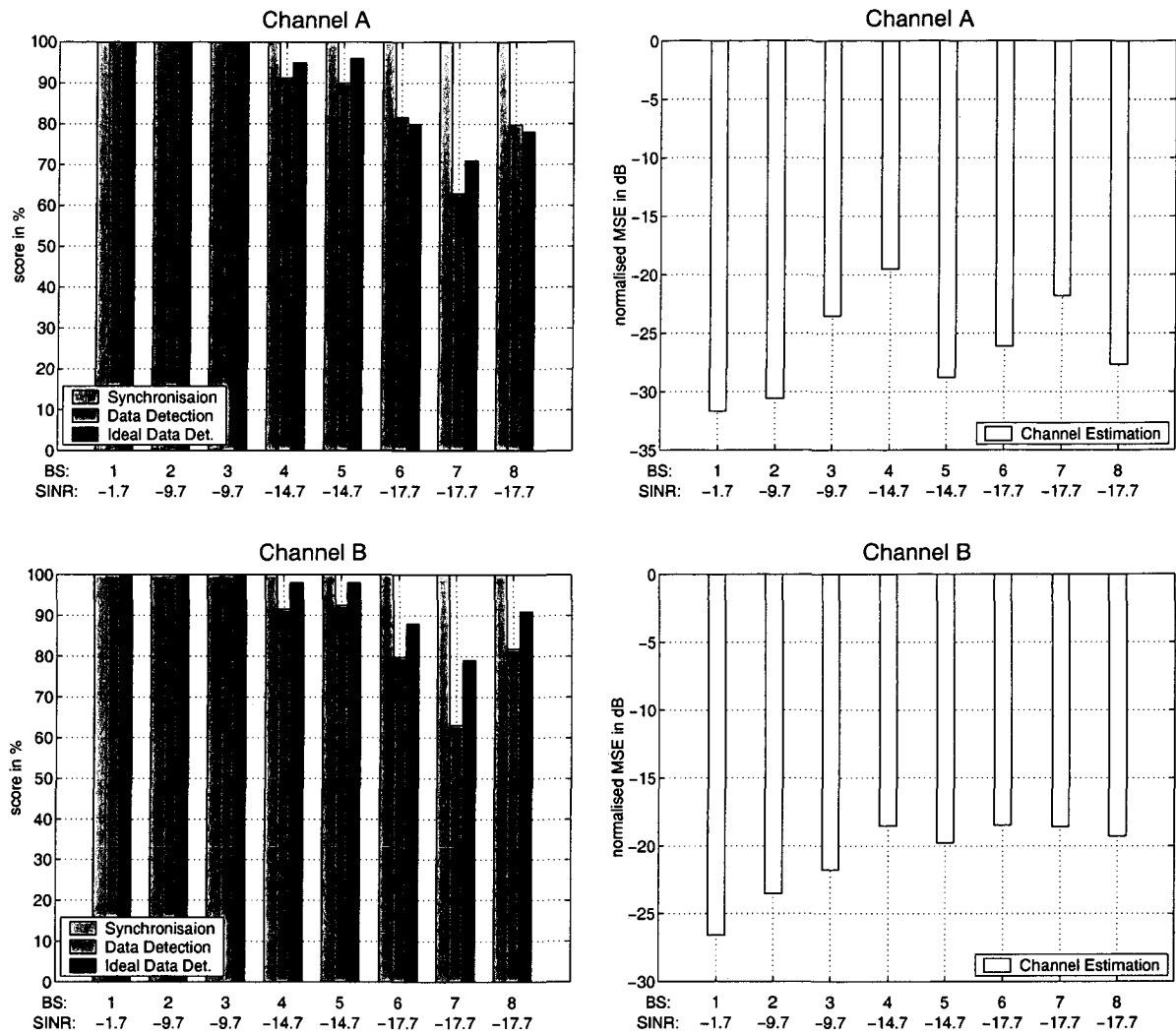
Figure 7.4: *Overall system simulation results for the indoor environment, scenario 1.*

Finally, at an SINR of $-22\,$dB, the detection process fails for both channels.

Indoor Environment

In the indoor environment, the synchronisation stage works virtually perfectly and hence the channel estimation results do not differ much from those obtained in Chapter 5 (cf. Figure 5.7). For channel A, the MSE of the channel estimation stage is well below $-20\,$dB for practically all base stations in all scenarios. This leads to a detection performance that is nearly equal to the ideal case in all scenarios. For channel B, the MSE is somewhat higher, but the maximum value of $-16\,$dB is still sufficiently low such that only a small degradation of detection performance is experienced in scenarios 2 and 3. Only for the weakest base stations (SINR $-17\,$dB) in scenario 1, the detection score drops by 10%, but it still lies around 70%.
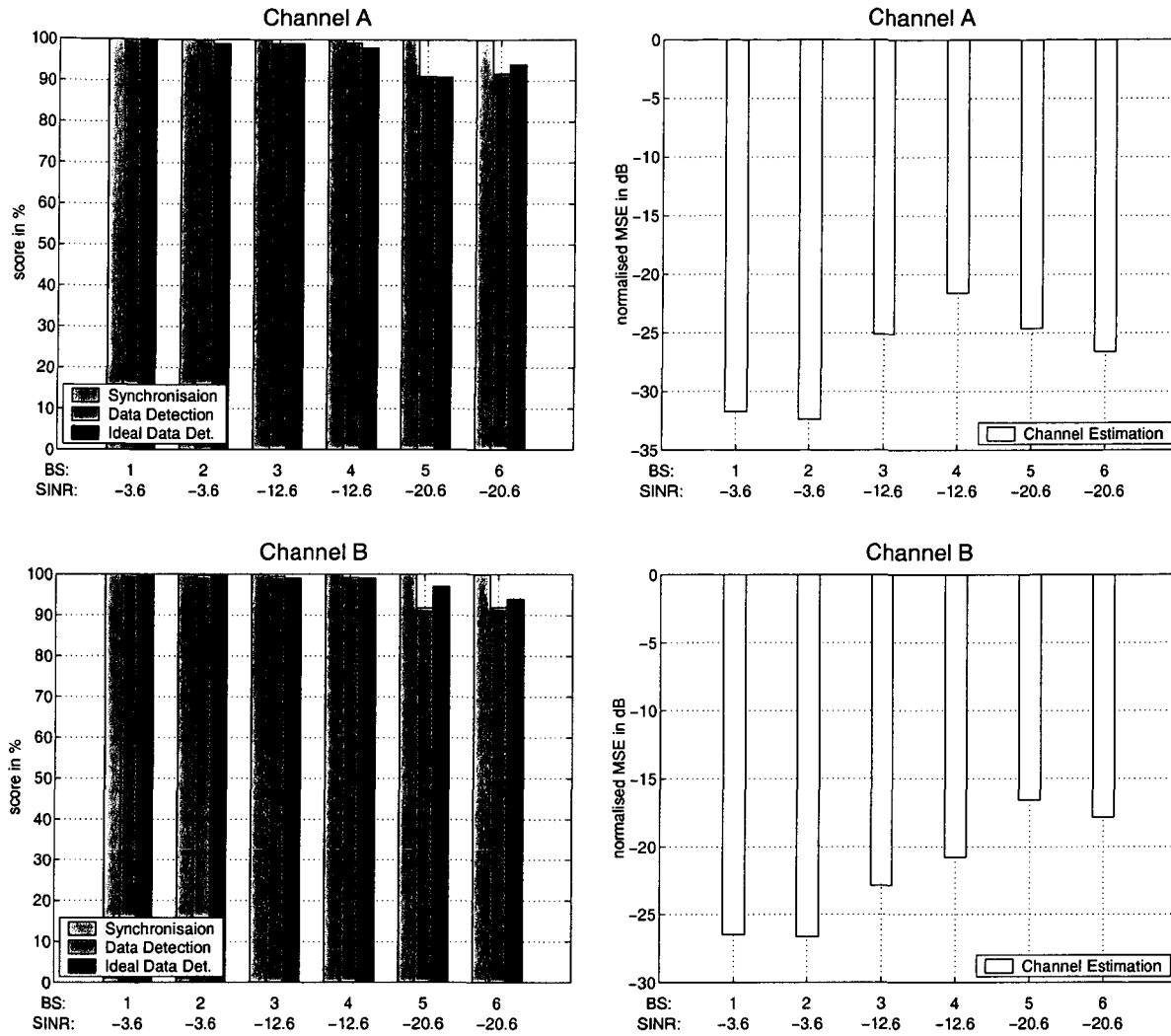
Figure 7.5: *Overall system simulation results for the indoor environment, scenario 2.*

Conclusions

In conclusion, it can be said that the detection stage is very sensitive to channel estimation errors. While for the strongest base stations in the pedestrian environment a channel estimation MSE of around $-10\,\text{dB}$ may be sufficient for nearly perfect detection performance, the weaker base stations experience a loss of about $20\,\%$ at a similar MSE. If the MSE rises to $-5\,\text{dB}$, a loss of even $50\,\%$ has to be expected. This difference is due to the decision feedback structure of the data detection stage, which causes inaccuracies for the strongest base stations to be passed on to weaker base stations. Furthermore, it is interesting that the detection scores for the shorter channel A now are higher than for channel B. The higher diversity offered by channel B, which led to better detection results in the ideal case, now is a disadvantage due to the larger inaccuracies of channel estimation.

100
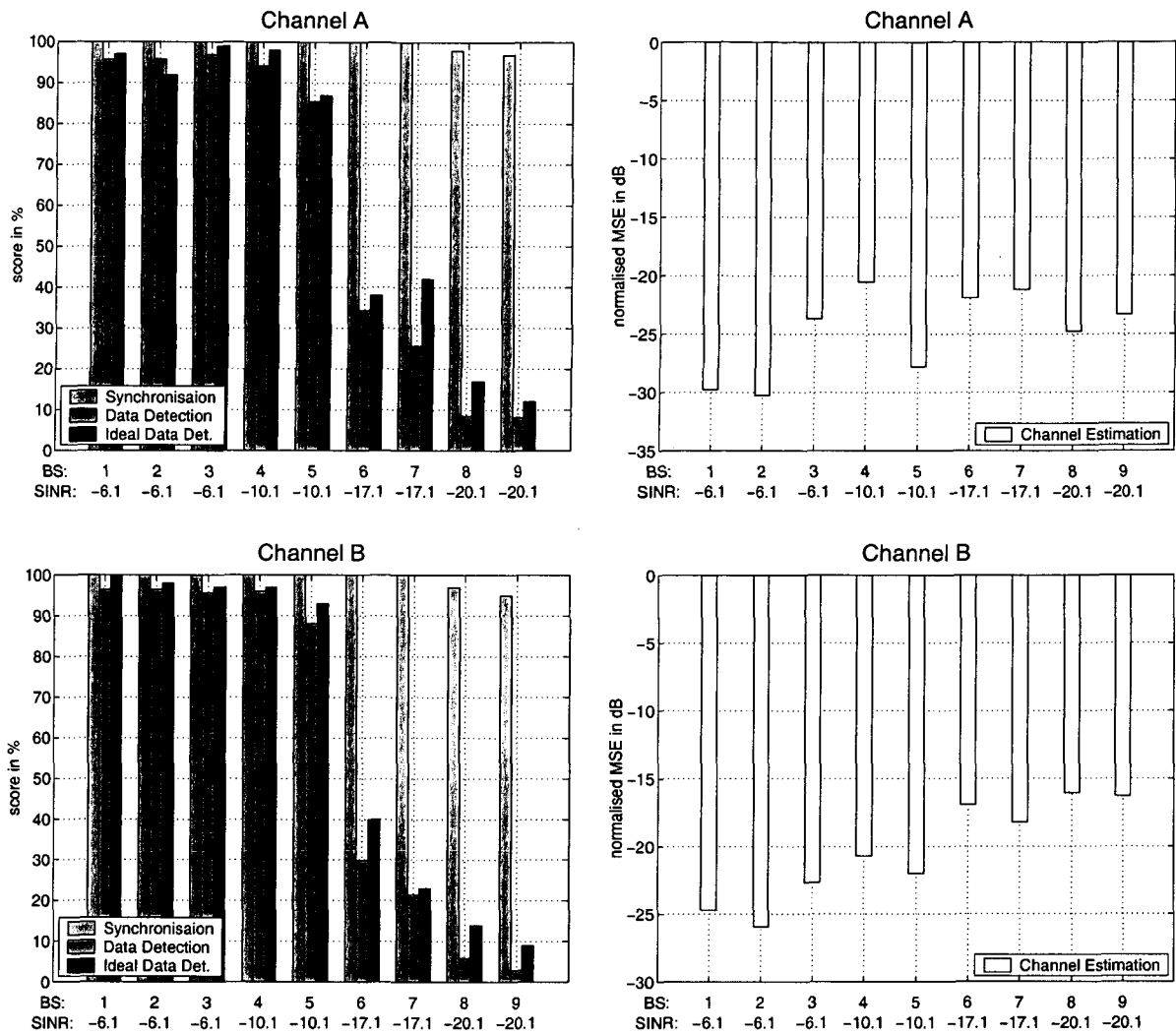
Figure 7.6: *Overall system simulation results for the indoor environment, scenario 3.*

The excellent channel estimation performance in the indoor environment results in similar detection scores for the ideal and nonideal systems. The clear connection between channel estimation accuracy and detection performance in both environments highlights the importance of high-performance channel estimation methods to achieve satisfactory results of data detection.

Chapter 8

Conclusions

In this final chapter, we summarise the most important results of our work and draw some conclusions, and suggest possible extensions and improvements of our methods.

8.1 Summary

This work has been performed within the project ANTIUM funded by the European Commission. The aim of ANTIUM was to develop a monitoring device for UMTS and DVB-T networks that allows to assess the interference situation present (Chapter 2). In this thesis, we considered signal processing algorithms for the TDD mode of UMTS (Chapter 3).

In order to classify interference, we have to know which base stations contribute to the overall received signal and what their respective power levels are. This information is gained by reading the broadcast channels (BCHs) of as many surrounding base stations as possible. Since the measurement device uses multiple antennas, space-time signal processing algorithms can be used for extracting the BCHs. However, before the BCHs can actually be detected, we have to perform synchronisation and channel estimation.

The aim of the *synchronisation stage* (Chapter 4) is to determine how many base station signals are present and where the corresponding BCHs are located temporally. For this purpose, UMTS/TDD offers a synchronisation channel (SCH) consisting of a primary and three secondary synchronisation codes. The presence of a base station's SCH is detected by means of the *primary synchronisation code* which is the same for all base stations in a UMTS/TDD network. At each possible time instant, we used a binary hypothesis test based on the generalised likelihood ratio to obtain a decision statistic for the presence of the primary synchronisation code. We presented three different detection algorithms which we termed the *spatial detector*, the *heuristic space-time detector*, and the *dispersive-channel detector*. The number and locations of peaks in these decision statistics corresponds to the number of base station signals present and the locations of the primary synchronisation codes within the received signal, respectively.

The code groups (which indicate the used scrambling codes and basic midambles) are extracted by means of *secondary synchronisation*, which can again be performed by us-

103

ing one of the proposed three detection algorithms. This time, decision statistics were computed for different synchronisation code combinations at one given time instant. The maximum value of these decision statistics corresponds to the synchronisation code combination present, which uniquely defines the code group. Because of its high SINR, we first performed secondary synchronisation for the strongest base station. After having verified its correctness using the midambles, we exploited the fact that UMTS/TDD networks are synchronous to reduce the computational complexity of secondary synchronisation for the weaker base stations. This was done by restricting secondary synchronisation to certain time windows. Simulations showed that averaging over as many timeslots as possible is advantageous and that reliable synchronisation is possible down to an SINR of

- -22 dB for channel A and -18 dB for channel B in the pedestrian environment;

- -20 dB for both channels in the indoor environment.

Based on the timing information and knowledge of the basic midambles gained during synchronisation, estimates of the base stations' channels can be computed in the **channel estimation stage** (Chapter 5). In UMTS/TDD, the data channels use eight different midambles which are constructed from the basic midamble. Since it is unknown how many data channels are present in the timeslot of interest and what their respective transmit amplitudes are, the actual composition of the total midamble is not known. However, by detecting which of the eight midambles are present and estimating their amplitudes, an estimate of the composite midamble can be gained. We presented two different midamble estimation schemes which we termed *basic midamble estimation* and *ML midamble estimation*. The first algorithm is based on the spatial detector of the synchronisation stage; the decision statistics obtained with the different possible midambles as reference sequences indicate which of the eight midambles are present in the timeslot. Also an amplitude estimate can be computed from these decision statistics. A more sophisticated way to determine the midambles is the ML midamble estimation scheme. Since this scheme requires knowledge of the channel, we first use the midambles estimated by the basic midamble estimation scheme for channel estimation. After having inserted this channel estimate into the model of the ML estimator, an improved midamble estimate can be computed.

Knowing the midambles of all base stations, we are able to construct a multiuser space-time data model which allows us to jointly estimate the channels of all base stations by means of an MMSE filter. Since this MMSE filter requires knowledge of the channels' second-order moments, we proposed an estimation scheme in which a *least-squares* estimator produces initial channel estimates. With these initial channel estimates, the second-order channel statistics can be estimated, and these estimates are finally used in the *MMSE filter*. The MMSE channel estimates obtained with this scheme were observed to be quite accurate, except in some cases for weak base stations. In order to enhance the channel estimation performance for the weak base stations, we proposed to recursively apply the MMSE estimator within a successive interference cancellation loop. This novel *successive cancellation MMSE (SC-MMSE)* channel estimator showed slightly improved performance. We were able to achieve a normalised channel estimation MSE of around

- $-5\,\text{dB}$ down to an SINR of $-22\,\text{dB}$ in the pedestrian environment;

- $-22\,\text{dB}$ (for channel A) and $-15\,\text{dB}$ (for channel B) down to an SINR of $-20\,\text{dB}$ in the indoor environment.

For the **data detection stage** (Chapter 6), we first developed a signal model where the received chips of a whole timeslot are given as functions of the input symbols. Based on this model, a *space-time MMSE equaliser* was derived in a straightforward way. Because knowledge of the presence of data channels and their respective amplitudes is not available, the correlation matrix of the received signal (which is required by the MMSE equaliser) is unknown. Although reformulation of the model into an equivalent vector-valued stationary process enabled a sample-mean estimation of the correlation matrix, simulations showed that the achieved estimation accuracy is quite poor. Instead of estimating the correlation matrix, we hence proposed to explicitly calculate it by detecting the presence of data channels and estimating their respective amplitudes. Since this works best for the strongest base station, we proposed a *decision feedback* structure where in each round only the correlation matrix of the strongest base station is calculated. The corresponding BCH data can then be detected by means of a conventional space-time MMSE filter (termed *DFB/MMSE receiver*). Replacing this MMSE filter by a decision feedback receiver (*DFB/DFB receiver*) additionally yielded small performance gains. Simulation results demonstrated that satisfactory detection scores can be achieved down to an SINR of

- $-18\,\text{dB}$ in the pedestrian environment;

- $-17\,\text{dB}$ in the indoor environment.

Finally, we combined the three stages of synchronisation, channel estimation, and data detection to one **overall system** and conducted simulations to study the influence of nonideal synchronisation and channel estimation on the performance of the BCH detection stage (Chapter 7). For these simulations, we selected the best methods of every stage, which are the *heuristic space-time detector* for synchronisation, the *SC-MMSE estimator* with *ML midamble estimation* for channel estimation, and the decision feedback detector with a decision feedback equaliser for each base station (*DFB/DFB receiver*) for data detection. In the indoor environment, because of the high accuracy of synchronisation and channel estimation, the detection scores were very close to the ideal case for almost all base stations down to the weakest ones. In the pedestrian environment, however, the effects of inaccurate channel estimates became obvious and the performance degraded compared to the ideal case. Overall, satisfactory detection scores were achieved down to an SINR of

- $-14\,\text{dB}$ in the pedestrian environment;

- $-17\,\text{dB}$ in the indoor environment.

8.2 Conclusions and Suggestions for Future Research

We finally provide some conclusions and suggestions for possible improvements of the receiver techniques presented in this thesis. Our simulations showed that the performance of the synchronisation stage was satisfactory in almost all situations, as long as we could average over eight frames or more. Also channel estimation accuracy was high in the indoor environment and for the strongest base stations in the pedestrian environment. For the weaker base stations in the pedestrian environment, however, we observed a significant degradation of channel estimation performance. Since the least-squares channel estimates were quite poor for the weak base stations, the corresponding estimates of the second-order channel statistics were not very accurate either. One possibility to obtain improved estimates of the channel statistics is to use the final SC-MMSE channel estimates instead of the least-squares estimates to compute them. Re-performing the whole SC-MMSE algorithm with these improved estimates of the second-order channel statistics can be expected to yield enhanced channel estimation performance for the weaker base stations.

Regarding the data detection stage, we saw that the performance was very sensitive to equally powered base stations. This sensitivity can possibly be reduced by including multiuser processing in every stage of the decision feedback structure, similarly as in group-wise interference cancellation [JR98]. Furthermore, we observed that channel estimation accuracies of $-16\,\mathrm{dB}$ to $-20\,\mathrm{dB}$ are needed for satisfactory detection performance; with an accuracy level of $-10\,\mathrm{dB}$, a loss in detection score of around 20 % has to be expected. A possible way to improve this situation is to incorporate channel estimation in the detection stage. After the data of the strongest base station has been detected, the content of the whole timeslot—instead of just the midamble—could be used for re-estimating the channel impulse response of the strongest base station. This results in an increased training sequence length, which should improve channel estimation accuracy. On the other hand, if we use the detected data as training information, decision errors (that will occur especially for the data channels, where error correction cannot be applied) will impair channel estimation performance. It is as yet unclear which one of these two contradictory effects has a stronger influence on the performance of channel estimation and, in turn, data detection.

Considering the significant difference in receiver performance between the pedestrian environment and the indoor environment, the strong influence of the channel model becomes obvious. Especially when selecting a "suitable" algorithm, the resulting choice will heavily depend on the considered simulation model. For instance, if the monitoring device were used only in indoor environments, the spatial synchronisation algorithm and basic midamble estimation algorithm would be sufficient. For the sake of comparability, we used the rather simple ETSI models [ETS98] in this work, but as more and more (also directional) measurements are being conducted, it would be interesting to compare our conclusions with those obtained with more advanced channel models (e.g. those described in [Ste01]).

It was seen that for data detection with ideal knowledge of the channel, longer channels are advantageous because they offer higher diversity. Unfortunately, this advantage is

diminished by the detrimental effects of larger channel estimation errors. This shows that great care has to be taken when analysing the performance of a given communication system assuming ideal channel knowledge. In order to exploit all the benefits offered by a space-time system, significant efforts must be dedicated to the development of a powerful channel estimation scheme.

Appendix A

List of Acronyms

Acronym	Description
ANTIUM	advanced network radio identification equipment for universal mobile communications
APS	azimuth power spectrum
AWGN	additive white Gaussian noise
BCH	broadcast channel
BER	bit error rate
BS	base station
cdf	cumulative density function
CDMA	code division multiple access
CG	code group
CPU	central processing unit
CRC	cyclic redundancy check
CP	chip period
CS	code set
DAB	digital audio broadcasting
DCD	dispersive-channel detector
DFB	decision feedback
DOA	direction of arrival
DVB-T	digital video broadcasting-terrestrial
ESPRIT	estimation of signal parameters via rotational invariant techniques
EU	european union
FDD	frequency division duplex
FFT	fast Fourier transform
GLRT	generalised likelihood ratio test
GP	guard period
GPRS	general packet radio service
GPS	global positioning system
GSM	global system for mobile communications

Acronym	Description
HD	hard disk
HST	heuristic space-time
I/O	input/output
ISI	intersymbol interference
IST	information society technologies
LMS	least mean square
LOS	line of sight
LS	least squares
MA	midamble
ML	maximum likelihood
MLSE	maximum likelihood sequence estimator
MMSE	minimum mean square error
MRC	maximum ratio combining
MSE	mean square error
MUSIC	multiple signal classification
MVM	minimum variance method
NLOS	non line of sight
OVSF	orthogonal variable spreading factor
PC	personal computer
P-CCPCH	primary common control physical channel
pdf	probability density function
QoS	quality of service
QPSK	quadrature phase-shift keying
RADAR	radio detection and ranging
ROC	receiver operating characteristics
SAGE	space alternating generalized expectation maximization
SCH	synchronisation channel
SC-MMSE	successive-cancellation MMSE
SF	spreading factor
SFN	system frame number
SNR	signal-to-noise ratio
SINR	signal-to-interference-and-noise ratio
ST	space-time
STTD	space-time transmit diversity
TDD	time division duplex
TFCI	transport format combination indicator
TPC	transmit power control
TPS	transmission parameter signalling
TTI	transmission time interval
UMTS	universal mobile telecommunications system

Bibliography

[3GP01a] 3GPP. TS 25.221 Physical channels and mapping of transport channels onto physical channels (TDD). www.3gpp.org, TS 25.221 v. 4.0.0, March 2001.

[3GP01b] 3GPP. TS 25.222 Muliplexing and channel coding (TDD). www.3gpp.org, TS 25.222 v. 4.0.0, March 2001.

[3GP01c] 3GPP. TS 25.223 Spreading and modulation (TDD). www.3gpp.org, TS 25.223 v. 4.0.0, March 2001.

[3GP01d] 3GPP. TS 25.944 Channel coding and multiplexing examples. www.3gpp.org, TS 25.944 v. 4.0.0, March 2001.

[AB93] S. A. Altekar and N. C. Beaulieu. Upper bounds on the error probability of decision feedback equalization. *IEEE Trans. Inf. Theory*, IT-39:145–156, Jan. 1993.

[AKH03] H. Artés, K. Kopsa, and F. Hlawatsch. A multi-antenna detection algorithm for UMTS/TDD receivers in strong interference environments. To appear in *Proc. IEEE Globecom 2003*, San Francisco, CA, Dec. 2003.

[And58] T. W. Anderson. *An introduction to multivariate statistical analysis*. Wiley, New York, 1958.

[App76] S. P. Applebaum. Adaptive arrays. *IEEE Trans. Antennas and Propagation*, AP-24:585–598, Sept. 1976.

[Aus67] M. E. Austin. Decision-feedback equalization for digital communication over dispersive channels. Technical Report 437, MIT Lincoln Laboratory, Lexington, Mass., Aug. 1967.

[Bar48] M. Bartlett. Smoothing peridiograms from time series with continuous spectra. *Nature*, No. 161, 1948.

[Bel63] P. A. Bello. Characterization of randomly time-variant linear channels. *IEEE Trans. Comm. Syst.*, 11:360–393, 1963.

[BK79] G. Bienvenu and L. Kopp. Principle de la goniometrie passive adaptive. In *Proc. 7éme Colloque GRETSI*, pages 106/1–106/10, Nice, France, 1979.

[BR82]   L. E. Brennan and I. S. Reed. An adaptive array signal processing algorithm for communications. *IEEE Trans. Aerospace and Electronic Systems*, 18(1):124–130, Jan. 1982.

[Bre59]   D. G. Brennan. Linear diversity combining techniques. *Proc. IRE*, 47:1075–1102, 1959.

[CGK67]   J. Capon, R. J. Greenfield, and R. J. Kolker. Multidimensional maximum likelihood processing of a large aperture seismic array. *Proc. IEEE*, 55:192–211, Feb. 1967.

[Cla68]   R. H. Clarke. A statistical theory of radiomobile reception. *Bell Syst. Tech. J.*, 47:957–1000, 1968.

[DS89]   D. M. Dlugos and R. A. Scholtz. Acquisition of spread spectrum signals by an adaptive array. *IEEE Trans. Acoust., Speech, Signal Processing*, 37(8):1253–1270, Aug. 1989.

[ETS98]   ETSI. TR 101.112 Universal Mobile Telecommunications System (UMTS); Selection procedures for the choice of the radio transmission technologies of the UMTS. www.etsi.org, TR 101.112 v. 3.2.0, April 1998.

[FH94]   J. Fessler and H. Hero. Space alternating generalized expectation maximization algorithm. *IEEE Trans. Signal Processing*, 42(10):2664–2677, Oct. 1994.

[For72]   G. D. Forney. Maximum-likelihood sequence estimation of digital sequences in the presence of intersymbol interference. *IEEE Trans. Inf. Theory*, IT-18:363–378, May 1972.

[For73]   G. D. Forney. The Viterbi algorithm. *Proc. IEEE*, 61:268–278, March 1973.

[Fro72]   O. L. Frost. An algorithm for linearly constrained adaptive array processing. *Proc. IEEE*, 60:926–935, 1972.

[Fuh97]   J. Fuhl. *Smart antennas for second and third generation mobile communication systems*. Dissertation, Technische Universität Wien, Vienna, Austria, 1997.

[Geo65]   D. A. George. Matched filters for interfering signals. *IEEE Trans. Inf. Theory*, IT-11:153–154, Jan. 1965.

[GV96]   G. H. Golub and C. F. Van Loan. *Matrix Computations*. Johns Hopkins University Press, Baltimore, 3rd edition, 1996.

[HN95]   M. Haardt and J. A. Nossek. Unitary ESPRIT: How to obtain increased estimation accuracy with a reduced computational burden. *IEEE Trans. Signal Processing*, 43(5):1232–1242, May 1995.

[Jak74]   William C. Jakes. *Microwave Mobile Communications*. Wiley, New York, 1974.

[JR98]   A.-L. Johansson and L. Rasmussen. Linear group-wise successive interference cancellation in CDMA. In *Proc. IEEE ISSSTA-98*, volume 1, pages 121–126, Sun City, South Africa, Sept. 1998.

[KAMH03] K. Kopsa, H. Artés, G. Matz, and F. Hlawatsch. Space-time algorithms for multiuser channel estimation in the downlink of UMTS/TDD. In *Proc. IEEE ICC 2003*, pages 2406–2410, Anchorage, AK, May 2003.

[Kay93]   S. M. Kay. *Fundamentals of Statistical Signal Processing: Estimation Theory.* Prentice Hall, Englewood Cliffs (NJ), 1993.

[Kay98]   Stephen M. Kay. *Fundamentals of Statistical Signal Processing: Detection Theory.* Prentice Hall, Upper Saddle River (NJ), 1998.

[KKB96]   A. Klein, G.K. Kaleh, and Paul W. Baier. Zero forcing and minimum mean square error equalization for multiuser detection in code-division multiple-access channels. *IEEE Trans. Veh. Technol.*, 45(2):276–287, May 1996.

[KMAH02] K. Kopsa, G. Matz, H. Artés, and F. Hlawatsch. Space-time synchronisation algorithms for UMTS/TDD systems with strong co-channel interference. In *Proc. IEEE Globecom 2002*, pages 254–258, Taipeh, Taiwan, Nov. 2002.

[KV96]   H. Krim and M. Viberg. Two decades of array signal processing research: The parametric approach. *IEEE Signal Processing Magazine*, 13(4):67–94, July 1996.

[Mon71]   P. Monsen. Feedback equalization for fading dispersive channels. *ieeeit*, IT-17:56–64, Jan. 1971.

[MS95]   S. Miller and S. Schwartz. Integrated spatial-temporal detectors for asynchronous Gaussian multiple access channels. *IEEE Trans. Veh. Technol.*, VT-40(2):472–482, May 1995.

[NP94]   A. Naguib and A. Paulraj. Performance of CDMA cellular networks with base-station antenna arrays. In *Proc. Int. Zürich Seminar on Digital Communications*, pages 87–100, Zürich, Switzerland, March 1994.

[PG58]   R. Price and P. E. Green. A communication technique for multipath channels. *Proc. IRE*, 58:555–570, March 1958.

[PP97]   A. Paulraj and C. B. Papadias. Space-time processing for wireless communications. *IEEE Signal Proc. Mag.*, 14(6):49–83, Nov. 1997.

[Pro95]   J. G. Proakis. *Digital Communications.* McGraw-Hill, New York, 3rd edition, 1995.

[Qur85]   S. U. H. Qureshi. Adaptive equalization. *Proc. IEEE*, 53(12):1349–1387, 1985.

[Rao65]   C. R. Rao. *Linear statistical inference and its applications.* Wiley, New York, 1965.

[Rap96]   T. S. Rappaport. *Wireless Communications: Principles & Practice.* Prentice Hall, Upper Saddle River (NJ), 1996.

[RPK86]   R. Roy, A. Paulraj, and T. Kailath. ESPRIT—A subspace rotation approach to estimation of paramters of cisoids in noise. *IEEE Trans. Acoust., Speech, Signal Processing,* ASSP-34:1340–1342, Oct. 1986.

[Sch91]   L. L. Scharf. *Statistical Signal Processing.* Addison Wesley, Reading (MA), 1991.

[Ste01]   M. Steinbauer. *The radio propagation channel—A non-directional, directional, and double-directional point-of-view.* PhD thesis, Vienna Univ. Technology, Vienna, Austria, Nov. 2001.

[TGM96]   J. S. Thompson, P. M. Grant, and B. Mulgrew. Smart antenna arrays for CDMA systems. *IEEE Personal Communications,* 3(5):16–25, 1996.

[VB88]   B. D. Van Veen and K. M. Buckley. Beamforming: A versatile approach to spatial filtering. *IEEE Acoust., Speech, Signal Proc. Magazine,* pages 4–24, April 1988.

[Ver98]   S. Verdú. *Multiuser Detection.* Cambridge Univ. Press, Cambridge (UK), 1998.

[vRLvW00]   P. van Rooyen, M. Lötter, and D. van Wyk. *Space-time processing for CDMA mobile communications.* Kluwer Academic Publishers, Norwell, Massachusetts, 2000.

[Wei91]   A. Weinmann. *Uncertain Models and Robust Control.* Springer, Vienna, Austria, 1991.

[Wid66]   B. Widrow. Adaptive filters, I: Fundamentals. Technical Report 6764-6, Stanford Electronics Laboratory, Stanford University, Stanford, Ca., Dec. 1966.

[Win84]   J. H. Winters. Optimum combining in digital mobile radio with cochannel interference. *IEEE J. Sel. Areas Comm.,* SAC-2(4):528–539, July 1984.

[Wis67]   J. Wishart. The generalized product moment distribution in samples from a normal multivariate population. *Biometrika,* 47:199–201, 1967.

Curriculum Vitae

Personal Data:

Name:	Klaus Kopsa
Address:	Edmund Weiß-Gasse 1/16, A-1180 Wien, Austria
Date of Birth:	27 Sep. 1974 in Vienna
Marital Status:	Single
Citizenship:	Austrian

School Education:

09/1980 – 06/1984:	Elementary School (Volksschule), Wien 18 Köhlergasse
09/1984 – 06/1992:	Grammar School (Gymnasium), Wien 19 Billrothstraße
June 1992:	Graduation (Matura) with highest honors

Mandatory Military Service:

07/1992 – 02/1993:	in Baden, Austria

Education at University:

10/1993 – 10/1998:	Studies of Electrical Engineering / Communications Engineering at Vienna University of Technology, Austria
October 1998:	Graduation (Dipl.-Ing. degree) with highest honors Diploma Thesis: *Software Implementation of a Pseudo-Blind Algorithm for Adaptive Antennas*
since 09/1998:	Doctoral studies at the Institute of Communications and Radio-Frequency Engineering (INTHF), Vienna University of Technology, Austria

Jobs and Professional Experience:

05/1993 – 09/1993:	Bundesamt für Eich- und Vermessungswesen, Vienna
07/1995 – 08/1995:	Siemens, PSE, Vienna
07/1996 – 08/1996:	Siemens, PSE, Vienna
07/1995:	Siemens, PSE, Vienna
since 11/1998:	Research Engineer at INTHF, working on the projects:
11/1998 – 02/2000:	*Adaptive Antennas for UMTS* in cooperation with the Alcatel Research Center Stuttgart, Germany
03/2000 – 12/2000:	*UMTS and Beyond* at the Telecommunications Research Center Vienna (FTW)
01/2001 – 10/2003:	*ANTIUM* funded by the European Commission within the 5$^{\text{th}}$ framework program

Awards:

1995 – 1998:	*Leistungsstipendium* scholarship granted by the Faculty of Electrical Engineering for excellent study performance

Languages:

German (mother tongue)
English (business fluent)